

AN MCNP STUDY OF FAST NEUTRON INTERROGATION FOR STANDOFF
DETECTION OF IMPROVISED EXPLOSIVE DEVICES

by

SAMUEL A. HEIDER

B.A., University of Nebraska at Lincoln, 2004

A THESIS

submitted in partial fulfillment of the requirements for the degree

MASTER OF SCIENCE

Department of Mechanical and Nuclear Engineering
College of Engineering

KANSAS STATE UNIVERSITY
Manhattan, Kansas

2012

Approved by:

Major Professor
Dr. William L. Dunn

Copyright

SAMUEL A. HEIDER

2012

Abstract

The signature-based radiation-scanning (SBRs) technique relies on radiation detector responses, called “signatures,” and compares them to “templates”, to differentiate targets containing nitrogen-rich explosives from those that do not. This investigation utilizes nine signatures due to inelastic-scatter and prompt-capture gamma rays from hydrogen, carbon, nitrogen, and oxygen (HCNO) as well as two neutron signatures, produced when a target is interrogated with a 14.1 MeV neutron source beam. One hundred and forty three simulated experiments were conducted using MCNP5. Signatures of 42 targets containing explosive samples (21 of RDX and 21 of Urea Nitrate), and 21 containing inert samples were compared with the signatures of 80 artificial templates through figure-of-merit analysis. A density filter, comparing targets with templates of similar average density was investigated. Both high and low-density explosives (RDX-1.8 g cm⁻³ and Urea Nitrate-0.69 g cm⁻³) were shown to be differentiated from inert materials through use of neutron and gamma-ray signature templates with sensitivity of 90.5% and specificity of 76.2%. Density Groups were identified, in which neutron signature templates, gamma-ray signature templates or the combination of neutron and gamma-ray signature templates were capable of improving inert-explosive differentiation. figure-of -merit analysis, employing the best Density Group specific templates, differentiated explosive from inert targets with 90.5% sensitivity and specificity of over 85%.

Table of Contents

List of Figures	vii
List of Tables	ix
Acknowledgements.....	x
Dedication	xi
Chapter 1 - The Threat and Toll of Improvised Explosive Devices	1
1.1 The IED Defined.....	1
1.2 The Human Toll of IEDs	2
1.3 The Financial Toll of Combating IEDs	4
1.4 Protection of Military Personnel from IEDs.....	5
1.4.1 Existing IED Protection Methods	5
1.4.2 Electronic Countermeasures to IEDs	5
1.5 IED Detection Techniques.....	6
1.5.1 Methods of Trace Explosive Detection.....	6
1.5.2 Methods of IED Detection by Inspection	6
1.6 The Advantage of Stand Off Bomb Detection.....	8
1.7 Objectives and Preview	9
Chapter 2 - Techniques for Detecting Explosives	10
2.1 Trace Detection Techniques	10
2.2 Bulk Detection Techniques.....	10
2.2.1 Advantages of Bulk Detection	12
2.2.2 X-Rays	12
2.2.3 Electromagnetic Detection Methods.....	14
2.2.4 Gamma Rays	15
2.2.5 Neutrons	16
Chapter 3 - Theory	20
3.1 Physics of Neutron Interactions	20
3.1.1 Neutron –Matter Interactions.....	20
3.2 The Composition of Explosives.....	23

3.3 Template Matching	25
3.4 Template Generation for SBRS Application	27
3.5 Explosive Discrimination Using Figure-of-Merit Analysis.....	29
3.6 Simulations Using MCNP Transport Code	32
3.7 Techniques Employed to Generate and Analyze MCNP Data	36
Chapter 4 - MCNP Simulation Model and Results.....	37
4.1 Target Model Specifications	37
4.1.1 Mockup Geometry	39
4.2 MCNP Data and Data Processing.....	41
4.2.1 Signature Peaks and Error.....	41
4.2.2 Figure-of-Merit Calculations	44
4.3 Results of Figure-of-Merit Analysis Using Cutoffs and Density	44
4.3.1 Application of a Density Filter.....	48
4.4 Particle Dependent Figure-of-Merit Analysis.....	56
4.4.1 Density Dependent Cutoffs Using Neutron Figure-of-Merit Analysis	56
4.4.2 Density Dependent Cutoffs Using Gamma-ray Figure-of-Merit Analysis.....	57
4.5 Results Using Density Dependent Cutoffs	58
Chapter 5 - Conclusions and the Way Ahead	61
5.1 Target Density.....	61
5.2 Particle Signatures	61
5.3 Explosive Density and Clutter Materials	62
5.4 Full-Scale Tests Using Operational D-T Neutron Generator	63
5.5 Implementation of a Larger Number of Templates	63
References.....	64
Appendix A - Template Signatures.....	68
Appendix B - Example MCNP Code.....	89
Appendix C - Sample Compositions and Density	96
Appendix D - Sample Pearl Script and C++ Codes for MCNP5 Data Processing.....	100
Appendix E - Sample MATLAB (2010a) codes for calculating Figures-of-Merit.	109
Appendix F - Lowest Figures-of-Merit for RDX, UNi, and inert samples versus all templates.	113
Appendix G - Lowest Figures-of-Merit using density filter.....	115

Appendix H - Lowest Figures-of-Merit using neutron signatures and density filter..... 117
Appendix I - Lowest Figures-of-Merit using gamma-ray signatures and density filter. 119

List of Figures

Figure 1-1: IED Incidents in Afghanistan, May 2008-May 2010 (Cordesman, 2010).....	3
Figure 1-2: Casualties by item: 2010 (Landmine & Cluster Munition Monitor, 2011).	3
Figure 1-3: JIEDDO Budget in Historical Perspective.....	4
Figure 1-4: Buffalo Mine Protected Clearance Vehicle (left), Husky Mine Detection Vehicle (center) and MRAP with Mine Roller System (right).	7
Figure 2-1: Existing Trace and Bulk Detection Technologies (NRC, 2004).....	11
Figure 2-2: Standoff X-ray detection showing hidden explosives and other items on personnel. Images were taken from a van moving at 0.3 to 6 miles per hour using X-ray backscattering in “drive-by” mode. The mock suicide vest contained simulated C4 explosives and pipe bombs. Both the explosives and the pipe bombs are easy to see and are distinguishable from normal objects under clothing (NRC, 2004).	13
Figure 2-3: (a) Schematic of DT111 fast neutron generator (Adelphi, 2012). (b) Photo of DT111 in Standoff Bomb Laboratory.	19
Figure 3-1: Various categories of neutron interactions. The letters separated by commas in the parentheses show the incoming and outgoing particles (Rinard, 1991).	21
Figure 3-2: Atomic percentages of the elements H, C, N and O, which constitute a selection of explosives, illicit drugs, and miscellaneous common materials (Buffler, 2004).	24
Figure 3-3: Graphical Depiction of Cutoff, ζ_0 , Being Used to Identify Inert, Suspect, and Explosive Materials.	30
Figure 4-1: Schematic of simulated target geometry, (a) 3-D mockup of car trunk, (b) detector configuration.	37
Figure 4-2: (a) Outside of Al target, (b) sample and clutter geometry, (c) sample close-up.	40
Figure 4-3: Sample Figure of Binned Responses Surrounding Signature Energies of 2.2232 MeV (Hydrogen Prompt-Capture Gamma-Ray) and 2.3128 MeV (Nitrogen Inelastic-Scatter Gamma-Ray).....	42
Figure 4-4: Lowest Figures-of-Merit with Cutoff of 9 Identifies All 21 Samples of RDX as Explosives	45

Figure 4-5: Lowest Figures-of-Merit with Cutoff of 9 Identifies All 21 Samples of UNi as
Explosives 46

Figure 4-6: Lowest Figures-of-Merit with Cutoff of 9 Identifies All 15 Inert Samples as
Explosives 47

Figure 4-7: Density Group-1, 13 targets with density between 0 and 1 g cm⁻³ 50

Figure 4-8: Density Group-2, targets 1-11 of 31 targets with density between 1 and 2 g cm⁻³... 51

Figure 4-9: Density Group-2, targets 12-21 of 31 targets with density between 1 and 2 g cm⁻³.52

Figure 4-10.: Density Group-2, targets 22-31 of 31 targets with density between 1 and 2 g cm⁻³.
..... 53

Figure 4-11: Density Group-3, 8 targets with density between 2 and 3 g cm⁻³ 54

Figure 4-12: Density Group-4 & 5, 9 targets with density between 3 and 9 g cm⁻³ 55

List of Tables

Table 2.1: Selected features of four common nuclear physics-based techniques for the non-intrusive interrogation of bulk samples. Adapted from Buffler (2004) and Johll (2009).	17
Table 3.1 Nine (9) HCNO prompt-capture and inelastic-scatter signature energies (Group T-16, 98-2007; Molnár, 2004 & Johll, 2009) and two (2) neutron signature energies.....	26
Table 4.1 Artificial Inert Clutter Materials	38
Table 4.2: Density Filter Values and Average Densities of Templates.....	48
Table 4.3 Clutter and Sample Average Densities.	49
Table 4.4 Density Dependent ζ_0 Using Neutron Signatures	57
Table 4.5 Density Dependent ζ_0 Using Gamma-ray Signatures	57
Table 4.6 Method Comparison Using Density Dependent Cutoffs	59
Table 4.7 Neutron and Gamma-ray ζ_ℓ for Group-3.....	60
Table A.1 Signature designations	68
Table A.2 Templates with RDX sample.....	69
Table A.3 Templates with Urea Nitrate sample.....	79
Table C.1 Inert Compositions (Williams III, 2006).....	96
Table C.2 Inert Compositions.....	97
Table C.3 Explosive Compositions.....	99
Table D.1 Pearl Script for isolating neutron signatures.....	100
Table D.2 C++ code for extracting gamma-ray signatures.....	102
Table E.1 Code calling “Response” script to retrieve signatures for templates and responses of targets.....	109
Table E.2 “Response” script, places signatures inside response vectors and calls “Template” script.....	110
Table E.3 “Template” script, places signatures inside template vectors and calls “FOM_Calc” script.....	111
Table E.4 “FOM_Calc” script, calculates FOM and normalization factor.....	112

Acknowledgements

The author would like to acknowledge Kennard Callender and the Kansas State Standoff Bomb Detection research team for contributions in development of the MCNP5 input code and various data processing codes.

Dedication

To my wife Amanda and children Annaliese, Evan and Owen, thank you for your loving support and dedication.

Chapter 1 - The Threat and Toll of Improvised Explosive Devices

1.1 The IED Defined

The Improvised Explosive Device or IED has become a household term evoking a sense of dread and fear in the hearts of many. The United States Military has described IEDs as “...nonstandard explosive devices used to target U.S. Soldiers, civilians, [Non-government Organizations], and government agencies. IEDs range from crude homemade explosives to extremely intricate remote-controlled devices. The devices are used to instill fear in U.S. Soldiers, coalition forces, and the local civilian population. Their employment is intended to diminish U.S. national resolve with mounting casualties. The sophistication and range of IEDs continue to increase as technology continues to improve and as terrorists gain experience.” (FM 3-21.8, Appendix I, 2007) The lethality combined with the simple construction of IEDs has made them the single most difficult foe on the modern battlefield and, as their employment increases the risks to innocent civilian populations also increases. The human and financial toll of IEDs has become a staggering reality felt the world over.

IEDs are generally classified by how they are triggered, the type of explosive accelerant used and by the means of delivery. Victim-activated IEDs, those that employ devices such as trip-wires, passive infrared receivers (PIR), crush-tubes, pressure-plates, or crush-wires to initiate the device, are often hard to detect and pose a tremendous threat to dismounted troops. Victim-activated devices also threaten civilian populations because they are in no way selective and can be activated by small children, herding animals, or anyone unfortunate enough to come in contact with the initiating device. Stacked conventional landmines can be used as part of the victim-activated IED group, threatening dismounted and mounted troops or civilians. Command-detonated devices relying on signals from devices such as telephones, two-way radios, or garage door openers, allow terrorists to be more selective in initiating an attack. These remotely controlled initiation devices are hard to detect and prevent, requiring that their signal be interrupted in some way. Command-wire initiated devices, requiring that a terrorist close to the IED simply touch wires to a battery to initiate the explosive, are resistant to electronic counter-measures but pose less of a threat because of the terrorists’ proximity to the IED.

IEDs using conventional munitions grade explosives or Explosive Remnants of War (ERW) are very dangerous because of their high explosive yield and their availability in many war-torn countries. The 155 mm shell, an ERW, has had devastating effects as an IED in Iraq and Afghanistan. However, there are several home-made explosives, like ammonium or urea nitrate, which have proven to be just as deadly as IED fuels (Almog, 2007). A particularly dangerous use of ammonium nitrate is in forming an explosively formed projectile (EFP). An EFP uses a metal tube, packed with an explosive, and a copper cone attached to one end. When the explosive is ignited, a molten slug capable of penetrating several inches of armor plating is formed (Matthew, 2010). By combining an EFP with any type of victim-activation device, terrorists can destroy heavily armored military vehicles with little chance of detection and without risking their own lives.

The means of IED delivery has many forms. Terrorist may opt to use a suicide bomber who uses a vest carrying explosives; this form of delivery is known as a Personnel Borne IED or PBIED. The use of Vehicle Borne IEDs (VBIEDs), where the explosives are concealed in a compartment, have proven very effective and extremely hard to prevent. No matter what the trigger, the explosive, or the means of delivery, IEDs persist as an ever-growing threat to a nation's security and peace.

1.2 The Human Toll of IEDs

Figures 1.1 and 1.2 demonstrate the human cost of IEDs and other explosive ordinance, with a focus on the areas with continued armed conflict. In Afghanistan, the number of IED victims in May 2010 was more than double that of May 2009. The highest number of IED casualties, in Afghanistan, came in August of 2009, peaking at 388. However, as the number of IED attacks continued to increase in the spring months of 2010 they were somewhat less effective when compared to other months with comparable numbers of attacks (Cordesman, 2010).

The number of victim-activated IED casualties is on the rise with nearly 70% of the casualties being civilians. Worldwide, victim-activated IEDs, Explosive Remnants of War (ERW) and other unspecified mine types were responsible for more than 2 000 casualties in 2010 (Landmine & Cluster Munition Monitor, 2011). In 2010, Afghanistan and Pakistan, the two countries with the highest numbers of casualties due to victim-activated IEDs, each had

increases, Afghanistan from 293 to 383 and Pakistan from 190 to 203. Also in 2010, Afghanistan accounted for 56% of the total victim-activated IED casualties worldwide (Landmine & Cluster Munition Monitor, 2011).

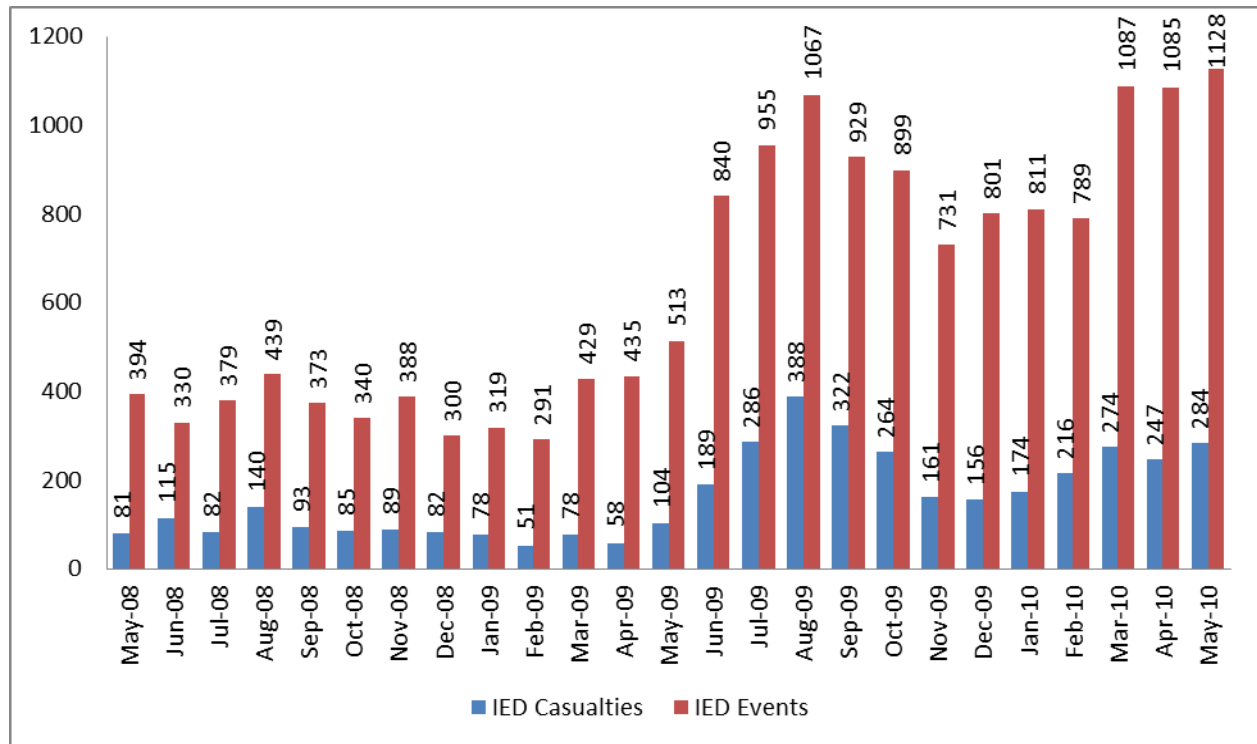


Figure 1-1: IED Incidents in Afghanistan, May 2008-May 2010 (Cordesman, 2010).

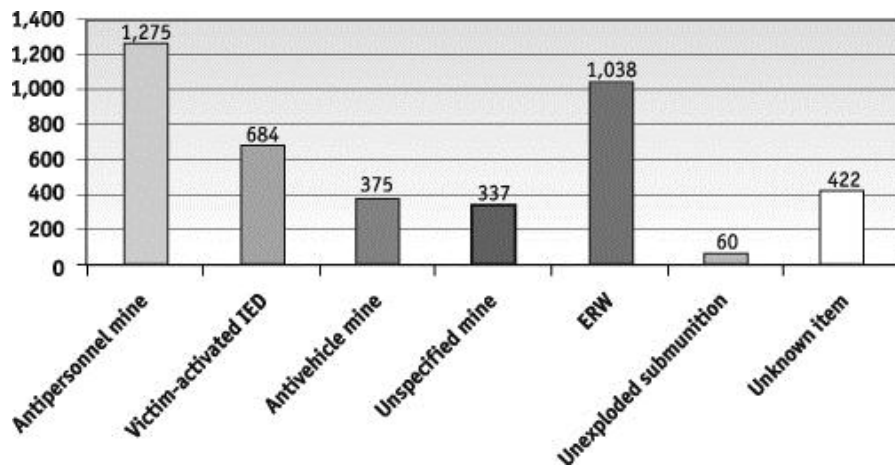


Figure 1-2: Casualties by item: 2010 (Landmine & Cluster Munition Monitor, 2011).

1.3 The Financial Toll of Combating IEDs

The focus of the majority of IED detection and defeat devices are military in nature because only the militaries of developed countries can afford their high cost. Military personnel are also often the targets of IED attacks in conflict areas and these forces demand a high level of protection. United States casualties in Afghanistan and Iraq have prompted the rapid development of several organizations with the purpose of developing and acquiring IED detection and defeat systems. The Joint Improvised Explosive Device Defeat Organization (JIEDDO) was created to combat the mounting death toll of American service men and women deployed in support of Operations Enduring Freedom and Iraqi Freedom. JIEDDO had an average budget of 3.48 billion dollars annually, from fiscal year 2006 to fiscal year 2010, and provided funding for IED defeat devices, training and education, and research and development of new IED detection and defeat technologies (JIEDDO, 2010). Figure 1.3 shows the funding of JIEDDO as compared with the number of IED attacks in Iraq and Afghanistan. JIEDDO provides many counter-IED (C-IED) technologies to the war-fighters in Iraq and Afghanistan and continues to spearhead advancements in training and force protection. In 2007 the Department of Defense (DoD) awarded \$2.2 billion, to Force Protection, Inc., and Armor Holdings, Inc., for armored vehicles and armor kits to help protect military personnel in combat zones (DoD Office of Inspector General, 2007).

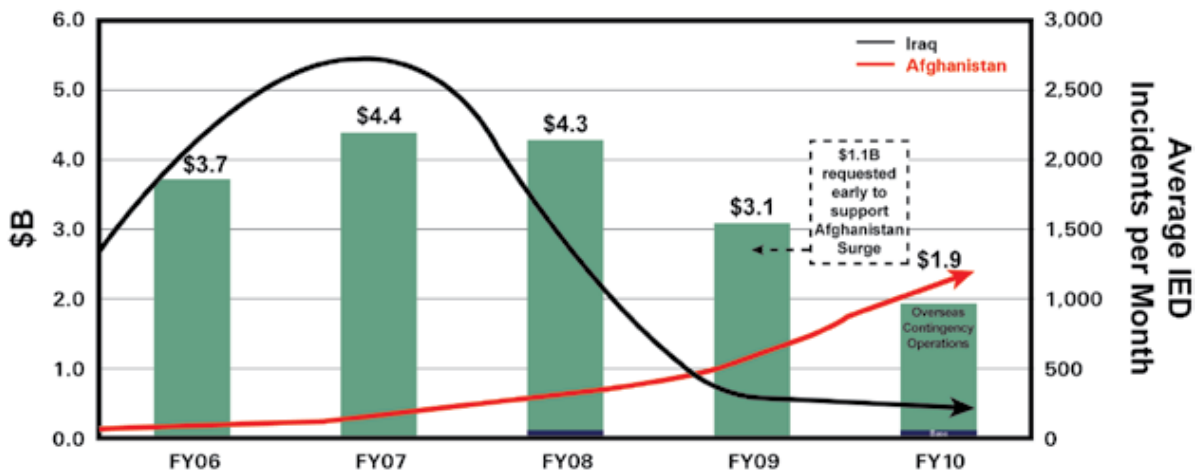


Figure 1-3: JIEDDO Budget in Historical Perspective.

In addition to the billions of dollars spent in protecting fighting men and women in conflict areas around the world the financial loss due to IEDs is nearly incalculable. The disruption to normal trade, by destroying roads and buildings, is immense. The costs to civilians in areas rife with IEDs, both in lost goods and repair costs, are also massive.

1.4 Protection of Military Personnel from IEDs

Protecting military personnel from IEDs is of great importance to any country currently involved in peacekeeping or combat operations. Any nation sending its military personnel into harm's way must contemplate how best to protect those individuals from small arms fire, rockets and mortars, landmines and IEDs. Soldiers, Airmen, and Marines of the US military are issued body armor to protect them from small arms fire and shrapnel, bunkers to protect them from mortars and rockets, and vehicles with increased protection to safeguard against attacks from IEDs.

1.4.1 Existing IED Protection Methods

One of the easiest ways to protect military personnel from IED attacks is to increase the armor of their vehicles. High Mobility Multipurpose Wheeled Vehicles (HMMWV) in Iraq and Afghanistan were given an "up-armored" or FRAG 5 package increasing the armor thickness on the doors, belly and roof of the vehicle (Matthew, 2010). However, any flat-bottomed vehicle is susceptible to damage from IEDs buried under roadways, in culverts or under bridges. To combat this vulnerability the Mine Resistant Ambush Protected (MRAP) vehicle, with its V-shaped hull and higher profile, was introduced to help protect service men and women. However, with the increased protection of thick armor two new disadvantages were introduced. Because the up-armored HMMWV and MRAP vehicles are heavier they are not as maneuverable and they are more likely to roll over at high speeds or on steep grades. The increase in armor thickness still does not provide complete protection from EFPs. As is the case with many protective measures, advantages in one area create disadvantages in another.

1.4.2 Electronic Countermeasures to IEDs

Electronic countermeasures (EC) target the remote electronic detonation radio frequency signals, such as a two-way radio or cordless telephone frequencies, used to detonate some IEDs. High power transmitters, jamming frequently used electromagnetic frequencies, prevent these

signals from reaching an IED initiation device. Once the frequencies are jammed foot-patrols and vehicle convoys can pass an IED safely, even if the whereabouts of the IED are unknown. Another EC pre-detonates IEDs by broadcasting the oft-used frequencies from an aircraft. As the aircraft passes over a vehicle or personnel route the IED receives a detonation signal and explodes before the military patrol reaches the intended engagement area.

1.5 IED Detection Techniques

Many detection techniques have been developed by military forces the world over. The most effective techniques employ extensive protection methods designed to safeguard equipment and personnel from shrapnel and the concussion of an IED explosion. To date few techniques developed are truly safe, but improvements are continuing to be made. Most detection methods require a great deal of time and that some person or machine physically inspect the location of a suspected IED. Mitigating these aspects of the detection process is the aim of nearly all advancements in IED detection.

1.5.1 Methods of Trace Explosive Detection

Traces of explosive chemicals are present on nearly any object that comes in contact with the explosive. These traces can be detected by a chemical analysis technique performed by wiping the suspect area with a cloth and examining the cloth in a machine for explosives. Detection by biosensors such as specially trained canines is also very effective. Another biosensor method involves specially trained bees that, when released, congregate in an area where they detect explosive chemicals. There are obvious drawbacks to these techniques. Chemical analysis is time consuming, as is canine detection, and bees, once released, may be hard to track and may be lost. Also, these techniques often require that highly trained personnel be in close proximity to an IED.

1.5.2 Methods of IED Detection by Inspection

Physical inspection is often the most effective method for detecting IEDs. Physical inspections are either passive or active in nature. Passive searches are conducted at checkpoints where military or police physically inspect a vehicle or person for explosives or contraband. These searches can be very tedious, time consuming and once again place personnel close to a possible IED. An active inspection method requires patrolling in areas where IEDs are likely to

be placed. Actively patrolling suspect areas requires highly trained men and women and a set of special tools.

The task of finding and destroying IEDs often falls to special military engineers and Explosive Ordnance Disposal (EOD) units employing anything from a knife and a hand-held metal detector to ground penetrating radar and infrared sensors. These units clear roads of mines and IEDs by driving over the road with special Husky Mine Detection Vehicles (MDV) as seen in Fig. 1.4. The Husky MDV vehicles utilize a light frame with wide wheels to help circumvent pressure plate mines or IEDs, and a V-shaped hull to protect the driver if there is an explosion directly beneath the cabin. Under the hull of the Husky MDV is an array of metal detectors or a ground penetrating radar system used to locate areas where mines or IEDs may be buried.



Figure 1-4: Buffalo Mine Protected Clearance Vehicle (left), Husky Mine Detection Vehicle (center) and MRAP with Mine Roller System (right).

After identifying a suspect area, it is the job of the crew of a Buffalo Mine Protected Clearance Vehicle (MPCV), also pictured in Fig. 1.4, to inspect the area. The crew utilizes the Buffalo MPCVs interrogating arm and video camera to locate the hidden IEDs and mines. Working in tandem these vehicles comprise the heart of a Rout Clearance Package (RCP). The responsibility of destroying the explosives often falls to EOD teams, but may also be done by specially qualified engineers.

The speeds at which an RCP can perform its duties is limited by the operators using the system and the terrain being investigated. Usually an RCP moves between 10-15 kilometers per hour. Although the Husky MDV and Buffalo MPCV protect their occupants from shrapnel and direct fire they still require personnel to be close to an IED and a potential explosion. The concussion of an IED blast can cause many internal injuries including Mild-traumatic Brain

Injury (MTBI). Many individuals with MTBI report that it affects their behavior and cognitive processes.

Another active patrolling method uses airborne infrared sensors to detect heat anomalies in vehicle or personnel routes. Detection via this method still requires that EOD or a RCP be used to investigate the suspect area, once again putting personnel in harm's way. In order to protect military and civil forces in areas where the dangers of IEDs are high, IEDs must be discovered and removed, tasks which often require expensive and sophisticated equipment and the lives of dedicated personnel.

1.6 The Advantage of Stand Off Bomb Detection

The ability to rapidly detect IEDs at standoff affords military and police the greatest protection. Standoff refers to the fact that all components of the detection system are at least several meters from the closest surface of the potential IED; of course, large standoff is preferred over short standoff. Whereas users would prefer standoff distances of many tens of meters, our research treats standoff as 1.5 m or more. Current methods of detection are neither fast nor provide service members the added protection of standoff. The future of IED detection systems must be centered on providing standoff techniques that are extremely fast and highly reliable. The goal of the Kansas State University Stand Off Bomb Detection research project is to develop just such a system. Utilizing a Signature Based Radiation Scanning technique, the project seeks explosive detection with appropriate levels of sensitivity and specificity to be accomplished within several seconds. In practice, high sensitivity, with its low number of false negative readings, is preferred over high specificity, with its low number of false positive readings. To accomplish this task a template matching procedure is employed, whereby back-streaming radiation signatures are compared to templates of known explosives signatures, to determine if a sample is an explosive or inert material. Back-streaming radiation is radiation that is backscattered from an interrogated object or generated inside the object by the interrogating radiation and emitted back toward the source where it is detected. Thus, use of back-streaming radiation requires only one side of an object be accessible for interrogation.

1.7 Objectives and Preview

The objective of this research was to demonstrate that the SBRS technique using high-energy neutron interrogation is capable of discriminating between explosive and inert targets with high levels of sensitivity and specificity. In practice, a detection method should correctly identify nine of every 10 IEDs encountered (sensitivity of 90%). However, the system should not be so sensitive that all objects tested are labeled as explosives. The number of tested objects falsely identified as explosives should be less than one in four (specificity of 75% or greater). In this work, explosive detection techniques using fast neutrons are explored with the intent of achieving sensitivity of 90% or better and specificity of at least 75%. In order to achieve high levels of sensitivity and specificity it is often necessary to employ filtering processes that enhance a detection technique's effectiveness. Identifying and exploring any filtering process that would yield the desired sensitivity and specificity was a secondary objective in this work. A final objective was to identify whether the use of neutron signatures offered any advantages in the discrimination of explosive from non-explosive materials.

The proceeding chapter deals with background information pertaining to existing techniques of IED detection (Chapter 2). The theoretical basis of explosive identification through neutron interrogation is described in Chapter 3. Chapter 4 outlines the experimental setup and the Monte Carlo Neutral Particle (MCNP5) simulations employed to replicate real objects for interrogation by neutrons. Explosive-non-explosive differentiation results, using Monte Carlo simulation data, are also presented in Chapter 4. Then, Chapter 5 highlights the results of the investigation with analysis and conclusions, concluding with suggestions for future investigations, which could improve on the results of this work.

Chapter 2 - Techniques for Detecting Explosives

In order to combat IEDs, one seeks to protect equipment and personnel from the hazardous effects of an explosion, by either shielding or protecting them from the blast or by preventing the IED from ever being detonated. Shielding is afforded by the armor surrounding military vehicles or by heavy concrete structures designed to withstand the devastating effects of an explosion. These shields, when combined with standoff, give personnel and equipment their best chance of surviving an IED blast. There are a host of countermeasures used to prevent the detonation of an IED, as mentioned, but their effectiveness is based mainly on their ability to interrupt electronic signals. These countermeasures blindly interrupt electronic signals even when there may be no IED present and their success is limited. Detection of IEDs prior to detonation affords the greatest protection for military and security forces. The focus of the remainder of this chapter will be to identify and explore techniques for detecting IEDs.

2.1 Trace Detection Techniques

In Section 1.5.1 examples of trace detection methods were briefly discussed. Figure 2.1 displays many more existing trace detection technologies either in use or under investigation. The interested reader should consult the work “Existing and Potential Standoff Explosives Detection Techniques” published by the National Research Council (NRC, 2004). While some of these methods have proven effective, they are not the subject of this work and are mentioned only to outline the many advances that have been made in attempting to solve the complex problem of IED detection.

2.2 Bulk Detection Techniques

There are a great number of bulk detection methods, also displayed in Fig. 2.1, several of which have shown great promise at detecting bulk explosives. Several of these methods are discussed and the application of a combination of these methods will be explored as the principal part of this investigation. Many bulk detection techniques rely on imaging of the associated spatial features of a bomb such as metal wires, detonators or batteries, or on the reflection, absorption or scattering of X rays, or microwaves, by the bulk explosive itself (NRC, 2004). It should be noted that while many bulk detection techniques rely on imaging, the research

presented in this work is designed to provide information about an IED without imaging. Thus, while imaging techniques are very useful, their use often requires access to multiple sides of an IED, and long imaging times, circumstances not practical in most field scenarios.

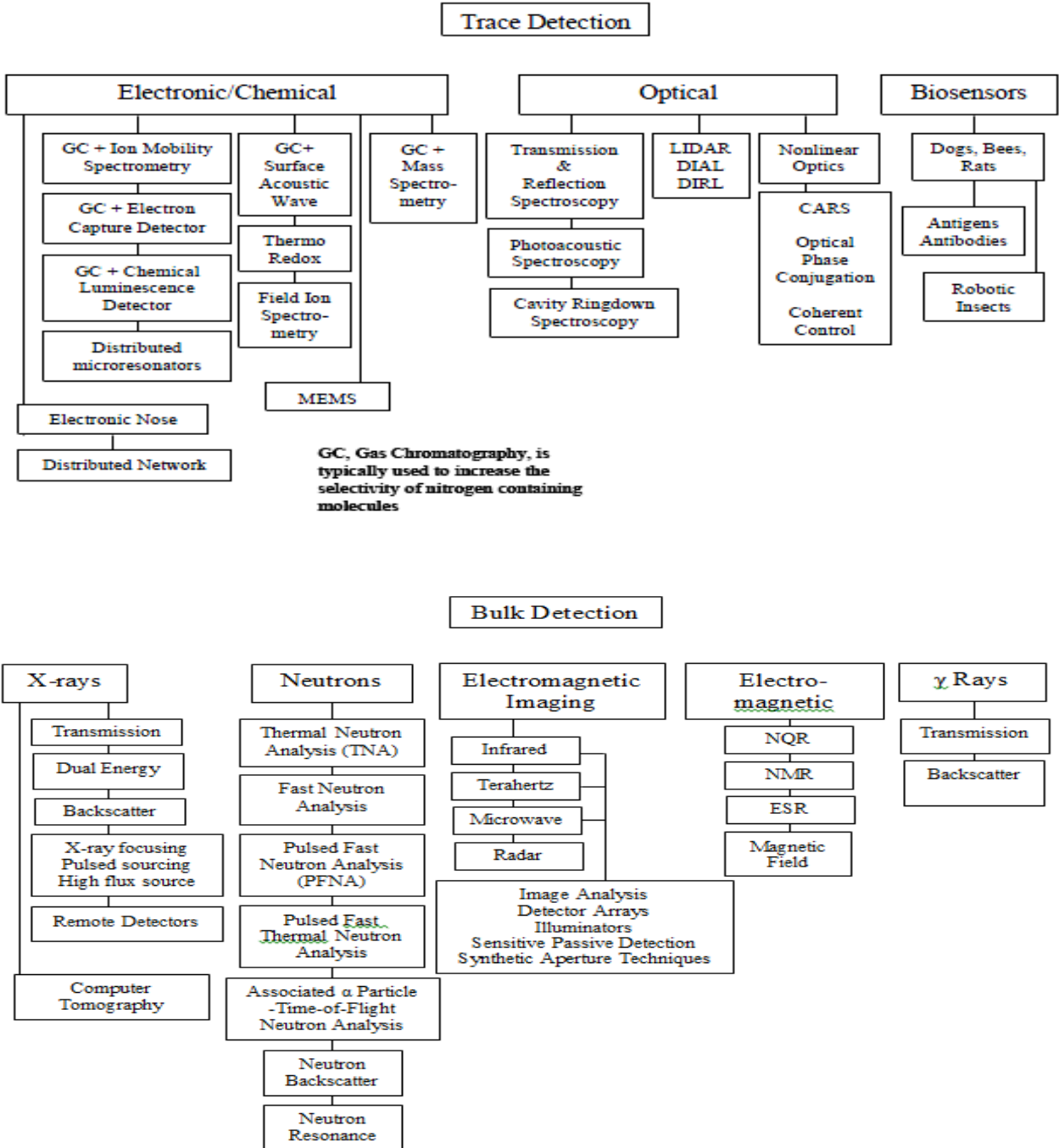


Figure 2-1: Existing Trace and Bulk Detection Technologies (NRC, 2004).

2.2.1 Advantages of Bulk Detection

Bulk detection, relying on the identification of the macroscopic characteristics of an explosive, often utilizes electromagnetic and particle radiation techniques. By using microwaves, neutrons or gamma rays, one can gain information about the shape, composition and density of the interrogated explosive. Charged particles are ineffective as interrogation radiation as they cannot penetrate deeply into a material or through clutter materials disguising an IED. Bulk detection of explosives also offers several advantages over trace detection methods. These advantages include:

Deep target penetration – Offers the ability to interrogate larger volumes, such as cargo containers.

Greater Specificity – Offers a lower number of non-explosives misidentified as explosives.

Greater Sensitivity – Offers a lower number of explosives misidentified as non-explosives.

Rapid Interrogation – Offers high intensity radiation leading to lower scanning times.

Standoff – Offers protection to equipment and operators by interrogating at a distance (Johll, 2009).

2.2.2 X-Rays

X rays have long been used to search luggage and cargo containers for illicit materials and explosives. The ionizing effects of X-ray radiation have detrimental effects on humans and thus health concerns surround the use of such scanning techniques on humans. However, at standoff distances of 10 to 20 meters the radiation effects are highly reduced. As transmitted X rays pass through a target they are absorbed according to the density and atomic number of the materials they encounter. Thus, an image and information about a target material's density can be found using transmission X-ray techniques. High-resolution images can be formed using an inexpensive detector placed on the opposite side of a target from a transmitter (NRC, 2004). Transmission X-ray techniques can detect the components of explosive devices in small volumes, but are ill suited for detection of explosives in large volumes due to the difficulty of identifying the many complex shapes explosive materials may take. This technique also suffers

from a high false positive rate making it a poor method for detecting explosives at standoff (Johll, 2009).

Images can also be formed from backscattered X rays, with the detector on the same side of the target as the transmitter. Images formed using backscattered X rays are shown in fig. 2.2, where the bright portions are organic materials and the dark spots are materials made of heavier elements. Backscatter X-ray imaging techniques are good at discriminating organic and inorganic materials, materials with larger than average densities and materials with low atomic number (Singh, 2003).



Figure 2-2: Standoff X-ray detection showing hidden explosives and other items on personnel. Images were taken from a van moving at 0.3 to 6 miles per hour using X-ray backscattering in “drive-by” mode. The mock suicide vest contained simulated C4 explosives and pipe bombs. Both the explosives and the pipe bombs are easy to see and are distinguishable from normal objects under clothing (NRC, 2004).

Computed Tomography (CT) is another imaging technique utilizing X-ray radiation, and can produce images with high spatial resolution. However, the technique requires scanning from many angles and thus requires a great deal of time, and data processing. There are CT systems that can scan and image large volumes at standoff distances of 20 feet (NRC, 2004). CT techniques require of the order of 100 views from 1 024 elements in a linear X-ray detector to produce a single slice image of 1 000 x 1 000 pixels (Singh, 2003). The number of transmitter-

detector geometries required to produce an acceptable image and the required expertise of the operator to interpret the image does not make this method practical for many standoff explosive detection scenarios.

2.2.3 Electromagnetic Detection Methods

Infrared (IR) Imaging

Most items including clothing and explosives are opaque to IR radiation with spectral wavelengths of 1 to 10 microns (NRC, 2004). Nearly all objects emit thermal IR radiation, which can be used to image the object with special cameras. This same technology is used extensively in military targeting applications. Because different objects have slightly different temperatures, they can be differentiated using thermal IR techniques. Temperature differences of a few tenths of a degree are detectable in many applications. Thermal IR imaging technology is capable of detecting temperature differences below the surface of an object. For instance, the image of a person wearing a suicide-bombing vest would show a temperature difference between the clothing touching the person's skin and the clothing touching the suicide vest. IR imaging is advantageous to standoff explosive detection because it is a well-developed technology offering real-time images, which allows fast response in suicide bomber situations. However, a major drawback of this method is its lack of specificity in differentiating explosives from non-explosives and between types of explosive materials. Nevertheless, this technology will likely remain an important method to screen personnel where there is a likelihood of suicide bomber attack.

Microwave Imaging

Microwaves, usually in the 100 to 300 GHz range, are used to form images that can be used to identify potential explosive threats carried by humans. With standoff distances of around 1 m or more, the ability to interrogate below clothing, and simple, inexpensive scanning equipment, microwave bomb detection is an area with great promise for person-borne IED identification (NRC, 2004; Jöhl, 2009). At frequencies of 300 GHz microwave imaging is limited by water vapor absorption to 50 m standoff and at 50 GHz the standoff is limited to just a few meters. The low frequency electromagnetic (EM) waves used in microwave interrogation are safe for humans. Although the resolution, on the order of 1 cm, is less than that for terahertz

or X-ray systems it is adequate to identify concealed explosives while limiting privacy issues to the individual being scanned (Kuznetsov and Evsenin, 2006).

Millimeter Wave Imaging

Millimeter waves, of 30 to 300 GHz and 1-10 mm wavelengths, are used to produce high-resolution images. The wavelengths used in this technique are considerably longer than optical wavelengths and will pass through a number of materials, such as smoke, fog, and clothing that are opaque to ordinary light. This fact coupled with the fact that metals, plastics, ceramics and the human body reflects millimeter waves, make millimeter wave imaging a good choice when screening individuals for concealed explosives (McMakin, 1996). Both microwave and millimeter wave imaging techniques are best suited for scanning humans rather than compartments or large containers.

Nuclear Quadrupole Resonance (NQR)

NQR is related to nuclear magnetic resonance (NMR) and magnetic resonance imaging (MRI), but has the advantage of not needing a large static magnetic field to split the levels of quadrupolar nuclei. NQR is a solid-state radio frequency (RF) spectroscopic technique that is used to detect quadrupolar nuclei present in isotopes such as ^{14}N , an isotope present in many high explosive compositions (Gudmundson, 2009). The nucleus of a quadrupolar element is slightly aligned by the electrostatic interactions with its valence electrons. By applying an electric pulse at the correct frequency the spin, or electric quadrupole moment, of the nucleus can be flipped, creating a NQR signal that can be used to identify the explosive quadrupolar elements in a target. A major drawback to this method is the proximity of the NQR device to the interrogated volume, between 10 and 100 cm, making it a poor standoff detection technique (Garroway et al., 2001).

2.2.4 Gamma Rays

Gamma rays can be used to locate or image targets with ^{14}N using resonance gamma-ray scattering at 9.17 MeV. Locating ^{14}N is important because it is an isotope present in many explosive substances. Additionally, gamma rays can be used in transmission and backscatter configurations reminiscent of the methods used for X-rays. Unfortunately, health concerns coupled with difficulties with sources capable of producing a sufficient gamma-ray flux make

this technology a less attractive avenue for future development as a standoff detection method (NRC, 2004).

2.2.5 Neutrons

As was mentioned in Sections 2.2.3 and 2.2.4, nitrogen is an important element in identifying explosives, because most explosive compositions can be separated from non-explosive compositions based on their proportions of hydrogen (H), carbon (C), nitrogen (N), and oxygen (O). A more in-depth discussion of this feature of explosive materials will be given in Chapter 3. For now, it is sufficient to state that most explosives consist almost exclusively of H, C, N, and O, and are mostly well separated from common benign materials by way of elemental composition. Further, explosives may be distinguished by their relatively low proportions of C and H and relatively high proportions of N and O. Neutron based explosive detection techniques rely on the characteristic gamma rays, emitted by the nuclei of H, C, N, and O when they are bombarded with neutrons or on the altered energy of the interrogating neutrons. The physics of these interactions is addressed in Ch. 3. Neutron interrogation is preferred to other forms of radiation interrogation because neutrons have the ability to penetrate deep into a target. Hence, the materials making up an interrogated object are identified based on the interrogating neutron energy and the spatial distributions of neutrons and de-excitation gamma rays (Buffler, 2004). Table 2.1 summarizes several relevant features of four prominent neutron interrogation techniques outlined below.

Thermal Neutron Analysis (TNA)

TNA is accomplished by detecting the prompt capture and or the delay gamma rays emitted in the (n, γ) reaction of the nuclides of an interrogated object. Fast neutrons are moderated within an interrogated object to thermal energies ($<$ about 0.2 eV). The capture gamma rays of ^1H (2.22 MeV) and ^{14}N (10.83 MeV) are primarily used for explosive identification in the TNA method (Buffler, 2004). Thermal neutrons generally have larger absorption cross sections than do fast neutrons increasing the likelihood of inducing the desired (n, γ) reaction and making TNA an oft preferred explosive detection technique (Johll, 2009).

Table 2.1: Selected features of four common nuclear physics-based techniques for the non-intrusive interrogation of bulk samples. Adapted from Buffler (2004) and Johll (2009).

Technique	Radiation Source^a	Probing Radiation	Main reaction type	Detection radiation	Primary (secondary) signatures
TNA	²⁵² Cf; d-D or d-T STNG	Thermalized neutrons	(n, γ)	Prompt γ -rays from neutron capture	H, N, Cl (others)
FNA	d-D or d-T STNG	Fast neutrons	(n, n' γ)	γ -rays from inelastic neutron scattering	C, O, Cl (N, others)
PFNA	ns-pulsed accelerator	Fast neutrons	(n, n' γ)	γ -rays from inelastic neutron scattering	C, O, Cl (N, others)
PFTNA	ns-pulsed accelerator	White spectrum of fast neutrons	All available (n, γ), (n, n' γ), (n, p γ)	Source neutrons which are transmitted	H, C, N, O (others)

^a STNG: Sealed tube neutron generator

Fast Neutron Analysis (FNA)

FNA utilizes the inelastic scattering of fast neutrons in an interrogated volume by detecting the de-excitation gamma rays produced in the (n, n' γ) reaction. Usually, collimated beams of continuous fast neutrons, produced in a sealed tube neutron generator, are used to bombard a target volume. Explosive elements are identified by detecting the gamma rays of ¹²C (4.43 MeV), ¹⁴N (1.64, 2.31, and 5.11 MeV) and ¹⁶O (6.131 MeV). FNA imaging is another form of FNA, but is limited to small volumes because of the lack of geometrical definition when there are large distances between a detector and the inner volume elements or “voxels” of the interrogated volume (Buffler, 2004 and associated references). The relative ease with which fast neutrons can be produced in interrogation devices makes FNA a feasible, although expensive, explosive detection method.

Pulsed Fast Neutron Analysis (PFNA)

PFNA, like FNA, makes use of de-excitation gamma rays produced in the (n, n' γ) reaction. Nanosecond pulses of neutrons, around 8 MeV, are produced in the (d, n) or (p, n)

reaction using a beryllium or lithium target in an accelerator, such as a Van de Graaff. Typically a target is scanned with pulsed neutrons while the de-excitation gamma rays are detected in arrays of NaI(Tl) crystals. By measuring the time between the creation of a neutron in the target and the detection of the de-excitation gamma ray, the location of an interacting nuclide may be found. This spatial information can be used to create a three-dimensional elemental image of the target volume (Buffler, 2004 and associated references). PFNA methods reduce the imaging problems encountered in FNA and allows larger volumes to be investigated.

Pulsed Fast-Thermal Neutron Analysis (PFTNA)

PFTNA employs sealed tube neutron generators (STNG) to create several microsecond long pulses of 14.1 MeV neutrons, from the ${}^3\text{H}(d, n){}^4\text{He}$ reaction. During a neutron pulse, detection of de-excitation gamma rays is used to identify C and O as in the FNA method. Between neutron pulses (about 100 microseconds), fast neutrons remaining in the sample are thermalized leading to the production of prompt capture gamma rays which are detected and identify the presence of H, N, Cl and Fe, similar to the TNA method. Detection of both de-excitation and prompt capture gamma rays is accomplished by the same detector arrays by simply storing each spectrum separately. After a few hundred pulses the neutron beam is left off for a longer period of time, around three milliseconds, during which time elements (O, Si, F and P) de-activate by emission of delayed gamma rays. Through the combination of fast inelastic neutron scattering, thermal neutron capture and delayed activation analysis a great deal of elemental information can be gathered about an interrogated volume, which can be used to identify potential explosive threats (Buffler, 2004 and associated references).

Through recent developments, compact systems using PFTNA have been marketed as Pulsed Elemental Analysis with Neutrons (PELAN) devices. PELAN systems, utilizing microsecond-pulsed d-T STNGs and bismuth germanium oxide (BGO) detectors, are designed to detect and characterize explosives and military ordinance (Buffler, 2004, Vourvopoulos and Womble, 2001). TNA techniques, using the radioisotopic source ${}^{252}\text{Cf}$, have found applications in detecting chemical agents, high explosives, and characterizing unexploded ordinance (Buffler, 2004, Caffrey et al., 1992).

2.3 Sealed Tube Fast Neutron Generators

The creation of fast neutrons in sealed tubes is not a new technology. By 1959 sealed tube fast neutron generators were being developed and tested. Models achieving 10^7 neutrons/sec with energy of 2.5 MeV through the $H^2(d, n)He^3$ reaction were explored, however for energy-calibration purposes monoenergetic neutrons of 14 MeV generated through the $H^3(d, n)He^3$ reaction are desired (Gow, 1959). Sealed tube fast neutron generators capable of producing 14 MeV neutrons are now commercially available through several manufacturers. One such manufacturer is Adelphi Technologies Inc., a company contracted to build a neutron generator for the Kanas State University Standoff Bomb Detection project. The DT111 model is expected to achieve a production rate of 10^{11} neutrons/sec and is pictured in Figs. 2.3 (a) and (b).

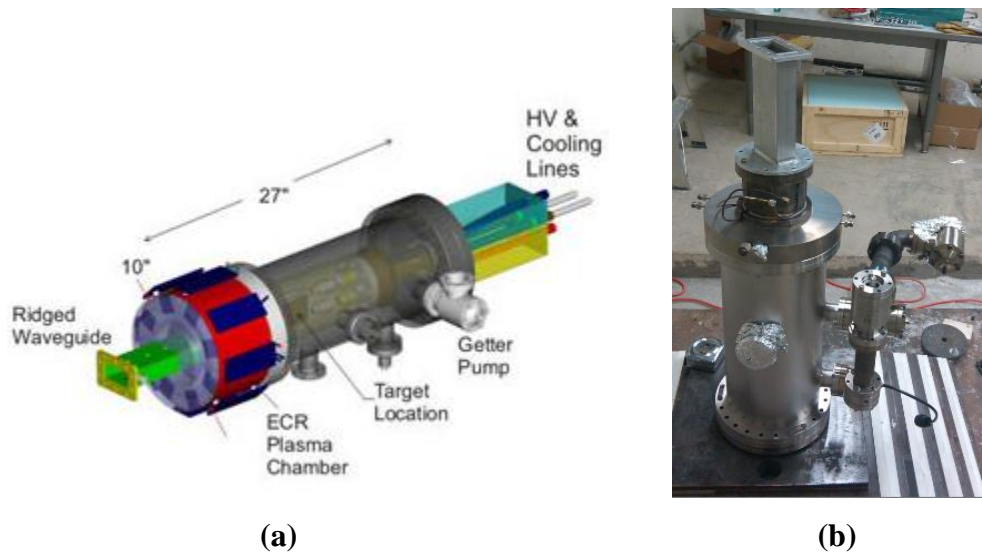


Figure 2-3: (a) Schematic of DT111 fast neutron generator (Adelphi, 2012). (b) Photo of DT111 in Standoff Bomb Laboratory.

Chapter 3 - Theory

3.1 Physics of Neutron Interactions

A description of neutron interactions in matter is helpful in grasping the role of neutron interrogation techniques for bulk explosive detection. As a neutral particle, a neutron interacts in ways quite different from charged particles. The neutral charge of the neutron allows it to pass, nearly unaffected, through the electrons orbiting the nucleus of an atom, whereas charged particles are likely to interact with atomic electrons. Therefore, most neutron interactions in matter are with the nuclei of atoms. Because atoms are mostly empty space, with the nucleus occupying only a small fraction of the volume of an atom, the distance between atomic nuclei is large and a neutron may penetrate deep into a material before it interacts with one of the widely spaced nuclei. It is intuitive that the kinetic energy of a neutron will govern its interactions in matter. There are three common categories associated with neutron energies: “fast” with energies greater than 0.1 MeV, “epithermal” with energies between 0.1 MeV and 0.2 eV and “thermal” with energies less than 0.2 eV.

3.1.1 Neutron –Matter Interactions

There are two broad neutron interaction categories, “scattering” and “absorption”. Each of these categories has several subcategories as seen in Fig. 3.1. A neutron-nucleus scattering event must conserve energy and thus the incident neutron will change its direction and velocity while the nucleus retains the same number of protons and neutrons it had prior to the collision. The velocity of the nucleus will change due to the collision and in some cases it will leave in an excited state, which may later de-excite in a radiative transition. If a nucleus absorbs a neutron in a capture event, a number of transitions are possible (Fig. 3.1) as well as a possibility of an induced fission (in some elements).

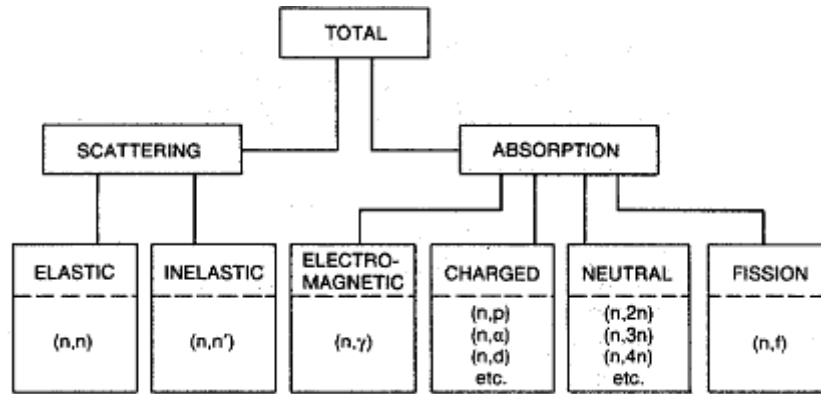


Figure 3-1: Various categories of neutron interactions. The letters separated by commas in the parentheses show the incoming and outgoing particles (Rinard, 1991).

Scattering

Scattering interactions can be divided into elastic and inelastic. In an elastic scattering event, with a fast or epithermal neutron, the nucleus gains kinetic energy as it leaves the location of the collision with a new direction and velocity. Similarly, the neutron loses an equal amount of kinetic energy in the collision as it leaves the collision location with a new direction and velocity. The average energy lost by a neutron in elastic scattering is given by (Shultis and Faw, 2000)

$$\frac{1}{2} \left[1 - \left(\frac{A-1}{A+1} \right)^2 \right] E, \quad (3.1.1)$$

where E is the energy of the incident neutron and A is the mass number of the target nucleus. Of note, from Eq. 3.1.1 one can easily see that as the mass number A of target nuclei is increased the average energy lost decreases. Thus, hydrogen with $A = 1$, is best for moderating or slowing down neutrons through elastic scattering (Rinard, 1991).

Inelastic scattering, while similar to elastic scattering, results in a nucleus in an excited state. The excited nucleus eventually de-excites by releasing radiation, such as an inelastic-scatter gamma ray, while the incident neutron leaves the collision location having had its velocity and direction changed. Inelastic scattering is only possible if the incident neutron has sufficient energy to excite the nucleus to one of its allowed excited energy levels. A case where inelastic scattering is impossible is in hydrogen where there are no excited states possible for the nucleus (Rinard, 1991) for neutron energies below a few hundred MeV.

Absorption

A nucleus may absorb a neutron, leaving the new nucleus in an excited state. The rearranged nucleus may de-excite by emission of delayed or prompt gamma rays, charged particles, more neutrons or fission fragments. Charged particles released from a capture event commonly include protons, deuterons, and alpha particles. The nucleus may rid itself of neutrons in order to return to a lower energy level, and in the case where two or more neutrons are ejected the number of neutrons is said to have been “multiplied” within the media. In the case of a fissioning event, two or more fission fragments, of intermediate atomic weight, and several neutrons are produced (Rinard, 1991).

Cross-Section

The idea of a cross section is used to quantify the probability of the occurrence of any of the above interaction events in appropriate units. To illustrate this concept, it is helpful to think of a number of mono-energetic neutrons incident on an atom-thick layer of material. As the neutrons move through the material some will scatter and some will be absorbed. The probability of a neutron not leaving the sample, i.e., being absorbed, is the ratio of neutrons absorbed to the number of neutrons incident on the material. Likewise, the probability of a neutron being scattered is the ratio of scattered neutrons to the number of incident neutrons. The microscopic cross section for an interaction is the probability of that interaction divided by the number of target atoms per unit area, thus the cross-sectional unit is centimeters squared (cm^2) and is denoted by the symbol σ . The unit of barns (b) is often used, where $1 \text{ b} = 10^{-24} \text{ cm}^2$. The microscopic cross section is largely dependent on the energy of the incident neutron and the type of nucleus involved in the interaction. However, in most applications involving bulk materials a different cross section is needed, one that may involve different elements in thicker samples than previously described.

For the transmission of a parallel beam of neutrons through a thick sample consisting of several atomic layers of material as described above, the neutron beam intensity, $I(x)$, of neutrons that have not interacted at a distance x inside the sample, is given by:

$$I(x) = I_0 e^{-N\sigma x}, \quad (3.1.2)$$

where I_0 is the incident neutron intensity, N is the atom density, and σ_t is the total microscopic cross section for scattering and absorption ($\sigma_t = \sigma_s + \sigma_a = \sigma_{elas} + \sigma_{inelas} + \sigma_f + \sigma_\gamma + \sigma_{n\alpha} \dots$) (Rinard, 1991; Duderstadt, 1976).

The total macroscopic cross section, or the probability, per unit path length, that a neutron traveling in a material will undergo a reaction, is given by:

$$\Sigma_t = N\sigma_t, \quad (3.1.3)$$

where Σ_t has units of cm^{-1} . Thus, the average distance a neutron travels in a material before an interaction is $\bar{x} = 1/\Sigma_t$ (Duderstadt, 1976). In the case of a material consisting of many elements forming a compound, the total cross section is given by:

$$\Sigma_t = \Sigma_1 + \Sigma_2 + \Sigma_3 + \dots = \frac{\rho N_a}{M} (n_1\sigma_1 + n_2\sigma_2 + n_3\sigma_3 + \dots), \quad (3.1.4)$$

where ρ is the density of the compound, M is the molecular weight of the compound, $N_a = 6.022 \times 10^{23}$ atoms mol^{-1} , and n_i , is the number of atoms of element i in one molecule (Rinard, 1991). One can easily see the importance of cross sections and cross-sectional data in calculating how neutrons will interact within a material, which is a key to detecting explosives with neutron interrogation.

3.2 The Composition of Explosives

During a chemical explosion, a rapid oxidation-reduction process produces hot gasses that quickly expand creating a shockwave. Chemical explosives are typically categorized by their “burn rate”, the rate at which their shock wave travels when detonated. Compositions with burn rates that are supersonic are called high explosives (HE), while those with subsonic rates are known as low explosives (LE). HE are generally preferred by terrorists and terror organizations because of their high explosive yield. HE tend to be rich in the oxidizers oxygen and nitrogen and the reducers hydrogen and carbon, required for the explosive chemical process. Explosives with high-nitrogen content are termed “nitrogen-rich” explosives.

A study of the elemental composition of 26 common nitrogen-rich HE compounds conducted by the National Research Council found similar proportions of hydrogen, carbon, nitrogen and oxygen (H, C, N, O). These compounds had average compositions (by weight) of about 3% H, 20% C, 31% N, and 46% O with standard deviations of 11% or less (NRC, 2004).

The density of many explosives are nearly 50% higher than the density of non-explosive HCNO compounds (Dunn, 2007a). A natural extension of these observations is that a detection method exploiting these common characteristics offers a potentially robust technique for explosive detection of nitrogen-rich explosives.

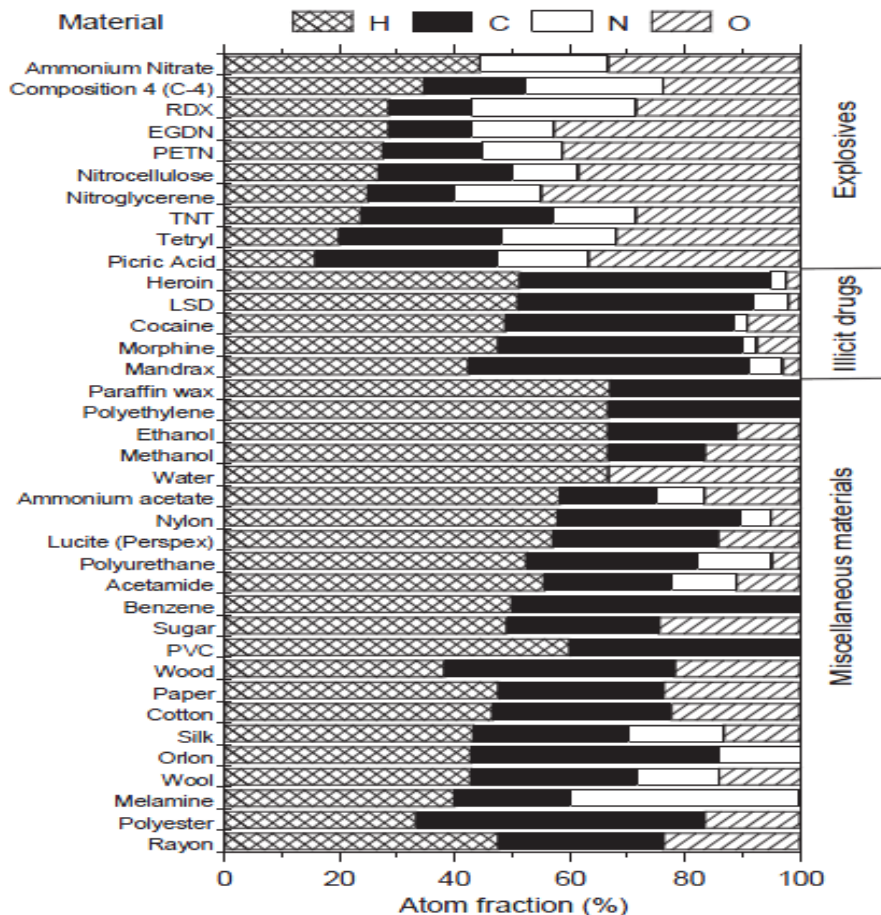


Figure 3-2: Atomic percentages of the elements H, C, N and O, which constitute a selection of explosives, illicit drugs, and miscellaneous common materials (Buffler, 2004).

Another compelling study demonstrates that explosive compositions are differentiated from non-explosive compounds by way of atom fraction composition of HCNO. Buffler's 2004 findings for 10 explosives, 5 illicit drugs, and 22 common HCNO compounds (see Fig. 3.2) showed that nitrogen-rich explosives had atom fractions of N and O that were higher than those in either illicit drugs or in 22 inert materials. Again, these results point to a detection method utilizing the presence of nitrogen and oxygen in explosive compounds.

The remainder of this thesis focuses on developing a method for differentiating only nitrogen-rich explosives using neutron interrogation techniques. Though there are many explosive materials available for investigation, the focus of the study outlined in this work will be to differentiate nitrogen-rich explosives from inert materials, those materials not identified as nitrogen-rich explosives. The remainder of this chapter is dedicated to outlining a theoretical procedure aimed at exploiting the elemental composition of nitrogen-rich explosives.

3.3 Template Matching

As discussed in Section 3.1.1, there are many neutron-matter interactions resulting in scattered neutrons, neutron multiplication, or the emission of gamma rays, charged particles, or fission fragments. The unique energies of inelastic-scatter and prompt-capture gamma-rays produced in interactions with H, C, N, and O allow one to form “signatures”. This is possible because as neutrons are thermalized in a material, particularly due to elastic collisions with hydrogen nuclei, the slowed neutrons are captured by the nuclei of hydrogen and nitrogen resulting in the production of prompt-capture gamma rays. Fast neutrons may also be scattered inelastically producing inelastic scatter gamma rays from collisions with carbon, nitrogen and oxygen nuclei (Dunn et al., 2007b). Similarly, signatures of backscattered neutrons below and above the “cadmium cutoff energy” (0.4 eV) may be used to help identify explosives.

Through neutron interrogation, the H, C, N, and O concentrations of a target can, in principle, be discovered. However, rather than measure the concentrations directly to determine if a sample is an explosive, signatures of an unknown sample are compared to known explosive signatures contained in a “template”. The process of comparing an unknown target “response”, or group of signatures, to known explosive templates is called “template matching”. The two candidate neutron energy signatures and the nine inelastic-scatter and prompt capture gamma-ray signatures used in this study are outlined in Table 3.1. Also shown are the average thermal cross section for the ${}^1_0\text{H}(n,\gamma){}^2_1\text{H}$ reaction and the inelastic scattering cross sections at 14.1 MeV for the C, N, O elements. Of course, the actual yield of each gamma ray will depend on the neutron spectrum in the target being interrogated. Comparing a response from an unknown sample to a known explosive template offers rapid identification of nitrogen-rich explosive compounds contained in a target sample.

Table 3.1 Nine (9) HCNO prompt-capture and inelastic-scatter signature energies (Group T-16, 98-2007; Molnár, 2004 & Johll, 2009) and two (2) neutron signature energies.

Gamma-Ray		Signatures		
Element	Energy (MeV)	Type of Reaction	Thermal σ (barns)	14.1-MeV σ (barns)
Hydrogen	2.2232	Prompt-capture	0.3326	-
Carbon	4.4390	Inelastic-scatter	-	0.2106
Nitrogen	2.3128	Inelastic-scatter	-	0.0557
	3.3786	Inelastic-scatter	-	0.0109
	4.9151	Inelastic-scatter	-	0.00687
	5.1059	Inelastic-scatter	-	0.0437
	6.4462	Inelastic-scatter	-	0.0122
Oxygen	6.1299	Inelastic-scatter	-	0.144
	6.9171	Inelastic-scatter	-	0.0317
Neutron		Signatures		
Below Cd cutoff	< 0.4×10^{-6}			
Above Cd cutoff	> 0.4×10^{-6}			

It is possible to create a large array of templates, utilizing a variety of target configurations and compositions, from the 11 signatures listed in Table 3.1. The characteristic responses of explosive HCNO compounds are utilized to make a library of templates, which lends itself for use in the signature-based radiation scanning (SBRS) technique. Based on a

template library representing various explosive types in a multitude of geometric and clutter configurations, the SBRS approach provides a means of quickly and efficiently identifying explosive compounds. The proposed SBRS technique interrogates an unknown target with neutrons, collecting backscattered responses for comparison to known explosive templates. The unknown response, when compared to a specific template, is scored with a figure-of-merit (FOM) and a variance, which can be used to determine if the interrogated sample contains an explosive. The automated SBRS approach requires little of the user while promising a robust method of inert-explosive differentiation through template matching. Testing and proving the SBRS method is important to IED detection because of its considerable improvements on existing neutron interrogation techniques. Application of the SBRS technique will allow IED identification in many real world scenarios including buried mines, shielded bulk cargo containers and personnel baggage.

3.4 Template Generation for SBRS Application

Confident that a finite number of L templates can accurately represent any proposed target type, one may proceed through the following SBRS technique. Suppose a template \mathbf{S}_ℓ is a vector of N signatures for a target that contains a sample of a known explosive. The subscript ℓ indicates a particular target configuration (position of sample in the target, clutter configuration and thickness, etc.) out of a total of L configurations, such that,

$$\mathbf{S}_\ell = (S_{\ell 1} \ S_{\ell 2} \ \dots \ S_{\ell N}), \ \ell = 1, 2, \dots, L. \quad (3.4.1)$$

After generating an appropriate number of templates to represent a specific target type, an unknown target, of the same type, is interrogated with neutrons, generating a response vector, \mathbf{R} . \mathbf{R} is a vector of the same N signatures as for the test target, and is represented as:

$$\mathbf{R} = (R_1 \ R_2 \ \dots \ R_N). \quad (3.4.2)$$

The response vector is compared to the library of L templates using a figure-of-merit procedure that is described in the Section 3.5. A computer code then calculates a FOM for unknown targets from the vectors \mathbf{S}_ℓ and \mathbf{R} , in a manner also explored in Section 3.5. Below are sample templates with N signatures, N standard deviations (σ) with $\ell = 2$.

Signature Energy I

$$S_{11} \quad S_{21}$$

$$\sigma_{11} \quad \sigma_{21}$$

$$\cdot \quad \cdot$$
$$\cdot \quad \cdot$$
$$\cdot \quad \cdot$$

Signature Energy N

$$S_{1N} \quad S_{2N}$$

$$\sigma_{1N} \quad \sigma_{2N}$$

The complex characteristics of possible explosive targets and the specificity required for explosive identification requires that a large library of templates be generated. Large volumes of thinly shielded explosives would require far fewer templates than would small explosive volumes with thick shields. Thus, many factors including beam intensity, interrogation time, the volume of explosive, thickness and density of both the target and shield, as well as interrogation standoff must be considered.

Though there are an infinite number of explosive configurations possible in real world scenarios, one can imagine that many of these scenarios can be modeled by a single template. Thus, a finite number of templates may be sufficient to differentiate nearly all explosive from inert materials. This argument hinges on the ability of a single template to fit many closely related explosive target configurations. Because an explosive target does not have to match perfectly to a template to be identified as an explosive, a template may represent a whole group of related target types. Thus, there is no need for a template library containing every possible scenario; rather a much smaller library may quickly identify nearly all explosive targets. In fact, it will be demonstrated that templates of artificial compositions, obscuring known explosives, adequately identify many real IED scenarios. Templates with artificial compositions are known as “artificial templates”, and are created with different proportions of H, C, N, O, as well as other real materials such as copper or chromium, at specific densities. Eighty such templates were created for this study and are given in Appendix A.

It will be shown that it is possible to minimize the number of FOM calculations required to identify an explosive based on a density filtering process. As mentioned in Section 2.2.2, X-ray interrogation provides information about the density of a sample, and work conducted by a “Senior Design Team” at Kansas State University showed promise for density discrimination

using backscattered X rays (Horton et al., 2011). X-ray imaging, producing what is essentially a density map, is ubiquitous and the Z-backscatter van (Chalmers, 2004) is a mobile imaging system that interrogates targets by forming a backscatter density image. Thus, if one knows the average density of a sample one may determine the appropriate templates to use in calculating a FOM. For example, a target with a very low density need not be compared to a template of medium or high density, thus reducing the number of required calculations. A detailed explanation of this process and its effectiveness are discussed later in this thesis.

3.5 Explosive Discrimination Using Figure-of-Merit Analysis

A SBRS method utilizing template matching, as described above, calculates the FOM,

ζ ,

$$\zeta_{\ell} = \sum_{i=1}^N \alpha_i \frac{(\beta R_i - S_{\ell i})^2}{\beta^2 \sigma^2 (R_i) + \sigma^2 (S_{\ell i})}, \quad (3.5.1)$$

where R_i is the i^{th} measured signature of an unknown sample, $S_{\ell i}$ is the i^{th} signature for the ℓ^{th} template, N is the number of signatures, β is a factor that scales the measured signature values to the template values (accounting, for instance, for differences in measuring times or beam intensities), σ^2 is the variance, and α_i is a normalized weight factor given by

$$\alpha_i = \frac{w_i}{\sum_{i=1}^N w_i}, \quad (3.5.2)$$

with w_i being a finite positive constant for the i^{th} signature. Note that $\alpha_i = 1/N$ for uniform weights ($w_i = 1, i = 1, 2, \dots, N$). The value of ζ_{ℓ} would be expected to be near unity if the R_i and $S_{\ell i}$ were drawn from the same distribution (or if the signatures obtained from a test sample differ only by statistical variations from those of one of the templates) but to be large if R_i and $S_{\ell i}$ differ substantially. The standard deviation in the figure-of-merit, which follows from the standard error propagation formula assuming uncertainties only in R_i and $S_{\ell i}$, can be estimated as

$$\sigma(\zeta_{\ell}) = 2 \left[\sum_{i=1}^N \alpha_i^2 \frac{(\beta R_i - S_{\ell i})^2}{\beta^2 \sigma^2 (R_i) + \sigma^2 (S_{\ell i})} \right]^{1/2}. \quad (3.5.5)$$

This estimate of standard deviation is a good approximation when R_i and S_{li} are larger than, say, 50 counts. In principle, effective use of ζ_ℓ and $\sigma(\zeta_\ell)$ allows one to differentiate inert from dangerous targets (Brewer, et al., 2011).

Use of normalized FOM values simplifies the task of finding appropriate cutoff values because the raw FOM values can assume values between zero and numbers exceeding 10^6 . Thus a normalized FOM is given by,

$$\zeta_\ell(\text{normalized}) = \frac{100}{\sum_{i=1}^N \alpha_i \frac{(S_{li})^2}{\sigma^2(S_{li})}} \sum_{i=1}^N \alpha_i \frac{(\beta R_i - S_{li})^2}{\beta^2 \sigma^2(R_i) + \sigma^2(S_{li})}. \quad (3.5.6)$$

The numerator of the normalization constant is an arbitrary scaling factor and the denominator is the figure-of-merit from Eq. (3.5.1) that would be obtained if all the R_i and $\sigma(R_i)$ were zero, i.e., there are no signature values for the unknown target. The normalized error is given by,

$$\sigma(\zeta_\ell(\text{normalized})) = \frac{100}{\sum_{i=1}^N \alpha_i \frac{(S_{li})^2}{\sigma^2(S_{li})}} 2 \left[\sum_{i=1}^N \alpha_i^2 \frac{(\beta R_i - S_{li})^2}{\beta^2 \sigma^2(R_i) + \sigma^2(S_{li})} \right]^{1/2}. \quad (3.5.7)$$

A cutoff value, ζ_0 , is used to determine if a sample is an explosive (its FOM is below ζ_0) or inert (its FOM is above ζ_0). There is also a third category deemed “suspects” for which a specified number of standard deviations of the FOM may include the cutoff value. These three cases are depicted below.

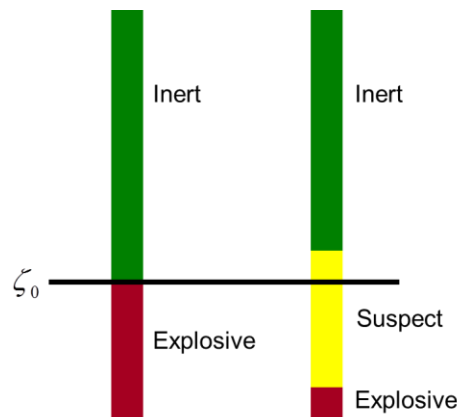


Figure 3-3: Graphical Depiction of Cutoff, ζ_0 , Being Used to Identify Inert, Suspect, and Explosive Materials.

A measure of the confidence one may report when identifying a substance as inert is given by the following,

$$\lambda_+ = \frac{\zeta_\ell(\text{normalized}) - \zeta_0}{\sigma(\zeta_\ell(\text{normalized}))}. \quad (3.5.8)$$

Similarly, the confidence, or margin-of-error, given to a sample identified as an explosive follows,

$$\lambda_- = \frac{\zeta_0 - \zeta_\ell(\text{normalized})}{\sigma(\zeta_\ell(\text{normalized}))}. \quad (3.5.9)$$

The value of λ_{\pm} gives an account of how closely the normalized FOM is to a pre-established cutoff value. While developing a systematic SBRS methodology one may also use λ_{\pm} to establish reasonable cutoff values. However, there are situations when a sample ζ is very close to ζ_0 , and the specified number of standard deviations λ_{\pm} allows the sample to be classified as either an inert or an explosive. In these cases the sample should be labeled as a suspect, and it is left to the user of the SBRS system to determine what course of action is to be taken with these samples.

An explosive correctly identified as an explosive is labeled a “true positive” (TP) and an inert correctly identified as an inert is labeled a “true negative” (TN). If an inert material is identified as an explosive it is labeled as a “false positive” (FP) and an explosive identified as an inert is labeled a “false negative” (FN). The “specificity” is related to the false positive rate through

$$\text{Sensitivity} = \frac{\text{Number of True Positives}}{\text{Number of True Positives} + \text{Number of False Negatives}}. \quad (3.5.10)$$

and the sensitivity is related to the false negative rate through

$$\text{Specificity} = \frac{\text{Number of True Negatives}}{\text{Number of True Negatives} + \text{Number of False Positives}}. \quad (3.5.11)$$

In Eq. (3.5.10), a sensitivity of 100% indicates no FN, and in Eq. (3.5.11), a specificity of 100% indicates no FP. In explosive detection both high specificity and high sensitivity are sought (Johll, 2009). The sensitivity and specificity may be adjusted by changing the cutoff value, ζ_0 . High levels of sensitivity are preferred over high levels of specificity because in real-world scenarios, not detecting explosives (large numbers of FN) endangers personnel and equipment,

while incorrectly identifying non-explosives as explosives does not. However, a high FP rate will limit the usefulness of any detection method, thus, a balance between sensitivity and specificity is required.

3.6 Simulations Using MCNP Transport Code

The Monte Carlo Neutral Particle (MCNP), code is used for problems requiring transport calculations for neutrons, photons, electrons, or combinations of neutrons/photons (where photons are produced by neutron interactions), neutrons/photons/electrons, photons/electrons, and electrons/photons (X-5 Monte Carlo Team, 2008). Developed and maintained by the Los Alamos National Laboratory, MCNP is an internationally recognized code for neutral particle transport. MCNP is capable of transporting neutrons of energies between 10^{-11} and 20 MeV for all isotopes and up to 150 MeV for some isotopes, photons of energies from 1 keV to 100 GeV, and electrons of energies from 1 keV to 1 GeV (X-5 Monte Carlo Team, 2008). To use the MCNP code the user creates an “input file” which specifies pertinent information about the specific problem being modeled. A simulated experiment is carried out by running the MCNP code with an input file modeling the important aspects of the experiment. An input file is a collection of “cards” including a title card, cell cards, surface and data cards, source cards, material cards and tally cards. A sample input code for MCNP is provided in Appendix B.

In MCNP the user may define three-dimensional configurations of materials in geometric cells bounded by surfaces or “macro bodies” (basic shapes such as spheres or boxes, etc.) already present in the MCNP code. The intersections, unions and complements of regions bounded by surfaces define cells. Surfaces are further defined by supplying coefficients (selecting a “+” for the outside of a surface and “-” for the inside of a surface) to the analytical surface equations or, for certain types of surfaces, known points on the surfaces. MCNP has more general geometry than is available in most other codes and provides the capability and flexibility of defining geometrical regions from user defined surfaces and then combining them with Boolean logic operators (X-5 Monte Carlo Team, 2008). Because the MCNP code is such a powerful modeling tool, allowing for a multitude of geometric and material configurations, it was used extensively to study the feasibility of the proposed SBRS method.

Once the geometry of a specific problem has been modeled the user must specify the materials contained in the cells. This is done by specifying a materials card, containing

elemental information, in the form of a Z Aid number, about the material. The Z Aid number of a cell is of the form ZZZAAA.nnX, where, Z and A are the atomic number and mass number, respectively, nn is a unique evaluation identifier corresponding to version of a cross-sectional data library, and X indicates the class of data to be used (X-5 Monte Carlo Team, 2008). By way of example the Z Aid number 1001.74c refers to hydrogen with Z=1 and A=1. Note that the first two zeros of the atomic number 001 are simply place holders and may be omitted, thus, the Z Aid number above is really of the form ZAAA.nnX. In addition, 74c tells the program to use the ENDF/B-VI cross section file designated endef74, with a continuous energy table. The ENDF/B-VI cross sections files are regularly updated using the most current experimental data.

The user, in source definition (SDEF) and tally cards, specifies sources and tallies to be used in a specific input file. Only one SDEF card is allowed per input file; however, each SDEF card may specify a wide variety of source conditions. Independent probability distributions may be specified for the source variables of energy, time, position, and direction, and for other parameters such as starting cell(s) or surface(s). In addition to input probability distributions, various analytic functions for fission and fusion energy spectra exist such as Watt, Maxwellian, and Gaussian spectra. In addition isotropic, cosine, and monodirectional probability distribution functions (PDF) are included in MCNP (X-5 Monte Carlo Team, 2008). The source used in the simulations for this study was a monodirectional beam of 14.1 MeV monoenergetic neutrons. Tallies are estimators used to calculate and score radiation events, a tally scores events similar to an actual detector with perfect efficiency, unless modified to represent a real detector (Johll, 2009). The F5, point detector tally, was used in simulations to score and sort, by energy, the particle flux at a point distant from a target whose bulk was interrogated with a neutron beam described above. The individual scores in an F5 tally are given by the following,

$$\frac{W \cdot p(\hat{\Omega}_p) e^{-\lambda}}{R^2} \quad (\text{particles cm}^{-2}), \quad (3.6.1)$$

where, W is the weight assigned to a particle history, $p(\hat{\Omega}_p)$ is the probability density function for scattering (or starting) in the direction $\hat{\Omega}_p$ towards the point detector (assuming azimuthal symmetry), $e^{-\lambda}$ is a term accounting for attenuation between the location of the last event and the detector point (λ is the total number of mean free paths from a particles location to the detector), and R is the distance to the detector from a source or collision event. The point detector is called

a “next-event estimator” because it is a tally of the flux at a point as if the “next event” were a particle trajectory directly to the detector without further collision (X-5 Monte Carlo Team, 2008). The physical quantity measured by the F5 tally, when the source has units of particles, is the particle fluence,

$$\Phi \equiv \frac{dN_p}{dA} \quad (\text{particles cm}^{-2}), \quad (3.6.2)$$

where, dN_p is the number of particles which penetrate into a sphere of cross-sectional area dA (Shultis and Faw 2000).

To account for the interactions of neutrons while traversing through a medium, extensive transport calculations are often required. In particular, a form of the Boltzmann transport equation, termed the Neutron Transport Equation (NTE), is employed to provide numerical solutions for the neutron flux or fluence density of neutrons in a media. Solutions to the NTE provide information about how the number of neutrons, with a specific energy and traveling in a specific direction, are affected by the media through which they are propagating. The steady state NTE can be written as,

$$\begin{aligned} \mathbf{\Omega} \cdot \nabla \varphi(\mathbf{r}, E, \mathbf{\Omega}) + \Sigma_t(\mathbf{r}, E) \varphi(\mathbf{r}, E, \mathbf{\Omega}) = \\ \frac{1}{2\pi} \int_0^{2\pi} \int_{-1}^1 \int_0^\infty \Sigma_s(\mathbf{r}, E') f_E(E' - E) f_\omega(\omega_s) \varphi(\mathbf{r}, E', \mathbf{\Omega}') dE' d\omega_s d\psi' + s(\mathbf{r}, E, \mathbf{\Omega}). \end{aligned} \quad (3.6.2)$$

In the steady state NTE, $\varphi(\mathbf{r}, E, \mathbf{\Omega})$ is the flux density (as a function of position, \mathbf{r} , energy, E , and direction, $\mathbf{\Omega}$); Σ_t is the total interaction cross section; Σ_s is the total scattering cross section; f_ω is the probability density function for the scattering angle cosine, $\omega_s = \cos \theta_s$, f_E is the energy probability density function and s is a source term.

Deterministic transport methods, such as discrete ordinates, solve Eq. (3.6.2) to find the average particle behavior, giving fairly complete information about the average flux density of particles throughout the phase space of the problem. MCNP, on the other hand, simulates individual particles and gives solutions based on aspects (tallies) of their average behavior. MCNP solutions yield only information about user specified tallies, however from the average behavior of many simulated particles the average behavior of real particles in a system is inferred through the central limit theorem (X-5 Monte Carlo Team, 2008). The central limit theorem gives clout to the Monte Carlo method by giving an estimate of uncertainty in the estimate of the

expected value; this uncertainty is proportional to $1/\sqrt{N}$ where N is the number of histories selected from an appropriate probability distribution function. Another pillar of Monte Carlo strength is the law of large numbers, which states that as long as the mean exists and the variance is bounded the following is true,

$$\lim_{N \rightarrow \infty} \bar{z} = \langle z \rangle. \quad (3.6.3)$$

Here, as the number of histories N goes to infinity the estimate of the expected value \bar{z} approaches the actual expected value $\langle z \rangle$ (Dunn and Shultis, 2011). Thus, both Monte Carlo and deterministic transport methods are capable of “solving” the NTE.

Monte Carlo methods are particularly useful when duplicating statistical processes (such as the interaction of particles with materials) and can model complex three-dimensional geometries that cannot be modeled by deterministic computer codes. The individual events that describe a transport process are governed by several probability distributions. Monte Carlo methods statistically sample these probability distributions to describe the total phenomenon. The number of trials comprising a Monte Carlo simulation is quite large and generally requires the use of digital computers (it should be noted that although many trials are needed to accurately approximate a solution, a large number of trials is not indicative of a precise result). Random numbers are generated through a random number generator and are used to statistically sample processes in a given problem. The statistical sampling process resembles dice throwing games in a casino, from which the name “Monte Carlo” is derived. The Monte Carlo method of particle transport is supremely realistic and constitutes a numerical experiment, tracing a particles history from source to termination. Probability distributions are randomly sampled using transport data to determine the outcome at each step of its life (X-5 Monte Carlo Team, 2008).

Because the X-5 Monte Carlo Team at the Los Alamos National Laboratory validates the MCNP5 code in several “benchmark” tests, it is presumed capable of precisely and accurately describing particle behavior in a medium. The accuracy of an MCNP5 experiment depends on the nuclear physics and cross section data supporting the code, and the ability of the user to accurately model the pertinent aspects of the problem. Given the precision and accuracy the code provides, it is theoretically possible to test the feasibility of an explosive detection technique utilizing simulated neutron interrogation.

3.7 Techniques Employed to Generate and Analyze MCNP Data

One hundred forty three MCNP5 experiments were performed requiring over 170 computer hours. Each of the 143 experiments generated over 1,600 lines of output. Experiments of comparable complexity and number of histories often utilize a cluster of computers to increase the speed of simulations. However, all experiments in this study were conducted on a personal laptop, demonstrating the incredible power and flexibility of the MCNP5 code. The extensive uses of auxiliary computer programs were necessary because of the bulk and format of MCNP5 output data. Much of the post-processing of data output was handled by programs written in the “Pearl” language. The regular expressions and other features of the Pearl language allow the user to create a program to search through a large output text file for a specific line of text and extract data to be stored in an array in the script. C++ programs were used to calculate needed values from the data contained in the Pearl arrays. Finally, MATLAB programs were used to calculate figures-of-merit, as described above, from the output of the C++ programs.

MCNP simulations save both time and resources by simulating experiments at a much faster rate and in more configurations than would be possible experimentally. Thus, for methods requiring more resources or time than are available, an MCNP simulation is a good alternative for acquiring results. However, no matter how well the problem is modeled in MCNP or how promising the results, the method should be verified through experimental means.

Chapter 4 - MCNP Simulation Model and Results

4.1 Target Model Specifications

Many IEDs are housed in metal containers and in the trunks of automobiles. Detecting such IEDs is the objective of the SBRS detection method. To this end, a mockup was developed with materials and geometry representing an average car trunk. The geometry used in all simulations is shown in Fig. 4.1.

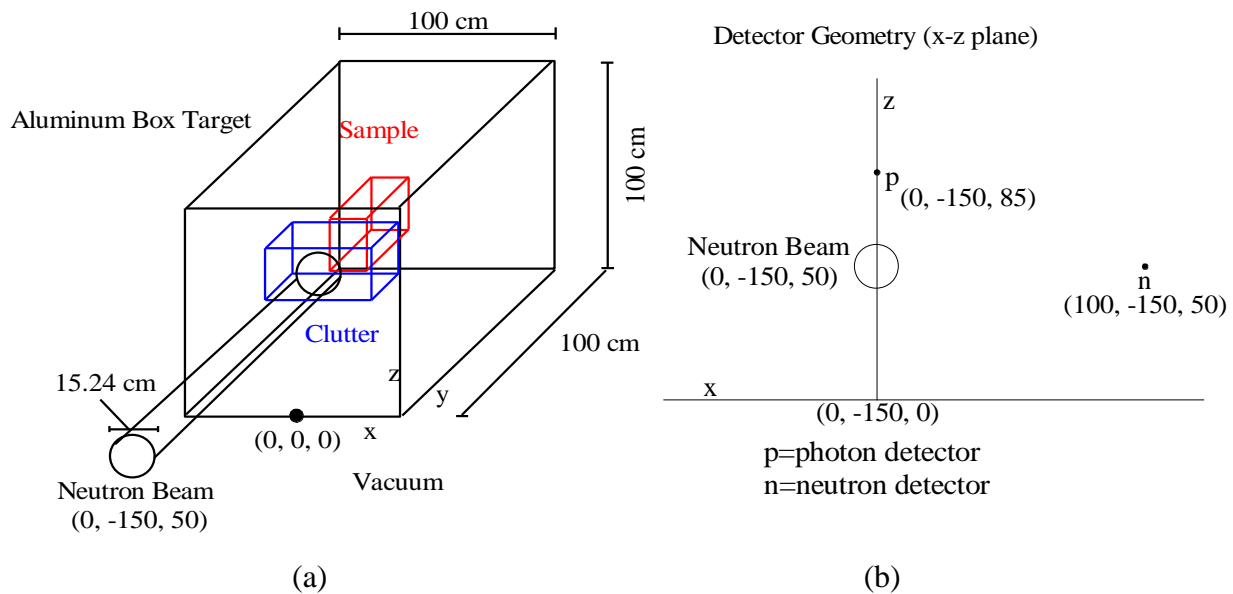


Figure 4-1: Schematic of simulated target geometry, (a) 3-D mockup of car trunk, (b) detector configuration.

It is crucial to define a common nomenclature to be used when describing aspects of the MCNP model.

Target – A 1 m³ aluminum box containing both the sample and clutter.

Clutter – A rectangular volume composed of an inert material that “shields” the sample within the target.

Sample – A rectangular volume (about 3.35 L) composed of either an explosive or an inert material contained in the target.

Source – A uniform, parallel, cylindrical neutron beam, 7.62 cm in radius, emitting 14.1 MeV neutrons.

Detector – A point detector, F5 tally in MCNP, to measure the particle fluence.

Inert – Any material that is not identified as a nitrogen-rich explosive occupying the clutter or clutter and sample positions.

Explosive – Nitrogen-rich explosive compound occupying the sample position.

Twenty-one materials commonly encountered in real detection scenarios were simulated as both clutter and sample materials; their densities and compositions are recorded in Appendix C. Explosive compounds of cyclonite (RDX) and Urea Nitrate (UNi) were also simulated as samples obscured by the other 21 materials, the densities and compositions of these explosives are also listed in Appendix C. Thus, 42 targets were created, 21 with an inert in both the clutter and sample positions (both the same inert material) and 21 with an inert in the clutter position and an explosive in the sample position. Additionally, 10 artificial materials were created and are listed in Table 4.1 below. All materials and explosives were modeled as being both uniform and homogeneous.

Table 4.1 Artificial Inert Clutter Materials

N0O50C0H0Crhd	N0O50C0H0Crmd	N0O50C0H0Crlld	N0O50C0H0Crvld
N0O60C20H0Crhd	N0O60C20H0Crmd	N0O60C20H0Crlld	N0O60C20H0Crvld
N0O0C50H50hd	N0O0C50H50md	N0O0C50H50ld	N0O0C50H50vld
N0O10C30H60hd	N0O10C30H60md	N0O10C30H60ld	N0O10C30H60vld
N0O20C30H50hd	N0O20C30H50md	N0O20C30H50ld	N0O20C30H50vld
N10O10C50H30hd	N10O10C50H30md	N10O10C50H30ld	N10O10C50H30vld
N20O0C30H50hd	N20O0C30H50md	N20O0C30H50ld	N20O0C30H50vld
N0O50C0H0Cuhd	N0O50C0H0Cumd	N0O50C0H0Culd	N0O50C0H0Cuvld
N0O60C20H0Cuhd	N0O60C20H0Cumd	N0O60C20H0Culd	N0O60C20H0Cuvld
N0O30C0H70hd	N0O30C0H70md	N0O30C0H70ld	N0O30C0H70vld

The artificial material nomenclature, N0O50C0H0Cr, represents a material consisting of 0% nitrogen (N0), 50% oxygen (O50), 0% carbon (C0), 0% hydrogen, and 50% chromium (Cr). The number following element designation (N#O#C#H#) denotes the weight percent of each element contained in the material. The chromium in the above example material, known as a

“filler” element, makes up the remaining weigh percent of the material composition. There are four materials listed above containing filler elements (50% and 20% chromium, and 50% and 20% copper respectively). Each column of Table 4.1 represents a specific density, as defined by the last few letters in the nomenclature of each material. “hd” stands for high density and represents a density of 7 g cm^{-3} , “md” denotes artificial materials of medium density (2.25 g cm^{-3}), “ld” indicates a low density of just 1 g cm^{-3} and finally “vld” connotes very low density (0.25 g cm^{-3}) clutter. The 40 materials listed above were placed in the clutter position shielding explosive samples of cyclonite and urea nitrate. Thus, a total of 80 artificial explosive templates were created, in MCNP5, by recording the backscattered radiation responses of targets with 40 artificial materials shielding a sample of RDX and the same 40 materials shielding UNi when interrogated with 14.1 MeV neutrons.

4.1.1 Mockup Geometry

The target, with six walls of 0.2 cm thick aluminum, housed clutter and sample volumes of 19.6 L and 3.35 L, respectively. Both the sample and clutter were modeled as rectangular parallelepipeds. The remaining 77 L inside the target were modeled as a void, that is, particles would not interact unless they were inside the aluminum shell of the target or inside the sample or clutter volumes. A sphere of 5 m radius surrounded the target. The volume inside the sphere, but outside of the target volume, was also modeled as a void so that the entire simulation was conducted in a vacuum.

One face of the sample, nearest the source, resided on the xy -plane, and was centered on the origin (refer to Fig. 4.1 (a)). The center of the target was positioned 50 cm from the origin in the z -direction. The sample was located inside the target so that it was centered at the coordinate (0, 41.5, 50). The parallelepiped of clutter had dimensions of 96 cm in total length (x -direction), 10 cm in width (y -direction) and 20 cm in height (z -direction). The clutter volume was further divided into three sections in the MCNP code; the left and right sections were equal in volume with dimensions ($x=32.38 \text{ cm}$, $y=20 \text{ cm}$, $z=10 \text{ cm}$) and the middle section had dimensions ($x=15.24 \text{ cm}$, $y=20 \text{ cm}$, $z=10 \text{ cm}$). The clutter volume was located inside the target between the source and the rectangular sample, as shown in Fig. 4.1 (a), and centered on the coordinate (0, 30, 50). The source, centered at (0, -150, 50), had a standoff of 1.5 m from the nearest face of the target. It was aimed directly on the centers of the target, clutter, and sample at $z=50 \text{ cm}$ traveling

parallel to the y-axis in the positive y-direction. A gamma-ray point detector (refer to Fig. 4.1(b)) was positioned 150 cm away from the closest point of the target at the coordinates (0, -150, 85). The F5 tally for gamma rays utilized 4-keV wide energy bins, selected so that signature gamma-ray energies would be at the center of a bin. The width of the energy bins was chosen to be similar to the energy resolution of some HPGGe detectors (Johll, 2009). A neutron point detector was located 158 cm from the nearest target surface at (100, -150, 50). Neutrons with energies above and below the cadmium cutoff (0.4 eV) were binned separately in the neutron F5 tally. Several pictures of the target geometry were taken using the MCNP5 Visual Editor program and are displayed below. Figure 4.2 (a) is a view from outside the aluminum box. Figures 4.2(a) & (b) show the inside of the target where both the clutter and sample are visible. It should be noted that there are several cells shown in Fig. 4.1(b) that had no clutter material in their volume. The cells shown in the figure were created in the MCNP code to allow more configurations of clutter than were used in this experiment.

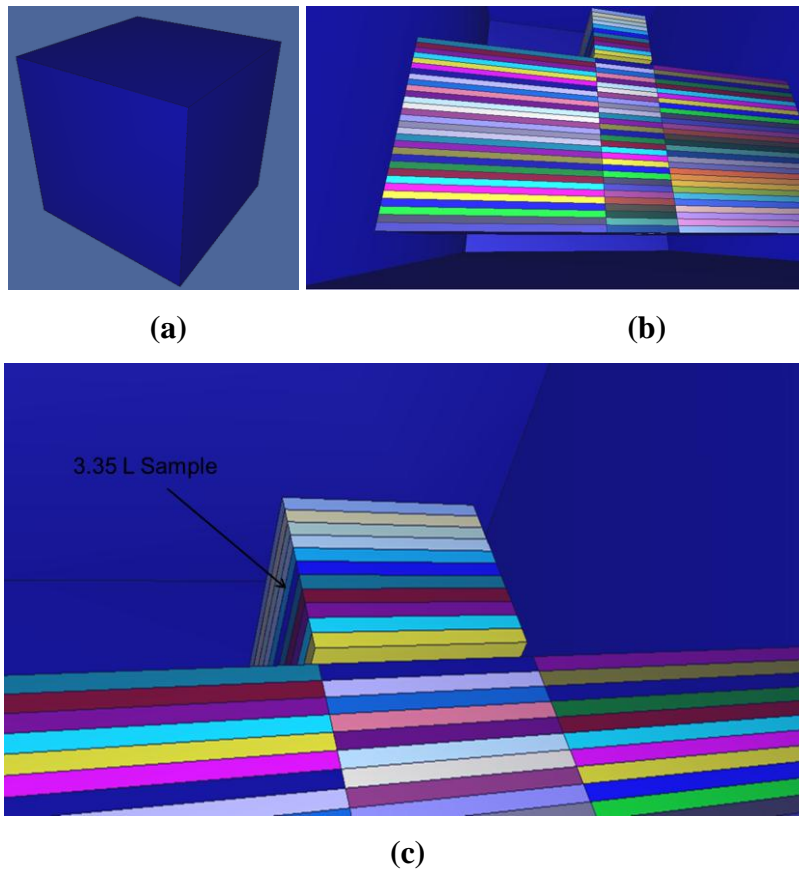


Figure 4-2: (a) Outside of Al target, (b) sample and clutter geometry, (c) sample close-up.

4.2 MCNP Data and Data Processing

Each Monte Carlo experiment traced 200 million particles through the geometry outlined in Section 4.1.1. Gamma rays were tallied in each of three 4-keV-wide energy bins centered around each of the nine gamma-ray signature energies; thus, each of the nine signature energy bins had a bin on either side of it. The MCNP5 code, provided in Appendix B, gives the energy bins used to detect gamma rays with energies near the desired signature energies. A group of three energy bins was centered on each of the gamma-ray signature energies outlined in Table 3.1. The three energy bins associated with each signature energy were used, in a method described in the following section, to determine if the response stored in a designated signature energy bin was larger than that of the bins on either side, representing a peak in the gamma-ray fluence. Neutrons were sorted into one of two energy bins ($E < 0.4$ eV and $E > 0.4$ eV). The fluences at all 11 (two neutron and 9 gamma-ray) explosive HCNO signature energies were tallied for use in the proposed SBRS detection technique.

4.2.1 Signature Peaks and Error

The output file of an MCNP experiment gives the results for a tally in three columns; the first is the energy of the bin, the second the fluence per source particle and the third the relative error of the measured fluence. Perl scripts were used to extract data from the many lines of text output. Once the pertinent data was extracted, it was fed into a C++ program that determined if the fluence in a signature energy bin represented a “peak” with a value larger than that of its neighbors. Figure 4.3 displays two responses of gamma-ray energies binned in MCNP experiments, the responses were from two different targets and figure was created for demonstration purposes only. A step-by-step method used to determine if the fluence in a signature energy bin represented a peak is presented below. A large number of counts in a signature energy bin denotes the presence of characteristic gamma rays (prompt capture or inelastic scatter) of one of the elements under investigation for explosive differentiation (Table 3.1). The method described below was applied only to the F5 tally used to measure gamma-ray fluence. A sample calculation follows the description of the method used to determine the presence of peaks in the signature energy bins, and utilizes data from Fig. 4.3.

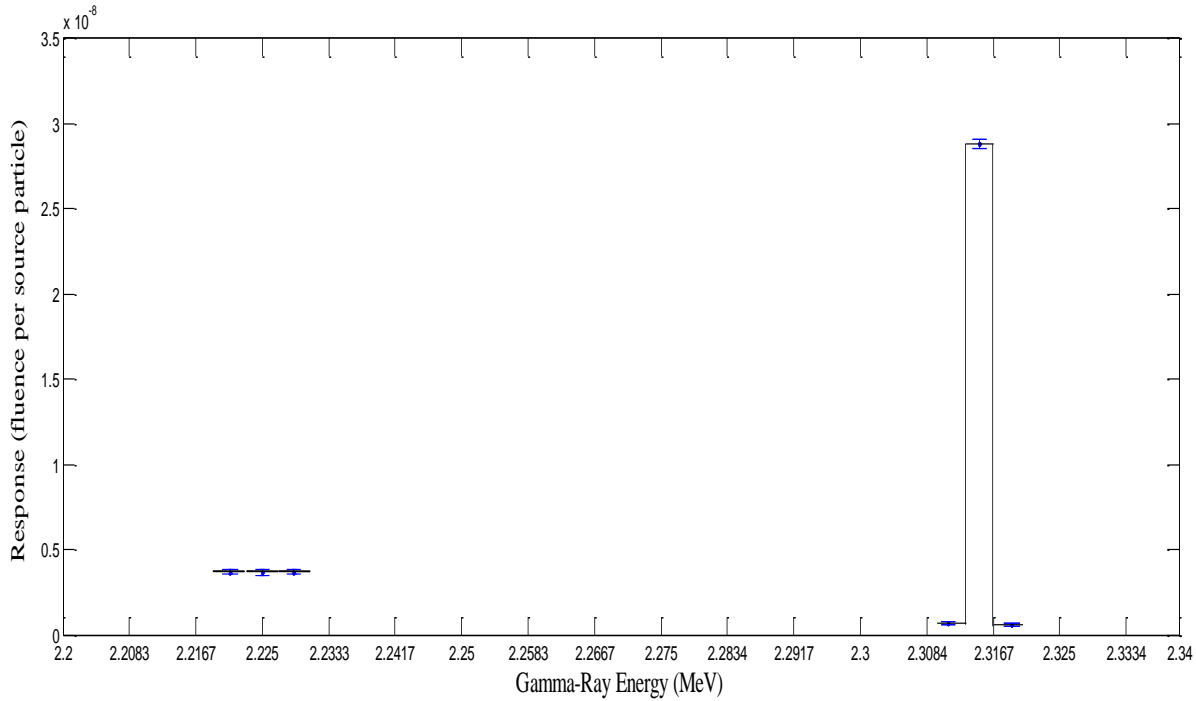


Figure 4-3: Sample Figure of Binned Responses Surrounding Signature Energies of 2.2232 MeV (Hydrogen Prompt-Capture Gamma-Ray) and 2.3128 MeV (Nitrogen Inelastic-Scatter Gamma-Ray)

In Fig. 4.3, solid horizontal lines are drawn, between the $\pm 3\sigma_{\bar{x}}$ bounds of each response, within each 4 keV wide energy bin. Because the error given in the MCNP output is a relative error R , the error must be multiplied by the tally to give the standard deviation of the sample mean, $\sigma_{\bar{x}} = \bar{x}R$, and $\bar{x} = \frac{1}{N} \sum_{i=1}^N x_i$, where x_i are the individual scores stored in a tally (X-5 Monte Carlo Team, 2008).

The following steps were performed to determine if there was a peak in the flux in a signature energy bin. Sample calculations follow the procedure outlined below.

1. An average “background” value was calculated by summing the tallies of the bins on either side of the signature energy bin and then dividing the result by two.
2. A confidence interval was found for the response of the signature energy bin ($\bar{x}_{Signature\ E}$) by multiplying the standard deviation of the sample mean by three ($3\sigma_{\bar{x}}$).

3. The background was then added to the value of 3σ and the result (termed a “three-sigma-check”) was compared to the tally in the signature energy bin.
4. Tallies larger than the three-sigma-check value were determined to be a peak; otherwise the tally was recorded as a zero for further analysis procedures.
5. If a tally was deemed a peak the background was subtracted from it to give a “net peak”, also used during further analysis.

To determine if there was a peak for the signature energy of 2.2232 MeV (hydrogen prompt-capture gamma-ray, left in Fig. 4.3, the response of the energy bin to the left ($\bar{x}_{Left Bin}$), centered at 2.221 MeV, and the response to the right ($\bar{x}_{Right Bin}$), centered at 2.229 MeV, were averaged to form a background value as follows (Step 1),

$$Background = \frac{\bar{x}_{Left Bin}}{2} + \frac{\bar{x}_{Right Bin}}{2} = \frac{3.68 \times 10^{-9} \text{ cts/source particle}}{2} + \frac{3.66 \times 10^{-9} \text{ cts/source particle}}{2} =$$

$3.67 \times 10^{-9} \text{ cts/source particle}$. Step 2 is to define a confidence interval for the response in the

signature energy bin, $3\sigma_{\bar{x}} = \bar{x}_{signature E} (R) = (3)3.65 \times 10^{-9} \text{ cts/source particle} (\pm 4.75 \times 10^{-11}) =$

$\pm 5.20 \times 10^{-19} \text{ cts/source particle}$. The value of $3\sigma_{\bar{x}}$ is then added to the background (Step 3) to

determine whether or not the response in the signature energy bin is a peak with the confidence interval:

$$3.67 \times 10^{-9} \text{ cts/source particle} + 5.20 \times 10^{-19} \text{ cts/source particle} = 3.67 \times 10^{-9} \text{ cts/source particle}.$$

Step 4 requires that the tally response in the signature energy bin be larger than value found in Step 3.

In this case, the background plus $3\sigma_{\bar{x}}$ of the signature energy bin is larger than the response contained in the signature energy bin and thus, there is no signature for the hydrogen prompt-capture gamma-rays of energy 2.2232 MeV.

There is a clearly defined peak to the right in Fig. 4.3 with signature energy 2.3128 MeV for nitrogen inelastic-scatter gamma rays. Steps 1-4 are the same as in the above example, however there is a peak at the signature energy, thus, a net peak value must be determined. The background is found to be, $6.13 \times 10^{-10} \text{ cts/source particle}$. This value is then subtracted from the peak value $2.88 \times 10^{-8} \text{ cts/source particle}$ to give a net peak of $2.88 \times 10^{-8} \text{ cts/source particle}$. Because the net peak for gamma-ray signature energies was found by subtracting random

variables from one another the propagation of errors was applied to find their standard deviations:

$$\sigma = \sqrt{\left(\bar{x}_{Signature\ E} (R_{Signature\ E})\right)^2 + \frac{\left(\bar{x}_{Left\ Bin} (R_{Left\ Bin})\right)^2}{4} + \frac{\left(\bar{x}_{Right\ Bin} (R_{Right\ Bin})\right)^2}{4}}. \quad (4.2.1)$$

The factor of one-fourth is needed because it was the values $\bar{x}_{Left\ Bin}/2$ and $\bar{x}_{Right\ Bin}/2$ that were subtracted from $\bar{x}_{Signature\ E}$. Calculating the standard deviation of the sample mean for both neutron and gamma-ray tallies was required. The standard deviation for the neutron F5 tally was found using the same method as described in Step 1 above ($\sigma = Tally(R) = \bar{x}(R)$). Sample Pearl and C++ codes used to calculate the standard deviations of neutron and gamma-ray signatures are provided in Appendix D.

4.2.2 Figure-of-Merit Calculations

Figure-of-merit calculations were made using the net peak and tally values found in the process outlined above. The standard deviations were also used in calculations involving Equations 3.5.6 and 3.5.7 of Ch. 3. MATLAB codes were used to calculate FOM and to generate several useful plots. Although calculations of FOM are easily accomplished using far less powerful software packages, it was the graphing capability and familiarity of use that lead the author to use the MATLAB platform. Samples of the codes used are provided in Appendix E.

4.3 Results of Figure-of-Merit Analysis Using Cutoffs and Density

The calculated FOM for samples containing RDX, UNi and an inert material were compared to 80 artificial templates containing either RDX or UNi. The 21 inert clutter materials used to shield the sample in each experiment were used to categorize the results. Uniform weights were used ($w_i = 1, i = 1, 2, \dots, N$) such that $\alpha_i = 1/N$. Normalized figures-of-merit and error ($\zeta_\ell(normalized)$ and $\sigma(\zeta_\ell(normalized))$) were used, and for brevity they are referred to as ζ_ℓ , and $\sigma(\zeta_\ell)$ for the remainder of this work. Plots, with $3\sigma(\zeta_\ell)$ confidence markers, of the lowest FOM, ζ_ℓ , for each shielding material are shown in Figs. 4.4-4.6 and tabulated in Appendix F. The lowest ζ_ℓ was used because a low ζ_ℓ represents a close match between the

template and the sample being interrogated. It is only necessary for one template to identify a target as containing an explosive; therefore, only one ζ_ℓ from each category was needed for identification purposes. By inspection, one may use a cutoff value of $\zeta_0 = 9$ (see Fig. 4.4)) to identify all explosive samples containing RDX. The lowest ζ_ℓ for all samples containing UNi were also below the cutoff of nine (Fig. 4.5), and again all explosive samples were correctly identified. However, when the same cutoff, $\zeta_0 = 9$, was applied to the targets containing inert materials, 15 of the 21 inerts were incorrectly identified as containing explosives.

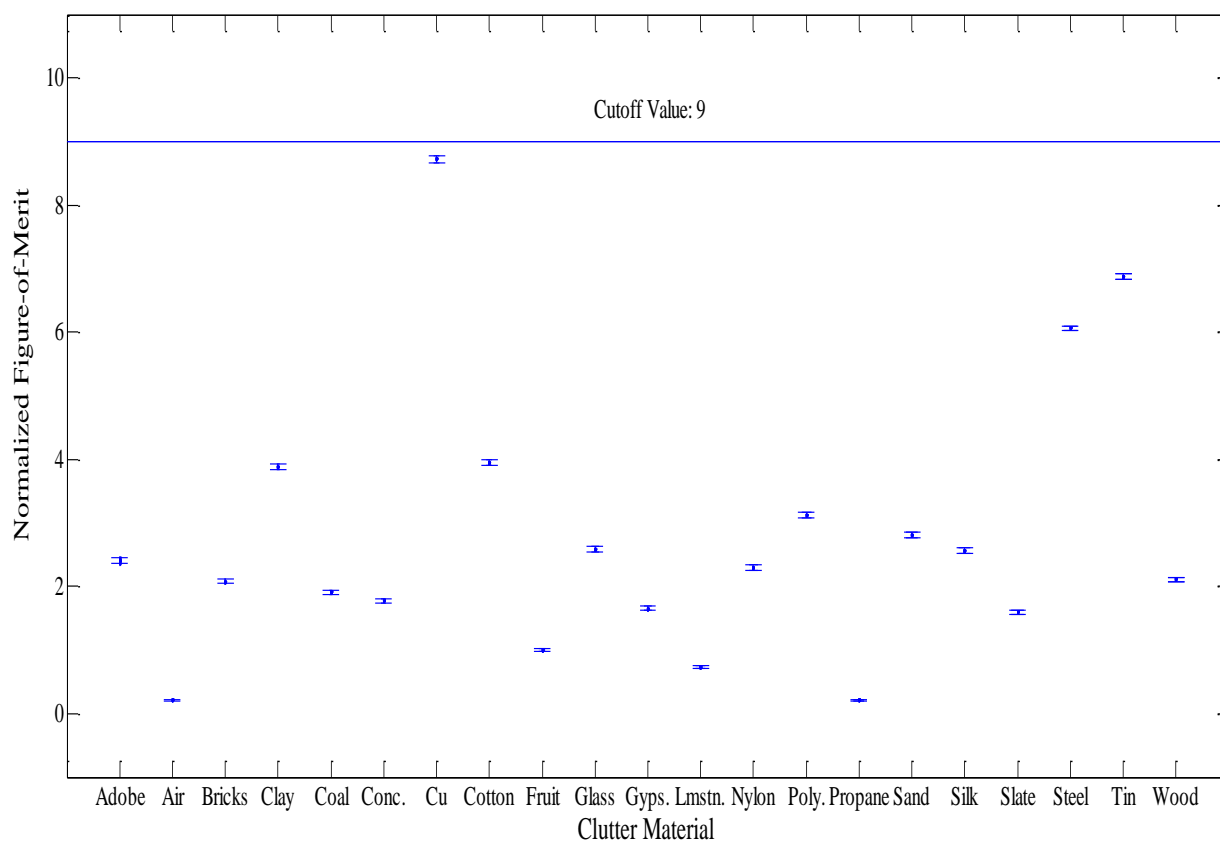


Figure 4-4: Lowest Figures-of-Merit with Cutoff of 9 Identifies All 21 Samples of RDX as Explosives

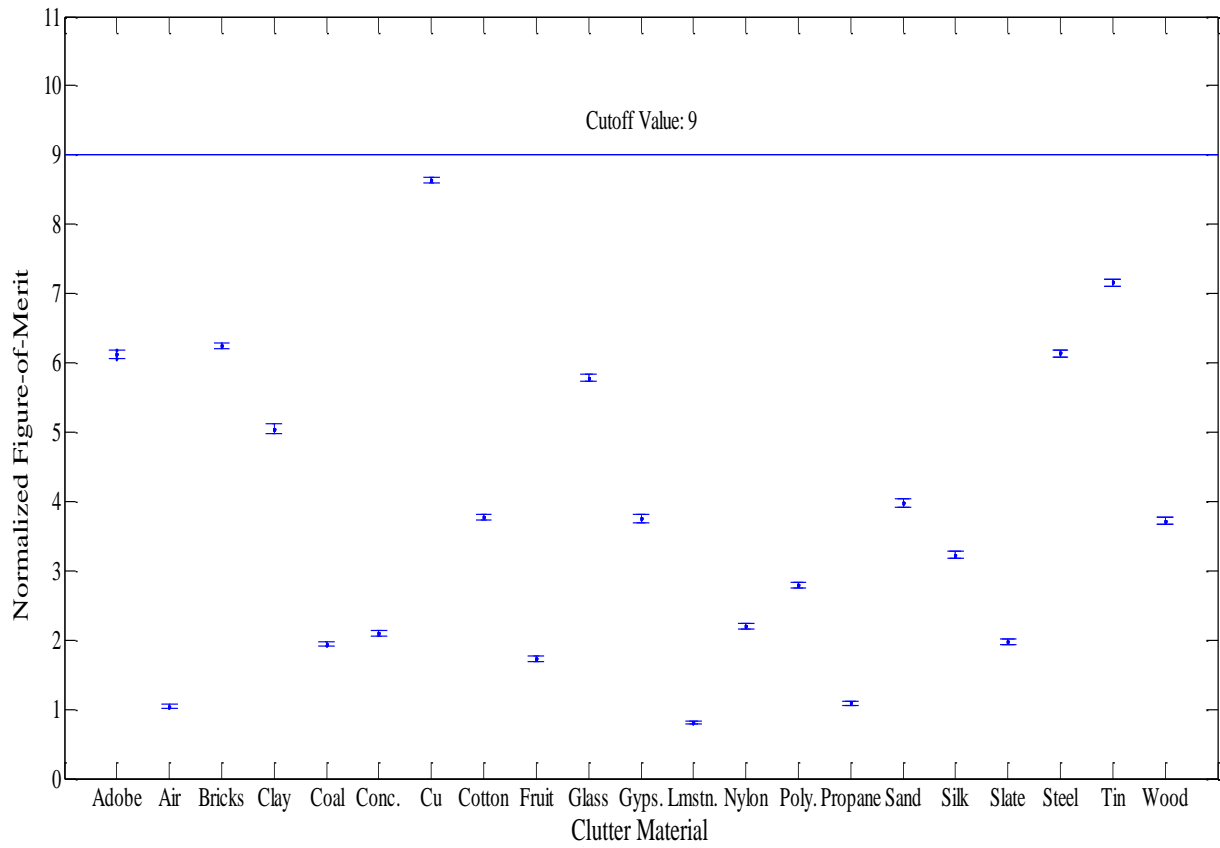


Figure 4-5: Lowest Figures-of-Merit with Cutoff of 9 Identifies All 21 Samples of UNi as Explosives

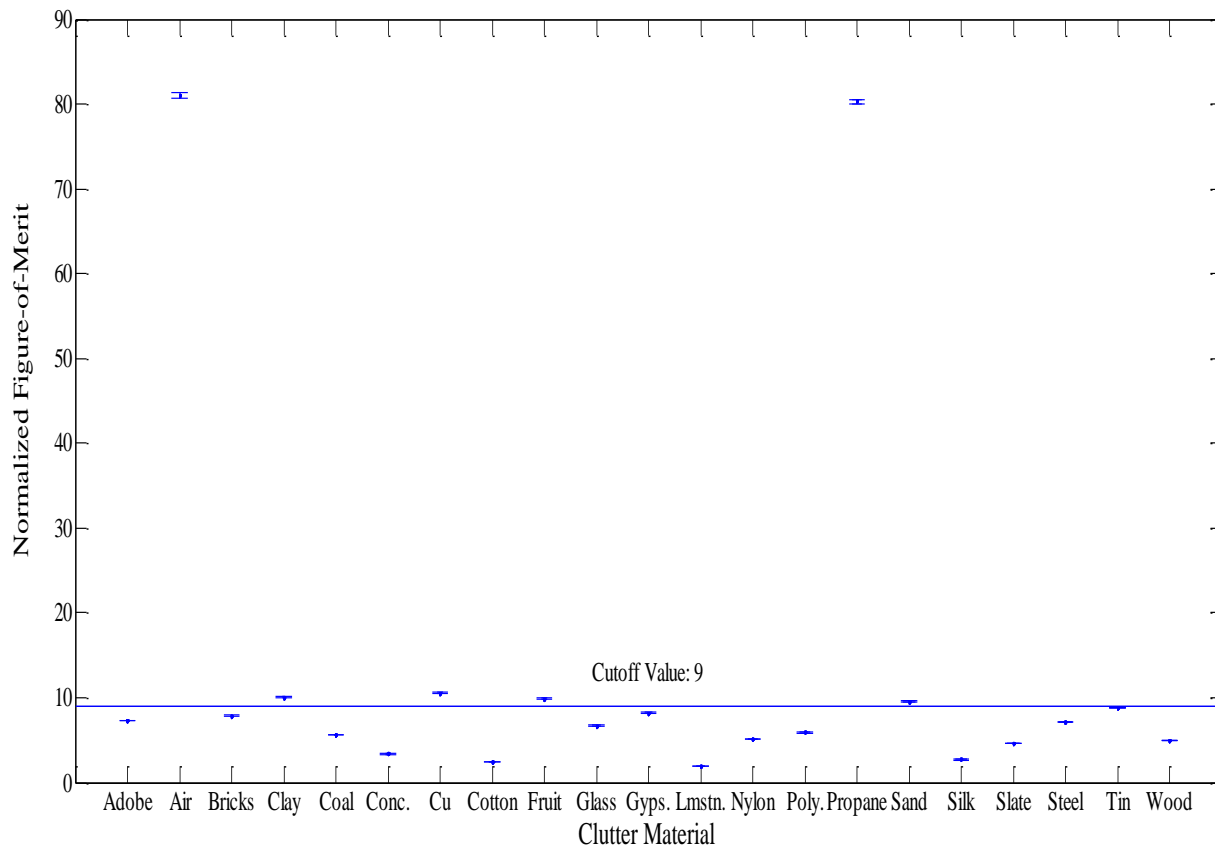


Figure 4-6: Lowest Figures-of-Merit with Cutoff of 9 Identifies All 15 Inert Samples as Explosives

Although all explosive samples were detected in this process (sensitivity of 100%), the resulting specificity (28.6% - with 15 FP) was deemed far too low for effective application. A cutoff value lowered to just five resulted in only six false positives, but the number of false negatives increased to 13. Applying the cutoff of five increased the specificity to nearly 71.4%, but the sensitivity was reduced by nearly one-fourth to just 76.2%. Clearly, a process that misses nearly 1-in-4 IEDs leaves much to be desired and is far more dangerous than is acceptable. Thus, a filtering process that would yield suitable levels of specificity (75% or greater) and sensitivity (90% or greater) was sought. Emphasis was placed on sensitivity in selecting appropriate cutoffs.

4.3.1 Application of a Density Filter

As was discussed in Section 3.4, the approximate density of a target can be identified via photon interrogation, and offers an avenue for categorizing targets. The number of backscattered photons from an interrogated volume is proportional to the density of the target. By measuring the intensity of backscattered radiation it is possible to gain rudimentary density measurements. However, density measurements made in this fashion are not highly accurate (Lawson and Severson, 2003). Comparing a target to templates of similar average density, thus filtering out templates that should not be used for comparison, eliminates many unnecessary FOM calculations. Another advantage of such a “density filter” is the possibility of differentiating explosive from inert targets.

A density filter was developed for comparing target signatures to templates with similar average densities. Backscatter X-ray methods can provide estimates of a target’s average density. Because information concerning the average density of a target is not precise, templates with a range of densities were used in the density filter approach. The range of target densities and the templates used in FOM calculations are given in Table 4.1.

Table 4.2: Density Filter Values and Average Densities of Templates.

Density Range (g cm ⁻³)	Templates Comprising Tier	Template Designation	Average Density (g cm ⁻³)
Group-1 0.0-1.0	RDX (VLD)	RDX (HD)	4.2773
	UNi (LD)	UNi (HD)	3.6961
	UNi (VLD)	RDX (MD)	2.0144
Group-2 1.0-2.0	RDX (MD)	UNi (MD)	1.4332
	UNi (MD)	RDX (LD)	1.4189
	RDX (LD)	RDX (VLD)	1.0616
	RDX (VLD)	UNi (LD)	0.8377
	UNi (LD)	UNi (VLD)	0.4804
Group-3 2.0-3.0	UNi (HD)		
	RDX (MD)		
	UNi (MD)		
Group-4 3.0-4.0	RDX (HD)		
	UNi (HD)		
	RDX (MD)		
Group-5 > 4.0	RDX (HD)		
	UNi (HD)		

An example of the filter methodology follows. Suppose a sample is measured to have an average density of 3.32 g cm^{-3} . The measured density places the sample in Group-4, where only templates having similar densities (4.2773 , 3.6961 and 2.0144 g cm^{-3}) are used to calculate a ζ_ℓ from the response of the sample after neutron interrogation. The ζ_ℓ is then compared to ζ_0 , to determine if the target contains a nitrogen rich explosive. Table 4.2 outlines the average density of all inert clutter with either inert samples and inert clutter with explosive samples.

Table 4.3 Clutter and Sample Average Densities.

Inert Clutter & Inert Sample	Average Density (g cm^{-3})	Inert Clutter & RDX Sample	Average Density (g cm^{-3})	Inert Clutter & UNi Sample	Average Density (g cm^{-3})
Air	0.0012	Air/RDX	0.9431	Air/UNi	0.3619
Propane	0.0019	Propane/RDX	0.9434	Propane/UNi	0.3622
Wood	0.75	Wood/RDX	1.2998	Wood/UNi	0.7186
Gypsum	0.752	Gypsum/RDX	1.3007	Gypsum/UNi	0.7195
Fruit	1.081	Fruit/RDX	1.4575	Fruit/UNi	0.8763
Nylon	1.14	Nylon/RDX	1.4856	Nylon/UNi	0.9044
Silk	1.16	Silk/RDX	1.4951	Silk/UNi	0.9139
Clay	1.285	Clay/RDX	1.5547	Clay/UNi	0.9735
Coal	1.29	Coal/RDX	1.5570	Coal/UNi	0.9758
Sand	1.391	Sand/RDX	1.6052	Sand/UNi	1.0240
Polyester	1.4	Polyester/RDX	1.6094	Polyester/UNi	1.0282
Cotton	1.55	Cotton/RDX	1.6809	Cotton/UNi	1.0997
Bricks	1.8	Bricks/RDX	1.8000	Bricks/UNi	1.2188
Adobe	1.85	Adobe/RDX	1.8238	Adobe/UNi	1.2426
Concrete	2.31	Concrete/RDX	2.0430	Concrete/UNi	1.4618
Limestone	2.35	Limestone/RDX	2.0620	Limestone/UNi	1.4808
Glass	2.4	Glass/RDX	2.0858	Glass/UNi	1.5046
Slate	2.84	Slate/RDX	2.2955	Slate/UNi	1.7143
Tin	7.365	Tin/RDX	4.4512	Tin/UNi	3.8700
Steel	7.8212	Steel/RDX	4.6685	Steel/UNi	4.0873
Copper	8.92	Copper/RDX	5.1920	Copper/UNi	4.6108

The above method was applied to all 21 RDX, 21 UNi, and 21 inert samples. All targets were collected into their respective groups and their signatures were then used to calculate ζ_ℓ with the templates in that group. The results are graphically depicted (with $3\sigma(\zeta_\ell)$ confidence markers) below in Figs. (4.4-4.7) and are tabulated in Appendix G.

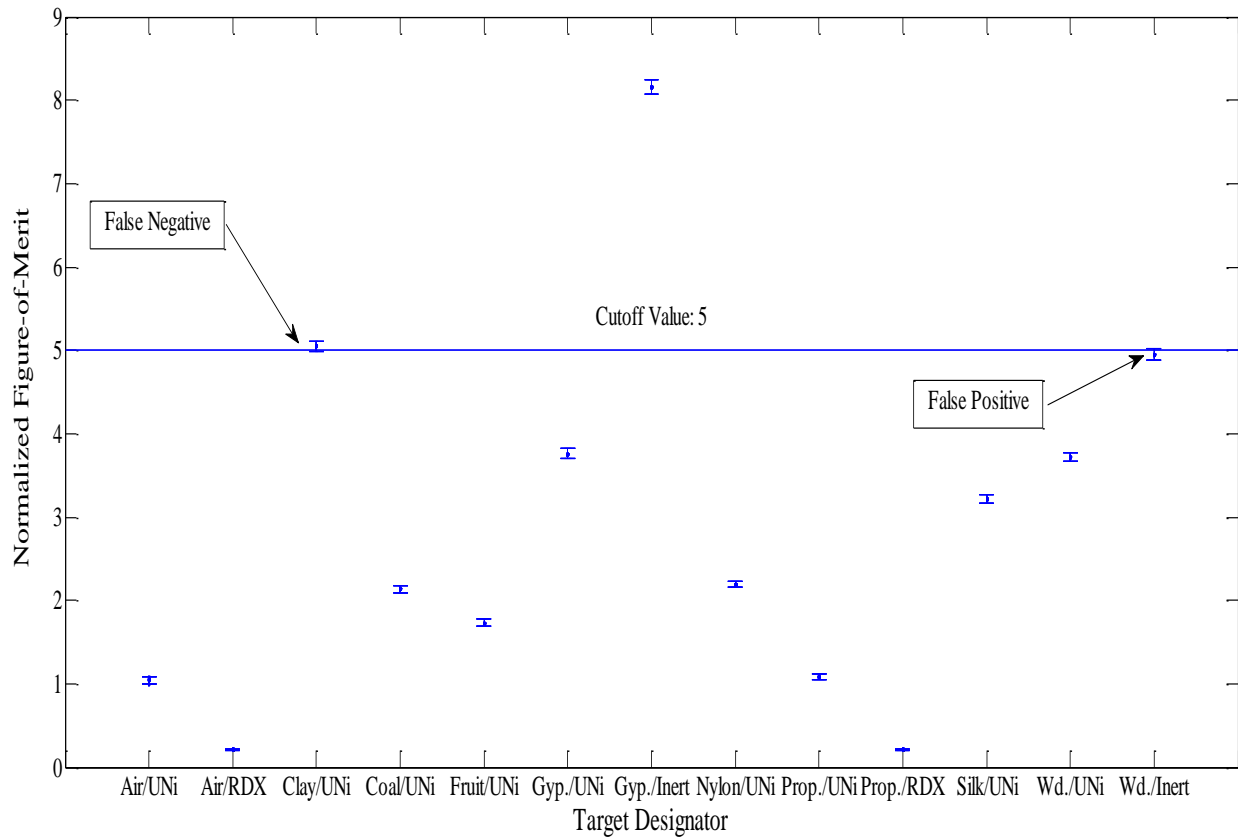


Figure 4-7: Density Group-1, 13 targets with density between 0 and 1 g cm⁻³.

The notation used in this and subsequent figures is “clutter/sample,” as in “Coal/UNi,” where a sample of Urea Nitrate is obscured by coal in the clutter configuration. With $\zeta_0 = 5$ there is one false negative (Clay/UNi, left in the figure) and one false positive (Wood/Inert, at the far right of the figure). The Clay/UNi target had $\zeta_\ell = 5.05$ and was only separated by $\lambda_+ = 2.22$ from the cutoff. Similarly the Wood/Inert target had $\zeta_\ell = 4.95$ and was just $\lambda_- = 2.17$ from ζ_0 . Each misidentified target is seen to be within $3\sigma(\zeta_\ell)$ of the cutoff and would be deemed “suspects.” This study does not deal with how suspect targets should be treated, but suggests that the user of a SBRS system be aware of the inherent difficulty in clearly identifying all explosive or inert targets. Within the bounds of this research any target whose ζ_ℓ is above ζ_0 is an inert and any target whose ζ_ℓ is below ζ_0 is an explosive.

There were 15 targets with density between zero and 1 g cm^{-3} but two targets (inert targets with clutter and sample composed of air and propane respectively) had ζ_ℓ that were over 80 and were not shown on the chart for clarity at lower values of ζ_ℓ . The targets with air and propane both had $\lambda_+ > 800$ and were very far removed ($> 800\sigma(\zeta_\ell)$) from targets with explosives shielded with air or propane as seen in Fig. (4.7).

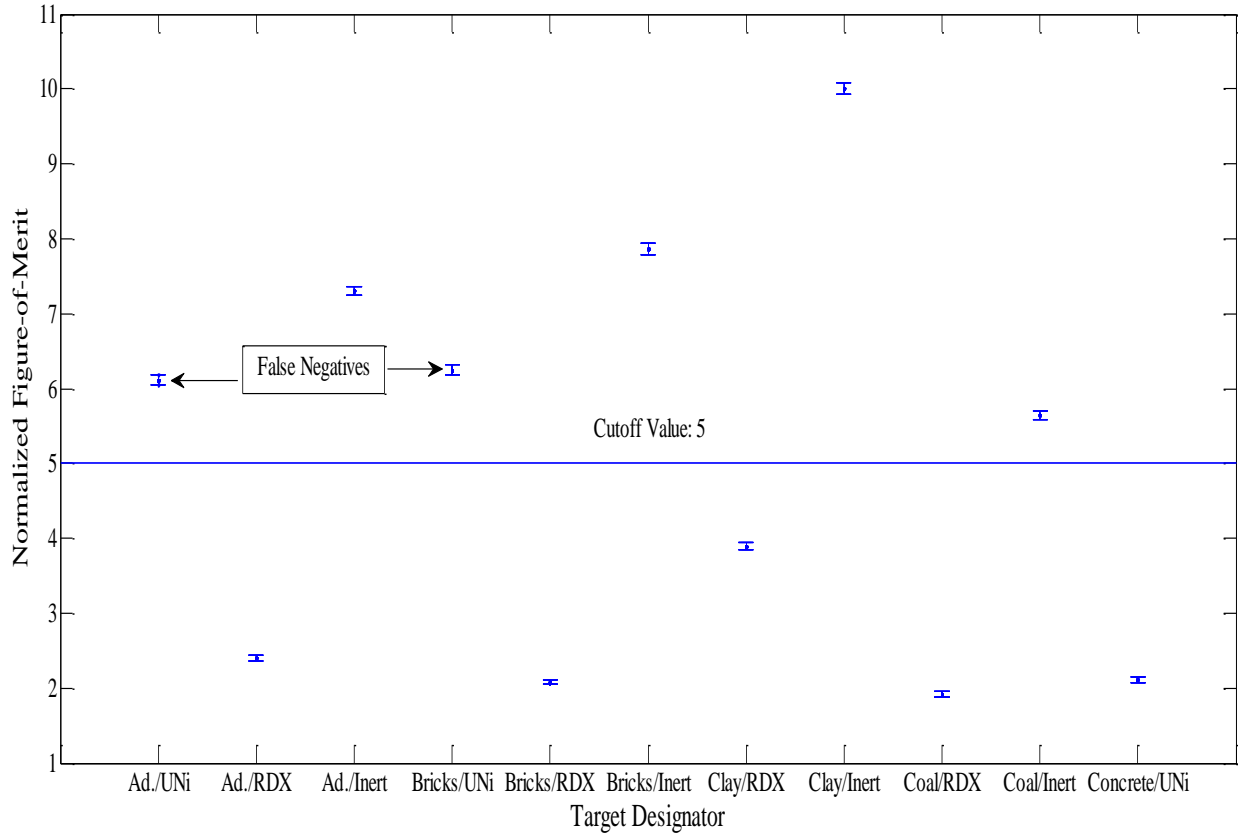


Figure 4-8: Density Group-2, targets 1-11 of 31 targets with density between 1 and 2 g cm^{-3} .

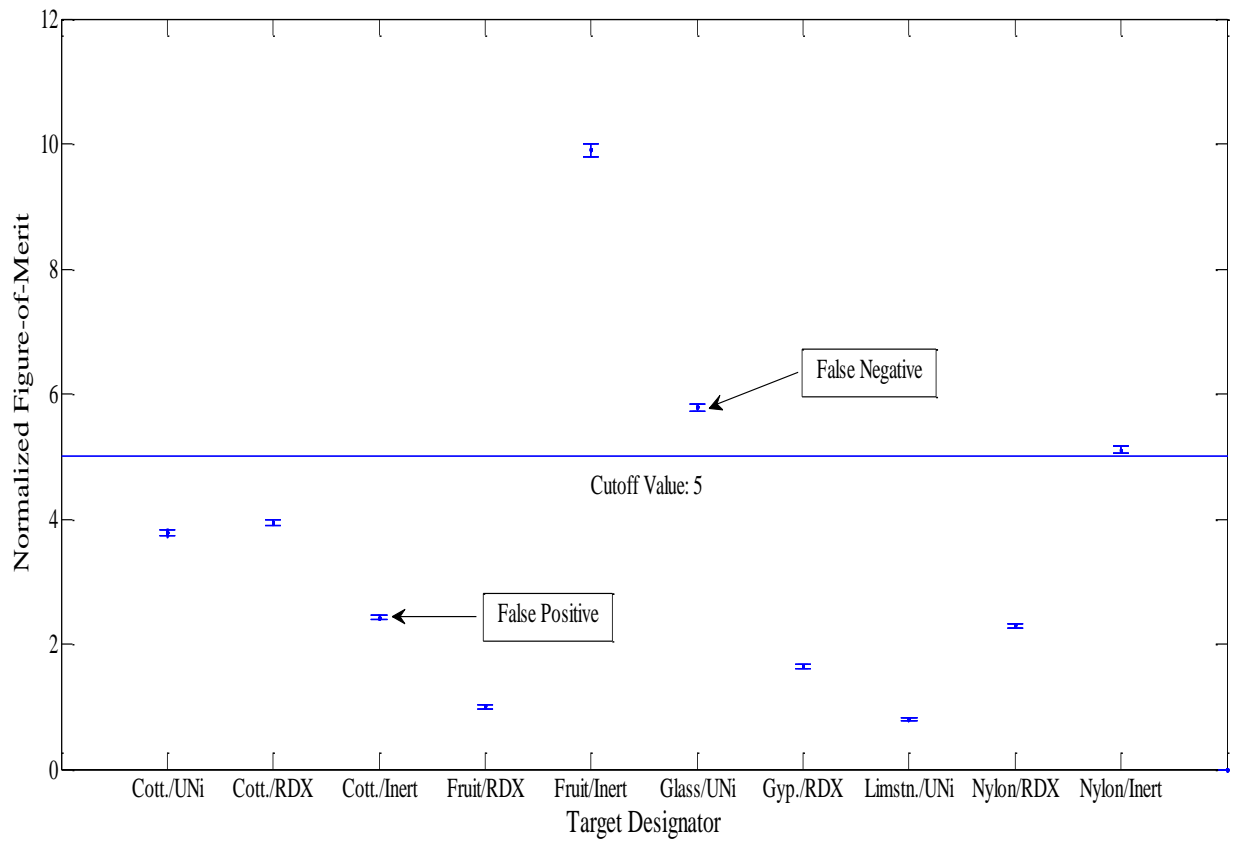


Figure 4-9: Density Group-2, targets 12-21 of 31 targets with density between 1 and 2 g cm⁻³.

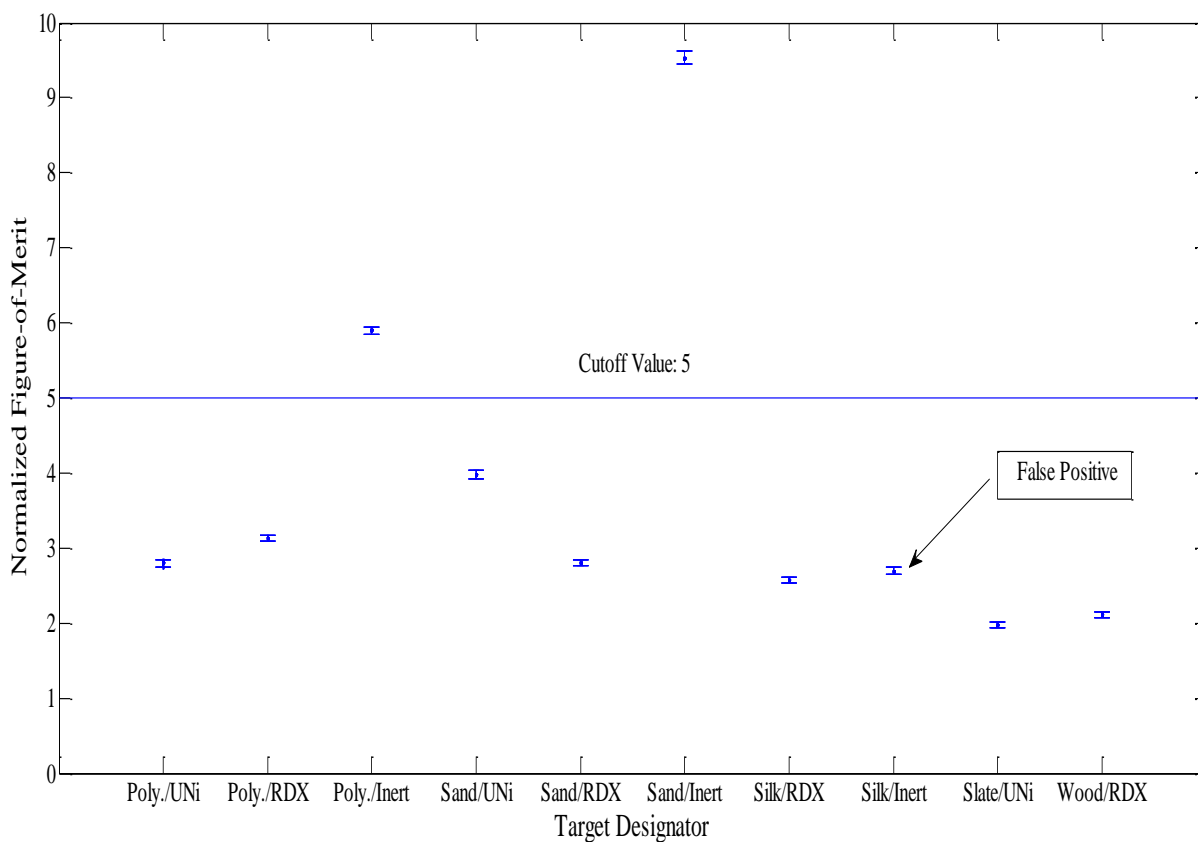


Figure 4-10.: Density Group-2, targets 22-31 of 31 targets with density between 1 and 2 g cm⁻³.

Three targets containing explosives in Group-2 had values of ζ_ℓ above five, and were not correctly identified as explosive hazards. Conversely, two targets that did not contain an explosive sample did have values of ζ_ℓ below five, and were deemed explosive threats. The cutoff value of five is common to both Group-1 and Group-2, thus targets with density between 0 and 2 g cm⁻³ are discriminated with $\zeta_0 = 5$.

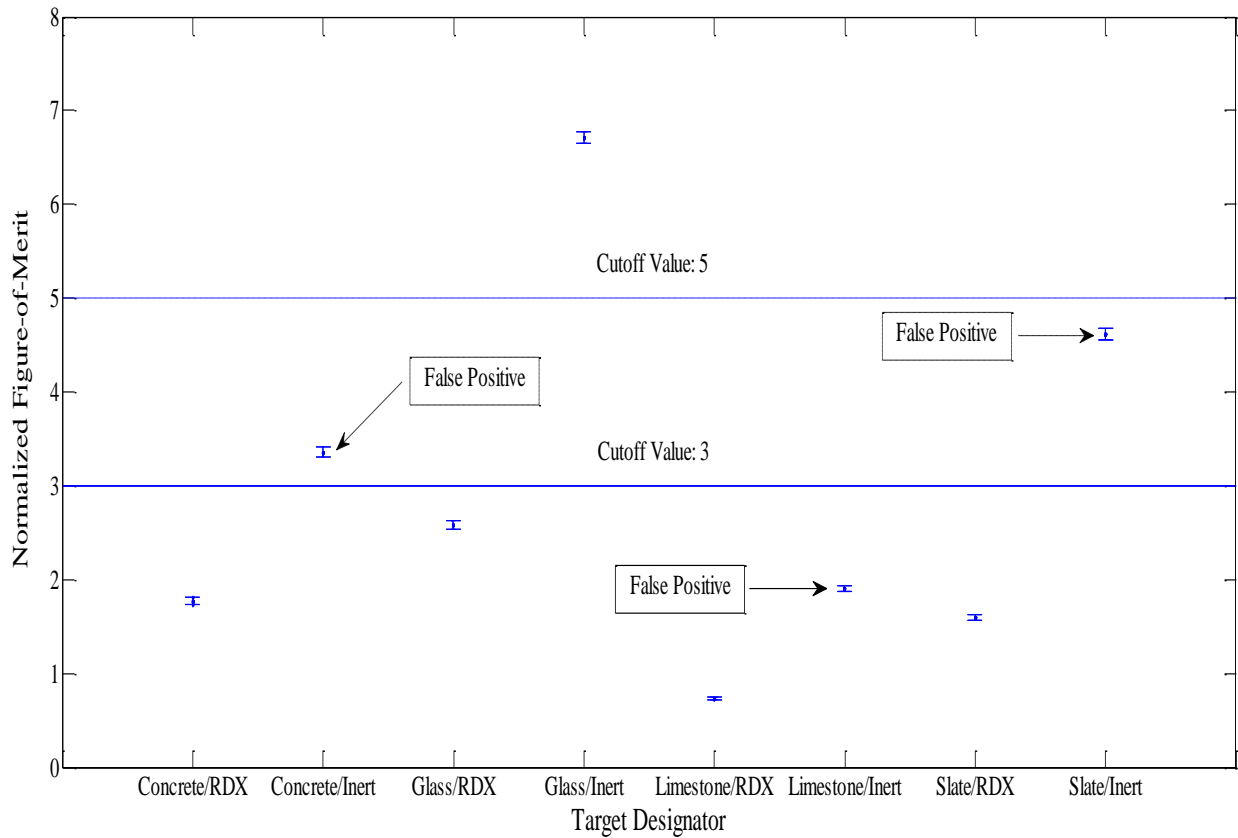


Figure 4-11: Density Group-3, 8 targets with density between 2 and 3 g cm⁻³.

The dashed line at the top of Fig. 4.9 represents $\zeta_0 = 5$ and was initially the cutoff used, however, a much lower cutoff, $\zeta_0 = 3$, was found to discriminate explosive from inert targets. Using $\zeta_0 = 3$, instead of $\zeta_0 = 5$, gives two fewer false positives, represented by the boxes with dashed lines, and still isolates all explosive targets in the group. Small changes in the cutoff value produce drastically different results in discrimination of explosive and inert targets.

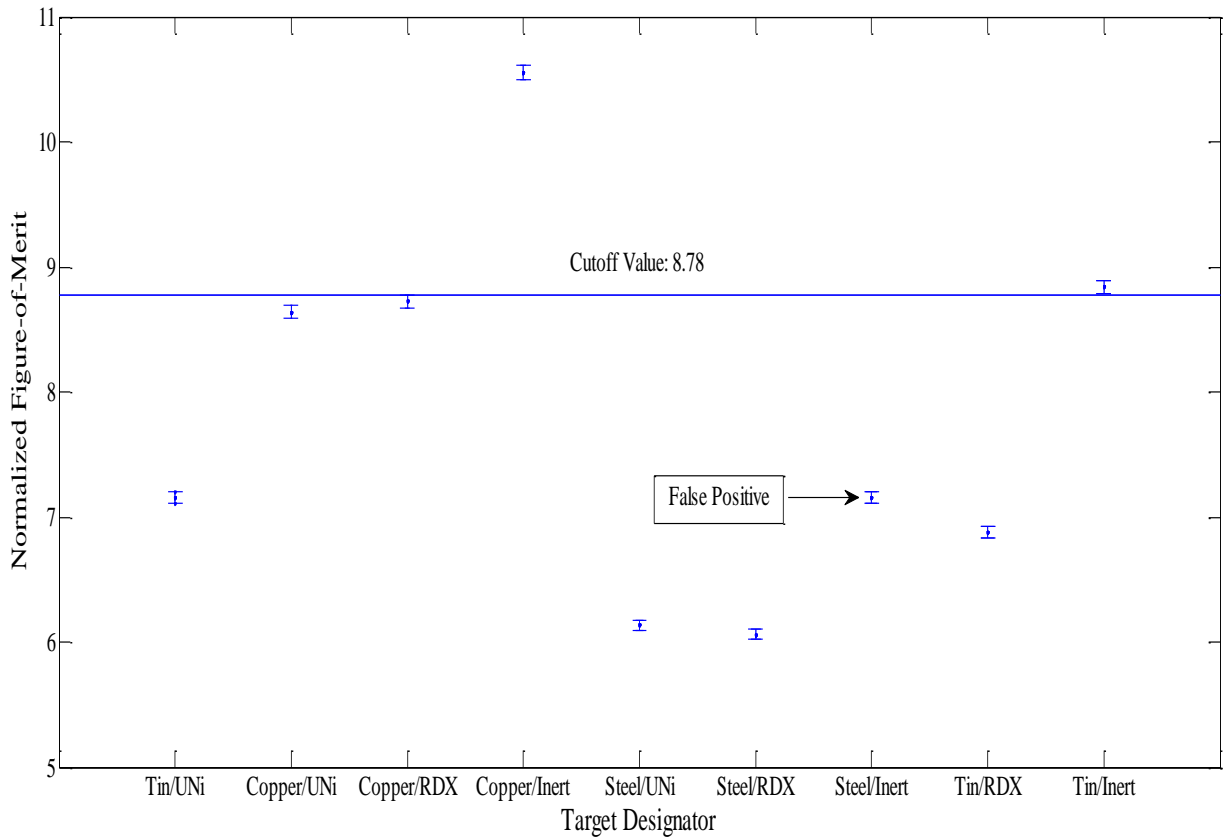


Figure 4-12: Density Group-4 & 5, 9 targets with density between 3 and 9 g cm⁻³.

The first target listed in Fig. (4.7) (Tin/UNi) had density of 3.87 g cm⁻³ and belonged to Group-4, however with only one target in the group it was not known what cutoff would be most effective. Because it had been observed that neighboring groups could share a common cutoff value, it was postulated that Group-4 would have the same cutoff as that of Group-5. The theory proved to be correct for the single target in Group-4, as seen above.

The cutoff shown in Fig. 4.10 was chosen because it separated the targets Copper/RDX and Tin/Inert. The Copper/RDX target had a $\zeta_\ell = 8.723$, and was separated from the cutoff by $\lambda_- = 3.4$. Above the cutoff by $\lambda_+ = 3.6$, the Tin/Inert target had a $\zeta_\ell = 8.841$. Although the difference between inert and explosive is narrow in Group-5, the use of $\zeta_0 = 8.78$ identified all explosive targets in the group and only lead to one false positive.

The use of $\zeta_0 = 5$ for Groups 1-3 and $\zeta_0 = 8.78$ in Groups 4 and 5 resulted in four false negatives and seven false positives. The resulting sensitivity (90.5%) is within the desired limit, but the specificity (66.7%) remained lower than preferred. However, if the cutoff in Groups 1-3 is raised to 6.5 all explosive targets are classified correctly, but the number of false positives climbs to 10 giving a sensitivity of 100% and a specificity of just 52.4%.

4.4 Particle Dependent Figure-of-Merit Analysis

The analysis completed in Section 4.3 used figures-of-merit calculated by combining the signatures of backscattered gamma rays and neutrons. The Standoff Bomb Detection project at Kansas State University has focused mainly on IED detection using gamma-ray signatures. The benefits, if any, of also using neutrons for the detection of IEDs is explored. The results of Section 4.3 are compared with the results of using only neutrons or only gamma rays in explosive detection. figures-of-merit are calculated using either gamma-ray signatures or neutron signatures and cutoffs are found for each case separately. These results are compared to those found above to determine if information carried by backscattered neutrons is valuable to IED detection.

4.4.1 Density Dependent Cutoffs Using Neutron Figure-of-Merit Analysis

The data retrieved from MCNP concerning neutrons above and below the cadmium cutoff, thus forming two signatures, were used in the same method as described in Section 4.3. Responses and templates with only neutron signatures were used to calculate figures-of-merit that were then filtered through the same density filters as in Section 4.3.1. Appropriate cutoffs in each density group were found using a non-graphical technique, opting instead for direct numerical comparisons. Numerical comparisons sought to minimize the number of false positives while maintaining a sensitivity of 90.5% (no more than 4 false negatives) across all five density groups. The numerical comparison technique also sought to limit the total number of cutoffs by seeking like cutoffs between adjacent groups. Table 4.4 outlines the density group cutoffs found in this manner.

The values of nearly all ζ_ℓ are significantly lower than were those found in Section 4.3, the result of neutron templates matching very closely to the signatures of individual targets. The lowest calculated ζ_ℓ for each target and its error are tabulated in Appendix H.

Table 4.4 Density Dependent ζ_0 Using Neutron Signatures

Group	ζ_0
1	0.581
2	0.581
3	0.048
4	0.83
5	0.83

Groups 1 and 2 share a common ζ_0 as do groups 4 and 5, while the cutoff of Group-3 is an order-of-magnitude smaller than any other group. The significantly lower ζ_0 for Group-3 is reminiscent of the ζ_0 for Group-3 observed in Fig. 4.9. The results of applying the above cutoffs, (number of false positives and false negatives) are tabulated in Table 4.6.

4.4.2 Density Dependent Cutoffs Using Gamma-ray Figure-of-Merit Analysis

The 9 gamma-ray signatures outlined in Section 3.3 were used to form templates, as in Section 4.4.1, for comparison to the signatures produced through MCNP simulated neutron interrogation. Calculated figures-of-merit were compared, using the same numerical comparison technique outlined in the above section, to find the best cutoff values for each density group. The cutoffs used are summarized below and the calculated figures-of-merit are displayed in Appendix I.

Table 4.5 Density Dependent ζ_0 Using Gamma-ray Signatures

Group	ζ_0
1	9.5
2	9.5
3	9.5
4	93
5	93

As in the analysis involving both neutron and gamma-ray signatures, a single cutoff value was found for groups 1-3 and another for groups 4-5.

4.5 Results Using Density Dependent Cutoffs

Table 4.6 compares the three methods discussed for FOM analysis in terms of sensitivity and specificity. Because all cutoff values found in Sections 4.3 and 4.4 were found by holding the sensitivity constant at 90.5% (4 false negatives), the following analysis compares each method on the basis of how many false positives were generated using the cutoffs detailed above. The findings are listed in the table by the type of particle used in the FOM analysis (*neutron*, γ -ray, and *neutron & γ -ray*). The targets producing a false negative or false positive result are also listed for further discussion.

The asterisks in the bottom right of the table, under the heading “*neutron & γ -ray*,” denotes the lower cutoff ($\zeta_0 = 3$) found in earlier analysis (see Fig. (4.9)). If the lower cutoff is applied the number of false positives is reduced to just five with a corresponding specificity of 76.2%, compared to 66.7% when $\zeta_0 = 5$ is used. The method using only neutron signatures had the largest number of false positives resulting in a specificity of just 47.6%, however in Group-3 no false positives or false negatives were recorded using $\zeta_0 = 0.048$. Finally, the 8 false positives found when using gamma-ray analysis techniques gives a specificity of 61.9%, still far below the desired 75%.

The method relying only on gamma-ray signatures did not exhibit a lower cutoff in Density Group-3 as did the other two methods. The use of neutron signatures when calculating the FOM markedly reduced the cutoff values in Density Group-3. This observation is highlighted in Table 4.6, where the calculated figures-of-merit are listed in ascending order. In Density Group-3 the figures-of-merit found using neutron signatures reveal drastically different values between explosive and inert targets (differing by an order-of-magnitude).

The lowest ζ_ℓ found using gamma-ray methods in Density Group-3 is for the target Limestone/Inert with all explosive targets having larger ζ_ℓ . No clear difference between the figures-of-merit of explosive and inert targets in Density Group-3 was found using gamma-ray techniques.

Table 4.6 Method Comparison Using Density Dependent Cutoffs

Group	<i>neutron</i>	FN	FP	γ -ray	FN	FP	<i>neutron & γ-ray</i>	FN	FP
Cutoff 1	0.581			9.5			5		
	Gypsum/Inert		X	Clay/UNi	X		Clay/UNi	X	
	Gypsum/UNi	X					Wood/Inert		X
	Coal/UNi	X							
Cutoff 2	0.581			9.5			5		
	Clay/Inert		X	Silk/Inert		X	Adobe/UNi	X	
	Polyester/Inert		X	Cotton/Inert		X	Bricks/UNi	X	
	Sand/Inert		X	Nylon/Inert		X	Glass/UNi	X	
	Adobe/Inert		X	Coal/Inert		X	Cotton/Inert		X
	Silk/Inert		X	Bricks/UNi	X		Silk/Inert		X
	Bricks/Inert		X	Adobe/UNi	X				
	Fruit/Inert		X	Glass/UNi	X				
	Coal/Inert		X						
	Nylon/Inert		X						
Cutoff 3	0.048			9.5			5 (*3)		
				Limestone/Inert		X	Limestone/Inert		X
				Slate/Inert		X	Concrete/Inert*		X
				Concrete/Inert		X	Slate/Inert*		X
Cutoff 4/5	0.83			93			8.78		
	Steel/Inert		X	Steel/Inert		X	Steel/Inert		X
	Copper/UNi	X							
	Copper/RDX	X							
Total		4	11		4	8		4	7
	Sensitivity (%)	90.5		Sensitivity (%)	90.5		Sensitivity (%)	90.5	
	Specificity (%)	47.6		Specificity (%)	61.9		Specificity (%)	66.7/76.2*	

Table 4.7 Neutron and Gamma-ray ζ_ℓ for Group-3

<i>neutron</i>			γ -ray		
Clutter/Sample	ζ_ℓ	$\pm\sigma(\zeta_\ell)$	Target	ζ_ℓ	$\sigma(\zeta_\ell)$
Concrete/RDX	0.003542	0.000595	Limestone/Inert	0.157531	0.004804
Glass/RDX	0.004888	0.000699	Limestone/RDX	0.525309	0.009234
Limestone/RDX	0.031877	0.001784	Slate/Inert	2.019122	0.024849
Slate/RDX	0.041522	0.002036	Concrete/Inert	2.205757	0.025972
Glass/Inert	0.112597	0.003354	Concrete/RDX	3.926767	0.029956
Slate/Inert	0.157054	0.003168	Slate/RDX	5.147706	0.034298
Concrete/Inert	0.168368	0.004101	Glass/RDX	7.449551	0.033037
Limestone/Inert	0.222573	0.004715	Glass/Inert	16.36977	0.048973

Chapter 5 - Conclusions and the Way Ahead

The need for explosive detection techniques that are both rapid and robust is evident from the battlefields of Iraq and Afghanistan, to the countryside of Cambodia, to port of entry security. The SBRS technique can provide rapid explosive identification with low rates of false alarms while maintaining adequate sensitivity. The implementation of various SBRS methods leads to increased levels of detection proficiency. Two proposed methods of implementing SBRS were explored.

5.1 Target Density

Target density was demonstrated to play an important role in the template-matching process. By utilizing target density as an indicator for which templates are best used in figure-of-merit analysis, needless calculations are eliminated and cutoff values are identified. X-ray interrogation can provide the needed target density information while neutron interrogation delivers stoichiometric evidence of explosives.

A tiered density approach was used to select optimum cutoff values, ζ_0 . Through the judicious use of ζ_0 , it was found that for targets with average density below 4 g cm^{-3} a single cutoff value ζ_0 differentiated most explosive from inert targets. Similarly, it was found that for targets with average density between a four and 9 g cm^{-3} a singular ζ_0 was needed for adequate explosive detection. Through the use of just two cutoff values, using figures-of-merit calculated from both neutron and gamma-ray signatures, for target interrogated volumes with average density between 0 and 9 g cm^{-3} , it is possible to achieve of sensitivity of 90.5% and specificity of 66.7%. However, a much lower cutoff was found for targets with density between 3 and 4 g cm^{-3} . Through the use of three cutoff values it is possible to achieve of sensitivity of 90.5% and specificity of 76.2%.

5.2 Particle Signatures

Signatures of both neutrons and gamma rays are used separately and in combination to calculate figures-of -merit, ζ_ℓ , used for target discrimination. The ζ_ℓ calculated using just neutron signatures were filtered by density to select ideal cutoff values. Three cutoff values were

found to give the most favorable outcomes in terms of sensitivity and specificity. Separate cutoffs were needed for targets with average densities 0-2 g cm⁻³, 2-3 g cm⁻³, and 3-9 g cm⁻³. However, the application of only neutron signatures in the discrimination process yielded specificity of only 47.6% (sensitivity was held constant at 90.5%). A similar analysis was conducted on ζ_ℓ calculated using only gamma-ray signatures. In the case of gamma-ray only ζ_ℓ calculations, only two cutoff values were needed (in density ranges 0-3 g cm⁻³ and 3-9 g cm⁻³). Maintaining sensitivity at 90.5%, the specificity was found to be 61.9%, a marked improvement over neutron only techniques. Finally, ζ_ℓ calculated using both neutron and gamma ray signatures, were analyzed using density filters. The analysis revealed that the choice in the number of cutoffs to be used determined the specificity (sensitivity being held constant at 90.5%). If only two cutoffs were used (in density ranges 0-3 g cm⁻³ and 3-9 g cm⁻³) the resulting specificity was found to be 66.7%. However, if three cutoffs were chosen (in density ranges 0-2 g cm⁻³, 2-3 g cm⁻³, and 3-9 g cm⁻³) a specificity of over 76% was found. Using neutron signatures in the calculation of the figure-of-merit provides better discrimination of targets in the density range of 2-3 g cm⁻³.

In the density groups investigated, different combinations of signatures give different results. By using only gamma-ray signatures in Density Group-1, neutron and gamma-ray signatures in Density Group-2, only neutron signatures in Density Group-3 and either neutron or neutron and gamma-ray signatures in Density Groups-4 and 5 (Table 4.4) a specificity of 85.7% can be achieved while maintaining a sensitivity of 90.5%. Thus, a SBRS system that has the capability of detecting and utilizing both neutron and gamma-ray backscattered radiation has the potential for discriminating explosive from inert targets with high levels of sensitivity and specificity.

5.3 Explosive Density and Clutter Materials

Targets containing the low density explosive Urea Nitrate (0.69 g cm⁻³) were misidentified (false positive result) 11 times more often than were targets containing the higher density RDX (1.8 g cm⁻³) in the experiments conducted. The clutter shielding the samples of Urea Nitrate consisted of materials mainly of density between 0 and 2 g cm⁻³. By adjusting the cutoff values in each of the Density Groups the number of false negative responses can be lowered or raised. The fact that targets with samples of Urea Nitrate were more often classified

incorrectly suggests that the templates used in this study were not adequate for low density explosive discrimination for targets with density between 0 and 2 g cm⁻³.

The targets identified as explosive when no explosive sample was present, consisted of materials one is likely to encounter in common explosive detection scenarios. Materials such as steel, clay, polyester, sand, and bricks are encountered more often in detection scenarios than are materials such as copper or gypsum. Although the artificial templates used in this study were not entirely successful in differentiating all explosive from inert targets, good sensitivity and specificity were obtained. Because the materials falsely identified as explosives are encountered often the number of false alarms given, using the templates used in this study, limits the effectiveness of the system in real-world application. Thus, research to identify superior artificial templates is warranted.

5.4 Full-Scale Tests Using Operational D-T Neutron Generator

A fully operational neutron generator is necessary for verifying the result of this study and to simulate actual physical conditions likely to face individuals tasked with identifying concealed explosives. Laboratory designs and shielding have been created for use with a D-T neutron generator capable of producing 14.1 MeV neutron at a rate of 10¹¹ neutrons per second. Full-scale tests should be conducted in preparation for a “field-use” model capable of being operated via remote control.

5.5 Implementation of a Larger Number of Templates

As previously mentioned, although the results of this investigation are encouraging more tests with a larger number of artificial templates are likely to improve on the results found here. As more tests are conducted the number of templates housed in a template library will grow. One cannot construct a library of an infinite number of templates, each of which will identify one or more IEDs. Thus, the goal must be to construct a library with a finite number of templates that are reasonably effective at differentiating explosives from inters. In order to limit the number of templates in a template library more experiments should be conducted to determine which templates perform well in a variety of situations and which most often fail to give valuable information.

References

- Adelphi, "Neutron Systems," San Carlos, California, 2012.
<http://www.adelphitech.com/products/neutrons_systemsMain.html>.
- Almog, J., G. Burda, Y. Shloosh, S. Abramovich-Bar, E. Wolf, T. Tamiri, "Recovery and Detection of Urea Nitrate in Traces," *Journal of Forensic Sciences*, Vol. 52, Issue 6, pp. 1284-1290, November 2007.
- Brewer, R.L., W.L. Dunn, S. Heider, C. Matthew, X. Yang, "The signature-based radiation-scanning approach to standoff detection of improvised explosive devices," *Applied Radiation and Isotopes*, Vol. 68, Issue 4-5, pp. 884-887, 2011.
- Buffler, A. "Contraband Detection With Fast Neutrons," *Radiation Physics and Chemistry*, Department of Physics, University of Cape Town, Vol. 71, pp. 853-861, 2004.
- Caffrey, A.J. Cole, J.D. Gehrke, R.J.; Greenwood, R.C., "Chemical warfare agent and high explosive identification by spectroscopy of neutron-induced gamma rays," *IEEE Transactions on Nuclear Science*, vol.39, no.5, pp.1422-1426, 1992.
- Chalmers, A., Single-sided X-ray inspection of vehicles using AS&E's Z-backscatter van, *Proc. SPIE*, Vol. 5199, pp. 19-25, 2004.
- Chawla, Krishan Kumar. Fibrous Materials. Cambridge, England: Cambridge UP, 1998.
- Department of Defense Office of Inspector General. "Procurement Policy for Armored Vehicles." Report No. D-2007-107, 2007.
<http://www.defense.gov/pubs/pdfs/Armored_Vehicles_Procurement.pdf> Accessed, February 12, 2012.
- Duderstadt, James J., and Louis J. Hamilton, Nuclear Reactor Analysis. Wiley, New York, 1976.
- Dunn, W. L., J. K. Shultis, Exploring Monte Carlo Methods. Elsevier, Amsterdam, 2011.
- Dunn, W.L., R. Brewer, K. Loschke, J. Lowrey, "Radiation Interrogation Using Signature Analysis for Detection of Chemical Explosives," *Proc. IEEE Conference on Technologies for Homeland Security: Enhancing Critical Infrastructure Dependability*, Boston, MA, 16-17 May, 2007, pp. 7-12. (a)
- Dunn, W.L., K. Banerjee, A. Allen, J. van Meter, "Feasibility of a method to identify targets that are likely to contain conventional explosives," *Nuclear Instruments and Methods in Physics Research B*, Vol. 263, pp. 179-182, 2007. (b)

- FM 3-21.8, "The Infantry Rifle Platoon and Squad," Headquarters Department of the Army Washington, DC. 2007.
- Garroway, A.N., M.L. Buess, J.B. Miller, B.H. Suits, A.D. Hibbs, G.A. Barrall, R. Matthews, L.J. Burnett, "Remote Sensing by Nuclear Quadrupole Resonance," *IEEE Transactions on Geoscience and Remote Sensing*, Vol. 39, No. 6, 2001.
- Gloyn, R. W. "Energy, Mineral, and Ground-water Resources of Carbon and Emery Counties, Utah". Utah Geological Survey, 2003.
- Goodings, A. C., & L. H. Turl, "The Density and Swelling of Silk Filaments In Relation to Moisture Content," The Journal of the Textile Institute: Transitions, pp. T69-T80, 1940.
- Gow, J., L. Ruby, "A Simple Pulsed Neutron Source Based on Crossed-Field Trapping," *Review of Scientific Instruments*, Vol. 30, Issue 5, pp. 315-317, 1959.
- Gudmundson, E., A. Jakobsson, P. Stoica, NQR-based explosives detection—an overview in Signals, Circuits and Systems, pp.1-4, July 2009.
- Horton, M., D. Ingersoll, M. Reichenberger, J. Weimer, "MCNP Simulation of Standoff Bomb Detection Using X-Ray Backscatter," Nuclear Senior Design Team, Kansas State University, 2011.
- Johll, Mark., "MCNP simulations for standoff bomb detection using neutron interrogation". Master's thesis, Kansas State University, 2009.
- Joint Improvised Explosive Device Defeat Organization. "JIEDDO annual report," 2010.
- Kuznetsov, A., A. Evsenin, MS-SRIP – Microwave System for Secret Standoff Inspection of People in Stand-off Detection of Suicide Bombers and Mobile Suspects, H. Schubert and A. Rimski-Korsakov, Springer, Netherlands, pp. 5-10, 2006.
- Landmine & Cluster Munition Monitor, "Landmine Monitor Report 2011: International Campaign to Ban Landmines," 2011. < http://www.the-monitor.org/index.php/publications/display?url=lm/2011/es/Casualties_and_Victim_Assistance.html > Accessed, February 12, 2012.
- Lawson, L. R., Severson, D., "Forestry White Paper: Nondestructive testing (NDT) of live trees," Wood Study Group, Bradford, PA, *Wood Study Zeitschrift*, Vol. 1, No. 3, 2003.
- Likos, W. J. and Lu, N., "A Laser Technique to Quantify the Size, Porosity, and Density of Clay Clusters During Sedimentation," *Geotechnical Testing Journal*, Vol. 24, No. 1, pp. 83–91, March 2001.

- Lo Presti, D. C. F., S. Pedroni, V. Crippa, "Maximum Dry Density of Cohesionless Soils by Pluviation and by ASTM D 4253-83: A Comparative Study," Geotechnical Testing Journal, Vol. 15, pp. 180-189, 1992.
- McMakin, D.L., D.M. Sheen, H.D. Collins, Remote concealed weapons and explosive detection on people using millimeter-wave holography in Security Technology, *30th Annual International Carnahan Conference*, pp.19-25, 2-4 Oct 1996.
- Micklich, B.J., C.L. Fink, T.J. Yule, "Accelerator requirements for fast-neutron interrogation of luggage and cargo," *Proceedings of the Particle Accelerator Conference*, pp.110-112, 1995.
- Molnár, G. L., Handbook of Prompt Gamma Activation Analysis with Neutron Beams, Kluwer Academic Publishers, Boston, London, 2004.
- Molnár, V., "Examination of Pressed Adobe Brick," Szechenyi Istvan University, Department of Architecture and Building Construction, *Hungarian Electronic Journal Manuscript no.: CEA-021227-A*, <<http://heja.szif.hu/ARC/ARC-021227-A/arc021227a.pdf>> Accessed, February 14, 2012.
- National Research Council, Existing and Potential Standoff Explosives Detection Techniques, National Academies Press, Washington D.C., 2004.
- Nelson, D. T., E. C. Eckel, W. F. Hillebrand, A. T. Coons, , Slate Deposits and Slate Industry of the United States. Washington: Govt. Print. Off., 1906.
- Nelson, S.A., "Weathering and Clay Minerals," Tulane University, New Orleans 2011 < <http://www.tulane.edu/~sanelson/eens211/weathering&clayminerals.htm>> Accessed February 14, 2012.
- Park, Seul-Hyun, Samuel L. Manzello, Dale P. Bentz, Tensei Mizukami. "Determining Thermal Properties of Gypsum Board at Elevated Temperatures." *Fire and Materials* 2009.
- Rinard, Phil M., Neutron Interactions with Matter in Passive Nondestructive Assay of Nuclear Materials, pp. 357-77, U.S. Nuclear Regulatory Commission, Washington D.C., 1991.
- Shultis, J.K., R.E. Faw, Radiation Shielding, American Nuclear Society Inc., La Grange Park, Illinois, 2000.
- Singh, S., M. Singh, "Explosives Detection Systems (EDS) for Aviation Security," *Signal Processing*, Vol. 83, pp. 31-55, 2003.
- USDA National Nutrient Database for Standard Reference, Release 23. U.S. Department of Agriculture. < <http://www.ars.usda.gov/services/docs.htm?docid=8964>> Accessed, February 14, 2012.

Vourvopoulos, G., P.C. Womble, "Pulsed fast/thermal neutron analysis: a technique for explosives detection," *Talanta*, Vol. 54, pp. 459-468, 2001.

Williams III, R., C. Gesh and R. Pagh, "Compendium of Material Composition Data for Radiation Transport Modeling," *Pacific Northwest National Laboratory*, prepared for DOE, PNNL- 15870, 2006.

Woodfin, Ronald L, Trace Chemical Sensing of Explosives. Wiley, Hoboken, NJ, 2007.

X-5 Monte Carlo Team, "MCNP – A General Monte Carlo N-Particle Transport Code, Version 5, Volume I: Overview and Theory," *Los Alamos National Laboratory*, 2008.

Appendix A - Template Signatures

Table A.1 Signature designations

Signature Number	Element	Energy (MeV)	Type of Reaction or Category
Gamma-ray Signatures			
1	Hydrogen	2.2232	prompt-capture
2	Nitrogen	2.3128	Inelastic-scatter
3	Nitrogen	3.3786	Inelastic-scatter
4	Carbon	4.439	Inelastic-scatter
5	Nitrogen	4.9151	Inelastic-scatter
6	Nitrogen	5.1059	Inelastic-scatter
7	Oxygen	6.1299	Inelastic-scatter
8	Nitrogen	6.4462	Inelastic-scatter
9	Oxygen	6.9171	Inelastic-scatter
Neutron Signatures			
10		$< 0.4 \times 10^{-6}$	Below Cd cutoff
11		$> 0.4 \times 10^{-6}$	Above Cd cutoff

Table A.2 Templates with RDX sample.

Template				
Nomenclature	N0O50C0H0Crhd	N0O50C0H0Crld	N0O50C0H0Crmd	N0O50C0H0Crvld
Signature				
1	2.273250E-10	3.786250E-10	2.519500E-10	4.398000E-10
$\sigma (\pm)$	8.919970E-11	5.966980E-11	7.273370E-11	4.488140E-11
2	2.150960E-09	4.701300E-08	2.252060E-08	7.295100E-08
$\sigma (\pm)$	1.339700E-10	5.418780E-10	1.039250E-10	1.502360E-10
3	2.822400E-10	9.029730E-09	4.516180E-09	1.344600E-08
$\sigma (\pm)$	1.315780E-10	7.204560E-11	6.507900E-11	7.826880E-11
4	5.193420E-08	2.959520E-07	1.721930E-07	4.230130E-07
$\sigma (\pm)$	1.407140E-10	3.279900E-10	2.283810E-10	4.240670E-10
5	5.162250E-10	9.485180E-09	4.948540E-09	1.404980E-08
$\sigma (\pm)$	5.835400E-11	7.147130E-11	5.978080E-11	8.687930E-11
6	2.042900E-09	3.966370E-08	2.089430E-08	5.828870E-08
$\sigma (\pm)$	6.074080E-11	1.080240E-10	7.453390E-11	1.365140E-10
7	4.362920E-07	3.327030E-07	3.718140E-07	3.039770E-07
$\sigma (\pm)$	4.408110E-10	4.026150E-10	4.128570E-10	3.672630E-10
8	6.686450E-10	1.127250E-08	6.057880E-09	1.651070E-08
$\sigma (\pm)$	4.880740E-11	6.143370E-11	4.753080E-11	7.590300E-11
9	1.000440E-07	7.708080E-08	8.501190E-08	7.214830E-08
$\sigma (\pm)$	2.050360E-10	1.725210E-10	1.823460E-10	1.680690E-10
10	3.885230E-10	1.069160E-09	6.941580E-10	1.518100E-09
$\sigma (\pm)$	7.420790E-12	1.903100E-11	9.787630E-12	2.201240E-11
11	4.526050E-06	1.906710E-06	2.462360E-06	1.705470E-06
$\sigma (\pm)$	1.810420E-09	9.533550E-10	1.231180E-09	8.527350E-10

Template				
Nomenclature	N0O60C20H0Crhd	N0O60C20H0Crlld	N0O60C20H0Crmld	N0O60C20H0Crvld
Signature				
1	0.000000E+00	3.144350E-10	3.182100E-10	4.310300E-10
σ (±)	0.000000E+00	5.140940E-11	8.031360E-11	4.284240E-11
2	1.699920E-09	4.394150E-08	2.007260E-08	7.193370E-08
σ (±)	1.747270E-10	1.101580E-10	9.986070E-11	1.475780E-10
3	2.738650E-10	8.583990E-09	3.936710E-09	1.331790E-08
σ (±)	7.760150E-11	1.566550E-10	7.052560E-11	7.205650E-11
4	4.213750E-07	4.264170E-07	4.082020E-07	4.599810E-07
σ (±)	4.668650E-10	4.282500E-10	4.515300E-10	4.608870E-10
5	4.361550E-10	8.987670E-09	4.391660E-09	1.385430E-08
σ (±)	5.347040E-11	7.048550E-11	5.474710E-11	8.517070E-11
6	1.453980E-09	3.770850E-08	1.876220E-08	5.760100E-08
σ (±)	5.472670E-11	1.062200E-10	7.387090E-11	1.405590E-10
7	7.826070E-07	4.551090E-07	5.948620E-07	3.385270E-07
σ (±)	6.303710E-10	5.039600E-10	5.391050E-10	4.088140E-10
8	5.356480E-10	1.081570E-08	5.499140E-09	1.634400E-08
σ (±)	3.805220E-11	5.933630E-11	4.525830E-11	7.481640E-11
9	1.837550E-07	1.046770E-07	1.372930E-07	7.974180E-08
σ (±)	2.795970E-10	2.122110E-10	2.506320E-10	1.855140E-10
10	1.300200E-09	8.237110E-10	5.747450E-10	1.443070E-09
σ (±)	1.781270E-11	1.136720E-11	1.034540E-11	2.395500E-11
11	4.428920E-06	1.804800E-06	2.390880E-06	1.649360E-06
σ (±)	1.328680E-09	9.024000E-10	9.563520E-10	6.597440E-10

Template					
Nomenclature		N000C50H50hd	N000C50H50ld	N000C50H50md	N000C50H50vld
	1	2.487680E-06	1.750110E-07	1.208540E-06	1.634840E-09
σ (\pm)		1.246410E-09	3.174110E-10	8.478390E-10	4.634040E-11
	2	2.441660E-10	3.446160E-08	1.099410E-08	6.793820E-08
σ (\pm)		4.449600E-11	9.384860E-11	5.651250E-11	1.454300E-10
	3	0.000000E+00	6.409020E-09	1.935690E-09	1.246990E-08
σ (\pm)		0.000000E+00	5.351320E-11	4.579860E-11	6.903950E-11
	4	2.175210E-06	1.297180E-06	1.823750E-06	7.198330E-07
σ (\pm)		1.088210E-09	9.084470E-10	1.094750E-09	6.483940E-10
	5	3.621100E-11	6.823110E-09	2.270850E-09	1.299540E-08
σ (\pm)		1.147150E-11	5.455340E-11	2.922760E-11	8.136810E-11
	6	0.000000E+00	2.884710E-08	9.731550E-09	5.411470E-08
σ (\pm)		0.000000E+00	8.870290E-11	4.826000E-11	1.317140E-10
	7	7.875970E-10	1.326560E-07	4.717180E-08	2.416690E-07
σ (\pm)		1.427960E-11	2.136590E-10	1.139630E-10	3.160790E-10
	8	4.794790E-11	8.312420E-09	2.896460E-09	1.544120E-08
σ (\pm)		9.401190E-12	4.960940E-11	2.737810E-11	7.346480E-11
	9	2.274950E-10	3.263150E-08	1.184180E-08	5.853190E-08
σ (\pm)		9.799650E-12	1.024250E-10	5.397460E-11	1.479350E-10
	10	2.703560E-07	8.830570E-08	2.164820E-07	3.106820E-09
σ (\pm)		7.840320E-10	4.238670E-10	4.762600E-10	1.124670E-10
	11	2.368750E-06	1.848140E-06	2.226450E-06	1.494110E-06
σ (\pm)		1.421250E-09	1.108880E-09	1.335870E-09	8.964660E-10

Template				
Nomenclature	N0O10C30H60hd	N0O10C30H60ld	N0O10C30H60md	N0O10C30H60vld
Signature				
1	2.913520E-06	3.505760E-07	1.729490E-06	3.009750E-09
$\sigma (\pm)$	1.167720E-09	4.576930E-10	8.664640E-10	5.317200E-11
2	1.562330E-10	3.261450E-08	9.441440E-09	6.720360E-08
$\sigma (\pm)$	4.260570E-11	9.268030E-11	5.500220E-11	1.438710E-10
3	0.000000E+00	5.937770E-09	1.712480E-09	1.226330E-08
$\sigma (\pm)$	0.000000E+00	5.314390E-11	4.458130E-11	6.832990E-11
4	1.347640E-06	9.186840E-07	1.185940E-06	6.090340E-07
$\sigma (\pm)$	8.091460E-10	7.354900E-10	8.307940E-10	5.486760E-10
5	0.000000E+00	6.426490E-09	1.901030E-09	1.282760E-08
$\sigma (\pm)$	0.000000E+00	5.403260E-11	2.983740E-11	8.179960E-11
6	0.000000E+00	2.701440E-08	8.295930E-09	5.334180E-08
$\sigma (\pm)$	0.000000E+00	8.886350E-11	4.951590E-11	1.352450E-10
7	3.199570E-07	2.927740E-07	3.035950E-07	2.903750E-07
$\sigma (\pm)$	4.178980E-10	3.827440E-10	3.966410E-10	3.796960E-10
8	0.000000E+00	7.757670E-09	2.419630E-09	1.516040E-08
$\sigma (\pm)$	0.000000E+00	4.789180E-11	2.482830E-11	7.231030E-11
9	7.326810E-08	6.806330E-08	6.987420E-08	6.893060E-08
$\sigma (\pm)$	1.848820E-10	1.718610E-10	1.762600E-10	1.672290E-10
10	2.375470E-07	1.145950E-07	2.097820E-07	4.913380E-09
$\sigma (\pm)$	5.701130E-10	4.469200E-10	4.824990E-10	8.057940E-11
11	1.941680E-06	1.658070E-06	1.875270E-06	1.423100E-06
$\sigma (\pm)$	1.359180E-09	1.160650E-09	1.312690E-09	8.538600E-10

Template				
Nomenclature	N0O20C30H50hd	N0O20C30H50ld	N0O20C30H50md	N0O20C30H50vld
Signature				
1	2.177890E-06	1.121120E-07	9.282420E-07	1.244430E-09
$\sigma (\pm)$	8.737560E-10	2.722200E-10	6.516540E-10	4.449450E-11
2	2.592530E-10	3.529620E-08	1.162000E-08	6.826640E-08
$\sigma (\pm)$	4.781710E-11	9.628660E-11	5.847130E-11	1.462120E-10
3	0.000000E+00	6.586370E-09	2.080900E-09	1.251700E-08
$\sigma (\pm)$	0.000000E+00	5.580240E-11	4.855080E-11	6.813060E-11
4	1.226420E-06	8.166360E-07	1.051840E-06	5.754770E-07
$\sigma (\pm)$	8.592890E-10	6.539060E-10	7.370560E-10	5.760410E-10
5	0.000000E+00	7.067200E-09	2.477820E-09	1.304920E-08
$\sigma (\pm)$	0.000000E+00	5.818640E-11	3.855520E-11	8.216680E-11
6	0.000000E+00	2.960610E-08	1.041590E-08	5.439130E-08
$\sigma (\pm)$	0.000000E+00	9.149500E-11	5.441010E-11	1.325960E-10
7	5.761420E-07	4.118220E-07	5.010210E-07	3.261470E-07
$\sigma (\pm)$	5.787760E-10	4.556260E-10	5.034780E-10	3.936940E-10
8	0.000000E+00	8.486570E-09	3.043500E-09	1.550610E-08
$\sigma (\pm)$	0.000000E+00	5.001920E-11	2.995830E-11	7.228070E-11
9	1.334960E-07	9.487840E-08	1.156190E-07	7.662600E-08
$\sigma (\pm)$	2.423800E-10	2.111730E-10	2.335450E-10	1.781460E-10
10	2.678420E-07	6.882020E-08	2.005430E-07	2.241670E-09
$\sigma (\pm)$	5.624680E-10	3.372190E-10	4.612490E-10	5.066170E-11
11	2.303830E-06	1.724170E-06	2.120830E-06	1.457370E-06
$\sigma (\pm)$	1.151910E-09	1.034500E-09	1.272500E-09	8.744220E-10

Template				
Nomenclature	N10O10C50H30hd	N10O10C50H30ld	N10O10C50H30md	N10O10C50H30vld
Signature				
1	5.141500E-07	1.083270E-08	1.430230E-07	6.413240E-10
$\sigma (\pm)$	4.143230E-10	8.004630E-11	2.466050E-10	4.088810E-11
2	7.663970E-08	7.102020E-08	7.130010E-08	7.883250E-08
$\sigma (\pm)$	1.736620E-10	1.525460E-10	1.609060E-10	1.602990E-10
3	1.303250E-08	1.314030E-08	1.269910E-08	1.450090E-08
$\sigma (\pm)$	8.827020E-11	7.645830E-11	8.176510E-11	7.523180E-11
4	1.846270E-06	1.037720E-06	1.462760E-06	6.374120E-07
$\sigma (\pm)$	9.238170E-10	7.269850E-10	8.783650E-10	5.742070E-10
5	1.355290E-08	1.353130E-08	1.298860E-08	1.509690E-08
$\sigma (\pm)$	9.015860E-11	8.746550E-11	8.604720E-11	9.126720E-11
6	5.906010E-08	5.729340E-08	5.598710E-08	6.262160E-08
$\sigma (\pm)$	1.557080E-10	1.452440E-10	1.474910E-10	1.459420E-10
7	2.668150E-07	2.598290E-07	2.549130E-07	2.803560E-07
$\sigma (\pm)$	3.753010E-10	3.398850E-10	3.586670E-10	3.666330E-10
8	1.643490E-08	1.614480E-08	1.569510E-08	1.779110E-08
$\sigma (\pm)$	8.340210E-11	7.695710E-11	7.784930E-11	7.911480E-11
9	6.294010E-08	6.141560E-08	6.013960E-08	6.679830E-08
$\sigma (\pm)$	1.655530E-10	1.552050E-10	1.578410E-10	1.621200E-10
10	1.440480E-07	1.496420E-08	8.111680E-08	1.051200E-09
$\sigma (\pm)$	3.457150E-10	1.256990E-10	3.244670E-10	2.859260E-11
11	2.858700E-06	1.854720E-06	2.448600E-06	1.537860E-06
$\sigma (\pm)$	2.001090E-09	9.273600E-10	1.224300E-09	7.689300E-10

Template				
Nomenclature	N20O0C30H50hd	N20O0C30H50ld	N20O0C30H50md	N20O0C30H50vld
Signature				
1	7.547050E-07	8.772480E-08	4.234630E-07	1.383900E-09
$\sigma (\pm)$	2.571650E-09	2.140720E-10	4.257470E-10	4.468550E-11
2	1.709970E-07	1.205920E-07	1.504620E-07	9.344290E-08
$\sigma (\pm)$	2.593280E-10	2.194570E-10	2.431620E-10	1.798570E-10
3	2.953870E-08	2.163670E-08	2.615130E-08	1.714090E-08
$\sigma (\pm)$	1.172750E-10	9.696860E-11	1.087910E-10	8.425020E-11
4	1.283810E-06	8.485070E-07	1.102430E-06	5.844000E-07
$\sigma (\pm)$	7.709120E-10	6.794060E-10	7.723590E-10	5.849270E-10
5	3.035610E-08	2.230360E-08	2.668180E-08	1.776340E-08
$\sigma (\pm)$	1.352170E-10	1.176050E-10	1.267020E-10	1.014020E-10
6	1.306760E-07	9.294480E-08	1.136590E-07	7.321430E-08
$\sigma (\pm)$	2.362990E-10	1.966000E-10	2.171420E-10	1.626350E-10
7	8.450010E-10	1.324660E-07	4.734160E-08	2.414670E-07
$\sigma (\pm)$	2.030050E-11	2.135260E-10	1.148500E-10	3.158620E-10
8	3.614150E-08	2.590870E-08	3.139230E-08	2.070220E-08
$\sigma (\pm)$	1.233870E-10	1.044420E-10	1.170090E-10	8.988240E-11
9	2.324130E-10	3.234970E-08	1.177060E-08	5.833210E-08
$\sigma (\pm)$	1.551130E-11	1.016440E-10	5.476870E-11	1.474410E-10
10	9.157240E-08	4.215670E-08	7.846770E-08	2.323250E-09
$\sigma (\pm)$	3.205030E-10	1.897050E-10	2.667900E-10	4.971750E-11
11	1.992020E-06	1.672430E-06	1.904010E-06	1.460710E-06
$\sigma (\pm)$	1.195210E-09	1.003460E-09	1.142410E-09	8.764260E-10

Template				
Nomenclature	N0O50C0H0Cuhd	N0O50C0H0Culd	N0O50C0H0Cumd	N0O50C0H0Cuvld
Signature				
1	0.000000E+00	3.256700E-10	4.617050E-10	4.849300E-10
σ (±)	0.000000E+00	8.086440E-11	1.214950E-10	4.977980E-11
2	2.276550E-09	4.664390E-08	2.267400E-08	7.293530E-08
σ (±)	2.123290E-10	1.240610E-10	1.054270E-10	1.505890E-10
3	6.158000E-10	8.999510E-09	4.446480E-09	1.350820E-08
σ (±)	9.380940E-11	7.892400E-11	7.568030E-11	7.521260E-11
4	4.684910E-08	2.934540E-07	1.679970E-07	4.222580E-07
σ (±)	1.340420E-10	3.250290E-10	2.227290E-10	4.233620E-10
5	4.679650E-10	9.418040E-09	4.849680E-09	1.405890E-08
σ (±)	5.715050E-11	6.894740E-11	6.235350E-11	8.676960E-11
6	2.125800E-09	3.969580E-08	2.086150E-08	5.833150E-08
σ (±)	5.965620E-11	1.088760E-10	7.803420E-11	1.367020E-10
7	3.575070E-07	3.070470E-07	3.243410E-07	2.969720E-07
σ (±)	4.691130E-10	3.713660E-10	3.926160E-10	3.587700E-10
8	6.495650E-10	1.124670E-08	6.018680E-09	1.650570E-08
σ (±)	3.590060E-11	6.318860E-11	4.628860E-11	7.725590E-11
9	8.136330E-08	7.122420E-08	7.395130E-08	7.052790E-08
σ (±)	1.836340E-10	1.667040E-10	1.737740E-10	1.643850E-10
10	6.744690E-10	3.135060E-09	1.663570E-09	5.692220E-09
σ (±)	1.079150E-11	2.414000E-11	1.680210E-11	4.667620E-11
11	5.174310E-06	2.085590E-06	2.794930E-06	1.753120E-06
σ (±)	1.552290E-09	1.042800E-09	1.117970E-09	8.765600E-10

Template Nomenclature	N0O60C20H0Cuhd	N0O60C20H0Culd	N0O60C20H0Cumd	N0O60C20H0Cuvld
Signature				
1	3.211650E-10	4.388850E-10	3.913200E-10	4.287700E-10
σ (±)	1.167940E-10	6.668030E-11	7.756470E-11	4.602680E-11
2	1.550190E-09	4.418610E-08	2.099430E-08	7.193590E-08
σ (±)	1.158780E-10	1.160770E-10	8.243660E-10	1.480790E-10
3	3.262450E-10	8.483180E-09	4.023290E-09	1.333850E-08
σ (±)	7.990860E-11	7.226860E-11	7.009020E-11	7.282650E-11
4	3.762370E-07	4.113690E-07	3.799840E-07	4.559610E-07
σ (±)	4.179460E-10	4.129930E-10	4.207180E-10	4.569260E-10
5	4.349650E-10	8.970710E-09	4.382350E-09	1.389700E-08
σ (±)	5.556160E-11	7.005870E-11	5.586950E-11	8.519160E-11
6	1.547640E-09	3.790780E-08	1.899990E-08	5.765590E-08
σ (±)	5.698730E-11	1.074270E-10	7.686800E-11	1.409980E-10
7	6.928600E-07	4.263960E-07	5.399010E-07	3.306430E-07
σ (±)	5.580820E-10	4.721530E-10	5.434430E-10	3.993130E-10
8	4.603940E-10	1.085680E-08	5.493140E-09	1.630980E-08
σ (±)	3.440980E-11	5.849930E-11	4.325450E-11	7.610900E-11
9	1.617180E-07	9.787430E-08	1.240120E-07	7.792410E-08
σ (±)	2.628060E-10	2.084330E-10	2.264700E-10	1.813400E-10
10	2.540550E-09	2.913830E-09	1.762060E-09	5.449220E-09
σ (±)	2.362710E-11	2.505890E-11	1.973510E-11	4.413870E-11
11	4.778960E-06	1.925010E-06	2.596590E-06	1.682790E-06
σ (±)	1.433690E-09	9.625050E-10	1.038640E-09	8.413950E-10

Template Nomenclature	N0O30C0H70hd	N0O30C0H70ld	N0O30C0H70md	N0O30C0H70vld
Signature				
1	3.134680E-06	5.151560E-07	2.067030E-06	5.089160E-09
$\sigma (\pm)$	1.256390E-09	5.684850E-10	1.035380E-09	6.279030E-11
2	1.636300E-10	3.098510E-08	8.310730E-09	6.650790E-08
$\sigma (\pm)$	4.404980E-11	9.152640E-11	5.451890E-11	1.424120E-10
3	0.000000E+00	5.554190E-09	1.515660E-09	1.213850E-08
$\sigma (\pm)$	0.000000E+00	5.269770E-11	4.443370E-11	6.911450E-11
4	6.722860E-08	2.266910E-07	1.120420E-07	3.940310E-07
$\sigma (\pm)$	1.775120E-10	2.959550E-10	2.034390E-10	4.342930E-10
5	0.000000E+00	5.999990E-09	1.670540E-09	1.269580E-08
$\sigma (\pm)$	0.000000E+00	5.493340E-11	3.845220E-11	8.166760E-11
6	0.000000E+00	2.548950E-08	7.250000E-09	5.255200E-08
$\sigma (\pm)$	0.000000E+00	8.757230E-11	5.093480E-11	1.336320E-10
7	9.255580E-07	6.314740E-07	8.162040E-07	3.984730E-07
$\sigma (\pm)$	7.439110E-10	5.713760E-10	6.561540E-10	4.410010E-10
8	0.000000E+00	7.306690E-09	2.074200E-09	1.496380E-08
$\sigma (\pm)$	0.000000E+00	4.998440E-11	3.004990E-11	7.155030E-11
9	2.094970E-07	1.424250E-07	1.845470E-07	9.225870E-08
$\sigma (\pm)$	3.169920E-10	2.588470E-10	2.980300E-10	2.051550E-10
10	5.387840E-07	3.212530E-07	4.927630E-07	2.335700E-08
$\sigma (\pm)$	8.620540E-10	6.425060E-10	7.391440E-10	1.845200E-10
11	1.199380E-06	1.191660E-06	1.191260E-06	1.307490E-06
$\sigma (\pm)$	9.595040E-10	9.533280E-10	9.530080E-10	7.844940E-10

Table A.3 Templates with Urea Nitrate sample

Template				
Nomenclature	N0O50C0H0Crhd	N0O50C0H0Crld	N0O50C0H0Crmd	N0O50C0H0Crvld
Signature				
1	0.000000E+00	2.639850E-10	1.160800E-06	2.423650E-10
σ (±)	0.000000E+00	5.489770E-11	8.140970E-10	7.025970E-11
2	1.252600E-09	2.338490E-08	5.574680E-09	1.119960E-08
σ (±)	9.472890E-11	4.303530E-10	5.939250E-11	8.272530E-11
3	0.000000E+00	4.550490E-09	1.018740E-09	2.292450E-09
σ (±)	0.000000E+00	5.830890E-11	4.179960E-11	5.953940E-11
4	4.066190E-08	7.758540E-08	1.759760E-06	5.852250E-08
σ (±)	1.362890E-10	1.743350E-10	1.056250E-09	1.472540E-10
5	3.179300E-10	4.794060E-09	1.149600E-09	2.528120E-09
σ (±)	5.824660E-11	5.671600E-11	2.338080E-11	5.570880E-11
6	8.789800E-10	1.956300E-08	4.780160E-09	1.021300E-08
σ (±)	5.591350E-11	8.352090E-11	3.637710E-11	6.494120E-11
7	4.315780E-07	2.698110E-07	3.129780E-08	3.366260E-07
σ (±)	4.359940E-10	3.811040E-10	9.764360E-11	4.077500E-10
8	3.179400E-10	5.467360E-09	1.424480E-09	2.942440E-09
σ (±)	4.340060E-11	4.680400E-11	2.172760E-11	3.960020E-11
9	9.914080E-08	6.100380E-08	7.646860E-09	7.590530E-08
σ (±)	2.029780E-10	1.617420E-10	4.580730E-11	1.786110E-10
10	1.777420E-09	2.190760E-09	1.905060E-09	2.665230E-09
σ (±)	2.186230E-11	2.913710E-11	2.286070E-11	4.157760E-11
11	4.413410E-06	1.299270E-06	2.091480E-06	8.508730E-07
σ (±)	1.765360E-09	7.795620E-10	1.045740E-09	5.956110E-10

Template				
Nomenclature	N0O60C20H0Crhd	N0O60C20H0Crlid	N0O60C20H0Crmid	N0O60C20H0Crvld
Signature				
1	3.511950E-10	2.621250E-10	2.712200E-10	2.695690E-10
$\sigma (\pm)$	9.065410E-11	4.820440E-11	7.639330E-11	3.646650E-11
2	6.720350E-10	2.171330E-08	9.971890E-09	3.550010E-08
$\sigma (\pm)$	1.068840E-10	8.894360E-11	7.901730E-11	1.138330E-10
3	3.660950E-10	4.404720E-09	1.984680E-09	6.763010E-09
$\sigma (\pm)$	8.094430E-11	1.464750E-10	5.893420E-11	5.296470E-11
4	4.124890E-07	2.157690E-07	3.031750E-07	1.374360E-07
$\sigma (\pm)$	4.830840E-10	3.472320E-10	3.966830E-10	2.759400E-10
5	0.000000E+00	4.561480E-09	2.192380E-09	7.012420E-09
$\sigma (\pm)$	0.000000E+00	5.744390E-11	5.012250E-11	6.471690E-11
6	5.545600E-10	1.854170E-08	9.200500E-09	2.849730E-08
$\sigma (\pm)$	5.377780E-11	8.010160E-11	6.292100E-11	1.023600E-10
7	7.788530E-07	3.930790E-07	5.608270E-07	2.499760E-07
$\sigma (\pm)$	6.274330E-10	4.749620E-10	5.646570E-10	3.774190E-10
8	3.079650E-10	5.263380E-09	2.713200E-09	7.926760E-09
$\sigma (\pm)$	3.899750E-11	4.642830E-11	4.052850E-11	5.532820E-11
9	1.829020E-07	8.868120E-08	1.283590E-07	5.723320E-08
$\sigma (\pm)$	2.783490E-10	2.067460E-10	2.342610E-10	1.622380E-10
10	5.636400E-09	1.701320E-09	1.461700E-09	2.471750E-09
$\sigma (\pm)$	4.734580E-11	2.347820E-11	2.192550E-11	4.152540E-11
11	4.357010E-06	1.284230E-06	2.110270E-06	8.317300E-07
$\sigma (\pm)$	1.307100E-09	7.705380E-10	1.055130E-09	4.990380E-10

Template Nomenclature	N0O0C50H50hd	N0O0C50H50ld	N0O0C50H50md	N0O0C50H50vld
Signature				
1	2.487480E-06	1.476060E-07	1.160800E-06	9.713650E-10
$\sigma (\pm)$	9.972900E-10	2.973240E-10	8.140970E-10	3.746950E-11
2	0.000000E+00	1.693850E-08	5.574680E-09	3.352870E-08
$\sigma (\pm)$	0.000000E+00	7.221510E-11	5.939250E-11	1.063770E-10
3	0.000000E+00	3.198010E-09	1.018740E-09	6.343630E-09
$\sigma (\pm)$	0.000000E+00	4.044530E-11	4.179960E-11	5.056910E-11
4	2.173860E-06	1.118970E-06	1.759760E-06	4.072210E-07
$\sigma (\pm)$	1.087430E-09	8.954740E-10	1.056250E-09	5.297170E-10
5	0.000000E+00	3.481760E-09	1.149600E-09	6.588130E-09
$\sigma (\pm)$	0.000000E+00	4.179040E-11	2.338080E-11	6.190970E-11
6	0.000000E+00	1.412530E-08	4.780160E-09	2.668730E-08
$\sigma (\pm)$	0.000000E+00	6.758580E-11	3.637710E-11	9.804490E-11
7	5.582060E-10	8.742680E-08	3.129780E-08	1.595390E-07
$\sigma (\pm)$	1.336680E-11	1.848460E-10	9.764360E-11	2.728740E-10
8	0.000000E+00	4.057360E-09	1.424480E-09	7.496880E-09
$\sigma (\pm)$	0.000000E+00	3.636270E-11	2.172760E-11	5.403740E-11
9	1.448890E-10	2.091320E-08	7.646860E-09	3.759380E-08
$\sigma (\pm)$	9.591730E-12	8.462270E-11	4.580730E-11	1.254340E-10
10	6.841080E-07	2.005740E-07	5.421200E-07	5.138820E-09
$\sigma (\pm)$	1.094570E-09	6.618940E-10	8.131800E-10	8.376280E-11
11	1.955030E-06	1.504180E-06	1.862550E-06	8.601760E-07
$\sigma (\pm)$	1.173020E-09	1.052930E-09	1.117530E-09	6.021230E-10

Template				
Nomenclature	N0O10C30H60hd	N0O10C30H60ld	N0O10C30H60md	N0O10C30H60vld
Signature				
1	2.914970E-06	3.045850E-07	1.679420E-06	1.846320E-09
$\sigma (\pm)$	1.168250E-09	4.279680E-10	1.009420E-09	4.313340E-11
2	1.399440E-10	1.603820E-08	4.667070E-09	3.321300E-08
$\sigma (\pm)$	4.373400E-11	9.850600E-11	4.702570E-11	1.087170E-10
3	0.000000E+00	2.996470E-09	8.526610E-10	6.246590E-09
$\sigma (\pm)$	0.000000E+00	4.045520E-11	4.251220E-11	4.994480E-11
4	1.345790E-06	7.565420E-07	1.133680E-06	3.038830E-07
$\sigma (\pm)$	8.080510E-10	6.813510E-10	7.940160E-10	4.562510E-10
5	0.000000E+00	3.251160E-09	9.981990E-10	6.475630E-09
$\sigma (\pm)$	0.000000E+00	4.166730E-11	2.719270E-11	6.136430E-11
6	0.000000E+00	1.326200E-08	4.037180E-09	2.634020E-08
$\sigma (\pm)$	0.000000E+00	6.810030E-11	3.667560E-11	9.946360E-11
7	3.192840E-07	2.490850E-07	2.895860E-07	2.083630E-07
$\sigma (\pm)$	4.170870E-10	3.756640E-10	4.073190E-10	3.353600E-10
8	0.000000E+00	3.813940E-09	1.220750E-09	7.356250E-09
$\sigma (\pm)$	0.000000E+00	3.781360E-11	2.315400E-11	5.310610E-11
9	7.316980E-08	5.687720E-08	6.610640E-08	4.809880E-08
$\sigma (\pm)$	1.846210E-10	1.608540E-10	1.735590E-10	1.459190E-10
10	6.054800E-07	2.648210E-07	5.304310E-07	9.047350E-09
$\sigma (\pm)$	9.687680E-10	5.826060E-10	9.017330E-10	1.176160E-10
11	1.573810E-06	1.316050E-06	1.532580E-06	8.154390E-07
$\sigma (\pm)$	1.101670E-09	9.212350E-10	1.072810E-09	6.523510E-10

Template				
Nomenclature	N0O20C30H50hd	N0O20C30H50ld	N0O20C30H50md	N0O20C30H50vld
Signature				
1	2.179640E-06	1.872200E-09	8.848280E-07	7.533760E-10
$\sigma (\pm)$	8.743210E-10	2.324580E-10	1.595130E-09	3.594930E-11
2	0.000000E+00	1.740770E-08	5.837750E-09	3.367500E-08
$\sigma (\pm)$	0.000000E+00	7.492320E-11	5.188180E-11	1.078270E-10
3	0.000000E+00	3.329190E-09	1.132760E-09	6.369040E-09
$\sigma (\pm)$	0.000000E+00	4.539340E-11	4.553710E-11	5.024570E-11
4	1.224980E-06	6.422840E-07	9.883690E-07	2.659340E-07
$\sigma (\pm)$	8.582480E-10	6.427820E-10	7.913070E-10	4.259770E-10
5	0.000000E+00	3.593690E-09	1.221050E-09	6.598050E-09
$\sigma (\pm)$	0.000000E+00	4.487090E-11	3.327970E-11	6.214880E-11
6	0.000000E+00	1.451110E-08	5.052830E-09	2.683960E-08
$\sigma (\pm)$	0.000000E+00	7.056250E-11	4.225730E-11	9.891840E-11
7	5.751430E-07	3.631880E-07	4.826110E-07	2.420770E-07
$\sigma (\pm)$	5.778210E-10	4.382890E-10	5.334570E-10	3.653150E-10
8	0.000000E+00	4.157660E-09	1.504070E-09	7.526270E-09
$\sigma (\pm)$	0.000000E+00	3.776780E-11	2.405160E-11	5.346780E-11
9	1.331690E-07	8.251050E-08	1.108640E-07	5.537060E-08
$\sigma (\pm)$	2.419690E-10	1.999860E-10	2.238660E-10	1.623270E-10
10	6.787960E-07	1.532790E-07	5.001870E-07	3.910010E-09
$\sigma (\pm)$	8.824350E-10	5.058210E-10	7.502800E-10	6.568820E-11
11	1.892830E-06	1.383500E-06	1.770620E-06	8.067880E-07
$\sigma (\pm)$	1.135700E-09	9.684500E-10	1.062370E-09	6.454300E-10

Template				
Nomenclature	N10O10C50H30hd	N10O10C50H30ld	N10O10C50H30md	N10O10C50H30vld
Signature				
1	5.146440E-07	8.099150E-09	1.318360E-07	3.799100E-10
$\sigma (\pm)$	6.207550E-10	7.354090E-11	2.403410E-10	3.312970E-11
2	7.653450E-08	5.101190E-08	6.380280E-08	4.325890E-08
$\sigma (\pm)$	1.740730E-10	1.408390E-10	1.566460E-10	1.284870E-10
3	1.317350E-08	9.504020E-09	1.124680E-08	8.191600E-09
$\sigma (\pm)$	8.798250E-11	6.797370E-11	7.783600E-11	5.834180E-11
4	1.843960E-06	8.453250E-07	1.380710E-06	3.209800E-07
$\sigma (\pm)$	9.227070E-10	7.612210E-10	8.290420E-10	4.497690E-10
5	1.355340E-08	9.671290E-09	1.148490E-08	8.476210E-09
$\sigma (\pm)$	9.274120E-11	7.769450E-11	8.482810E-11	7.238610E-11
6	5.867170E-08	4.048740E-08	4.915380E-08	3.435210E-08
$\sigma (\pm)$	1.551160E-10	1.277540E-10	1.397620E-10	1.152780E-10
7	2.656950E-07	2.084960E-07	2.329120E-07	1.956650E-07
$\sigma (\pm)$	3.738540E-10	3.356180E-10	3.511280E-10	3.149930E-10
8	1.629540E-08	1.132760E-08	1.368720E-08	9.612240E-09
$\sigma (\pm)$	8.244520E-11	6.865470E-11	7.607930E-11	6.211290E-11
9	6.251600E-08	4.816930E-08	5.438500E-08	4.531700E-08
$\sigma (\pm)$	1.643430E-10	1.461200E-10	1.537040E-10	1.420480E-10
10	3.885130E-07	3.397660E-08	2.092260E-07	1.975340E-09
$\sigma (\pm)$	1.592900E-09	2.140530E-10	5.230650E-10	4.009940E-11
11	2.613760E-06	1.517550E-06	2.228840E-06	8.428690E-07
$\sigma (\pm)$	1.306880E-09	9.105300E-10	1.114420E-09	5.900080E-10

Template				
Nomenclature	N20O0C30H50hd	N20O0C30H50ld	N20O0C30H50md	N20O0C30H50vld
Signature				
1	7.505730E-07	7.335910E-08	4.064180E-07	7.989150E-10
$\sigma (\pm)$	5.278610E-10	1.938100E-10	4.086820E-10	3.621790E-11
2	1.711610E-07	1.010610E-07	1.440180E-07	5.790490E-08
$\sigma (\pm)$	2.594700E-10	2.041570E-10	2.328070E-10	1.524980E-10
3	2.955770E-08	1.823870E-08	2.503650E-08	1.091480E-08
$\sigma (\pm)$	1.170760E-10	9.050800E-11	1.062270E-10	6.899470E-11
4	1.282510E-06	6.774660E-07	1.042380E-06	2.761980E-07
$\sigma (\pm)$	7.701470E-10	6.778440E-10	7.301910E-10	4.147110E-10
5	3.026890E-08	1.879880E-08	2.549980E-08	1.126720E-08
$\sigma (\pm)$	1.345620E-10	1.122740E-10	1.263760E-10	8.612950E-11
6	1.304430E-07	7.738680E-08	1.083670E-07	4.527140E-08
$\sigma (\pm)$	2.360900E-10	1.869560E-10	2.178630E-10	1.373360E-10
7	5.791490E-10	8.735680E-08	3.137270E-08	1.594500E-07
$\sigma (\pm)$	1.883790E-11	1.848350E-10	9.822140E-11	2.727470E-10
8	3.605610E-08	2.150390E-08	2.974280E-08	1.265870E-08
$\sigma (\pm)$	1.231190E-10	9.748850E-11	1.138330E-10	7.401590E-11
9	1.782910E-10	2.080180E-08	7.592930E-09	3.749720E-08
$\sigma (\pm)$	1.763370E-11	8.422520E-11	4.752850E-11	1.251160E-10
10	2.531840E-07	1.038810E-07	2.146870E-07	4.154380E-09
$\sigma (\pm)$	5.316860E-10	3.531950E-10	4.508430E-10	8.225670E-11
11	1.830350E-06	1.391050E-06	1.735060E-06	8.243250E-07
$\sigma (\pm)$	1.098210E-09	9.737350E-10	1.041040E-09	5.770280E-10

Template Nomenclature	N0O50C0H0Cuhd	N0O50C0H0Culd	N0O50C0H0Cumd	N0O50C0H0Cuvld
Signature				
1	0.000000E+00	1.750550E-10	4.450650E-10	0.000000E+00
σ (±)	0.000000E+00	7.161990E-11	8.613820E-11	0.000000E+00
2	1.080030E-09	2.308420E-08	1.121920E-08	3.597580E-08
σ (±)	1.022200E-10	9.988650E-11	1.215660E-10	1.172740E-10
3	4.205850E-10	4.592640E-09	2.301520E-09	6.878730E-09
σ (±)	8.508380E-11	6.843080E-11	6.941080E-11	5.715430E-11
4	3.545290E-08	7.541840E-08	5.489340E-08	9.677840E-08
σ (±)	1.281740E-10	1.772030E-10	1.387950E-10	2.143940E-10
5	1.842250E-10	4.773630E-09	2.442650E-09	7.141440E-09
σ (±)	5.535980E-11	5.559330E-11	5.053400E-11	6.617210E-11
6	1.119380E-09	1.954720E-08	1.017580E-08	2.886650E-08
σ (±)	6.771280E-11	8.293190E-11	6.718670E-11	1.036830E-10
7	3.532530E-07	2.446890E-07	2.896820E-07	2.083730E-07
σ (±)	3.925640E-10	3.453640E-10	3.799390E-10	3.147690E-10
8	3.466970E-10	5.481290E-09	2.989570E-09	8.005150E-09
σ (±)	4.231540E-11	4.673910E-11	4.208280E-11	5.599500E-11
9	8.032280E-08	5.558610E-08	6.514190E-08	4.814070E-08
σ (±)	1.811410E-10	1.529670E-10	1.667160E-10	1.464200E-10
10	5.319840E-10	1.672220E-09	1.054950E-09	2.568470E-09
σ (±)	9.575710E-12	2.157160E-11	1.371430E-11	4.058180E-11
11	5.055510E-06	1.457680E-06	2.397570E-06	8.945840E-07
σ (±)	1.516650E-09	8.746080E-10	1.198790E-09	6.262090E-10

Template Nomenclature	N0O60C20H0Cuhd	N0O60C20H0Culd	N0O60C20H0Cumd	N0O60C20H0Cuvld
Signature				
1	5.580400E-10	0.000000E+00	0.000000E+00	2.608560E-10
σ (±)	1.212080E-10	0.000000E+00	0.000000E+00	4.020170E-11
2	8.441050E-10	2.177840E-08	1.008460E-08	3.547690E-08
σ (±)	1.079350E-10	9.342460E-11	8.765000E-11	1.144180E-10
3	0.000000E+00	4.311190E-09	1.958670E-09	6.826290E-09
σ (±)	0.000000E+00	6.045840E-11	6.356950E-11	5.469920E-11
4	3.671790E-07	2.004190E-07	2.748420E-07	1.332600E-07
σ (±)	4.079770E-10	3.427350E-10	3.876650E-10	2.677450E-10
5	1.892950E-10	4.579460E-09	2.186190E-09	7.050440E-09
σ (±)	5.426680E-11	5.579850E-11	4.808990E-11	6.550020E-11
6	7.328500E-10	1.868570E-08	9.249270E-09	2.852390E-08
σ (±)	5.488270E-11	8.052590E-11	6.530270E-11	1.023890E-10
7	6.895030E-07	3.644010E-07	5.060320E-07	2.420500E-07
σ (±)	5.553790E-10	4.402980E-10	5.095430E-10	3.654540E-10
8	2.395970E-10	5.277750E-09	2.642710E-09	7.906690E-09
σ (±)	3.671950E-11	4.733040E-11	3.827890E-11	5.874810E-11
9	1.608520E-07	8.226260E-08	1.154030E-07	5.553660E-08
σ (±)	2.614540E-10	1.919370E-10	2.227850E-10	1.575490E-10
10	1.988420E-09	1.493190E-09	1.120350E-09	1.120350E-09
σ (±)	2.087840E-11	1.941150E-11	1.680520E-11	1.680520E-11
11	4.711610E-06	1.385650E-06	2.297680E-06	2.297680E-06
σ (±)	1.413480E-09	8.313900E-10	1.148840E-09	1.148840E-09

Template Nomenclature Signature	N0O30C0H70hd	N0O30C0H70ld	N0O30C0H70md	N0O30C0H70vld
1	3.134420E-06	4.528230E-07	2.014750E-06	2.914040E-09
$\sigma (\pm)$	1.256280E-09	5.449960E-10	1.009130E-09	4.920150E-11
2	1.218930E-10	1.534910E-08	4.225680E-09	3.286080E-08
$\sigma (\pm)$	4.416330E-11	6.978370E-11	5.346160E-11	1.085230E-10
3	0.000000E+00	2.899240E-09	7.846570E-10	6.179210E-09
$\sigma (\pm)$	0.000000E+00	4.261820E-11	4.335230E-11	5.064980E-11
4	6.694520E-08	8.299330E-08	7.113190E-08	9.907480E-08
$\sigma (\pm)$	1.766860E-10	1.841300E-10	1.727050E-10	2.187900E-10
5	0.000000E+00	3.078120E-09	8.411510E-10	6.408330E-09
$\sigma (\pm)$	0.000000E+00	4.480360E-11	3.463490E-11	6.184340E-11
6	0.000000E+00	1.249190E-08	3.481280E-09	2.599890E-08
$\sigma (\pm)$	0.000000E+00	6.641250E-11	4.189080E-11	9.845530E-11
7	9.254420E-07	5.873860E-07	8.025540E-07	3.155940E-07
$\sigma (\pm)$	7.438230E-10	5.905450E-10	6.452060E-10	4.127780E-10
8	0.000000E+00	3.530690E-09	1.027590E-09	7.247430E-09
$\sigma (\pm)$	0.000000E+00	3.414740E-11	2.483920E-11	5.225960E-11
9	2.094600E-07	1.314230E-07	1.811180E-07	7.142840E-08
$\sigma (\pm)$	3.169530E-10	2.521820E-10	2.925450E-10	1.877190E-10
10	5.387970E-07	2.919700E-07	4.893500E-07	1.315590E-08
$\sigma (\pm)$	8.620750E-10	6.715310E-10	7.340250E-10	1.578710E-10
11	1.199360E-06	1.057830E-06	1.179580E-06	7.326120E-07
$\sigma (\pm)$	9.594880E-10	8.462640E-10	9.436640E-10	6.593510E-10

Appendix B - Example MCNP Code

Mockup of Car Bomb experiment

c THIS HAS A GAMMA PNT DETECTOR MOVED ALONG THE POSITIVE Z-AXIS
 c AND TWO NEUTRON PNT DETECTORS MOVED ALONG THE POSITIVE X-AXIS

c

C ***** BLOCK 1 -- CELLS *****

1 0 -20 (-200:-100:103:-110:111:245) imp:n,p=1 imp:n,p=1 \$between Al box & clutter

7 3 -2.7 20 -21 imp:n,p=1 \$aluminum box

8 0 21 -999 imp:n,p=1 \$inside void

13 0 999 imp:n,p=0 \$outer void/killzone

c

c -----clutter boxes-----

c -THE FIRST BOX of each set IS NEAREST TO THE SOURCE-

c the boxes to the left of the source are the 400s

c the middle boxes are the 200s

c the boxes to the right of the source are the 300s

c =====

c -----

401 0 102 -103 110 -111 200 -201 imp:n,p=1 \$Right Clutter Box 1

402 0 102 -103 110 -111 201 -202 imp:n,p=1 \$Right Clutter Box 2

403 0 102 -103 110 -111 202 -203 imp:n,p=1 \$Right Clutter Box 3

404 0 102 -103 110 -111 203 -204 imp:n,p=1 \$Right Clutter Box 4

405 0 102 -103 110 -111 204 -205 imp:n,p=1 \$Right Clutter Box 5

406 0 102 -103 110 -111 205 -206 imp:n,p=1 \$Right Clutter Box 6

407 0 102 -103 110 -111 206 -207 imp:n,p=1 \$Right Clutter Box 7

408 0 102 -103 110 -111 207 -208 imp:n,p=1 \$Right Clutter Box 8

409 0 102 -103 110 -111 208 -209 imp:n,p=1 \$Right Clutter Box 9

410 0 102 -103 110 -111 209 -210 imp:n,p=1 \$Right Clutter Box 10

411 0 102 -103 110 -111 210 -211 imp:n,p=1 \$Right Clutter Box 11

412 0 102 -103 110 -111 211 -212 imp:n,p=1 \$Right Clutter Box 12

413 0 102 -103 110 -111 212 -213 imp:n,p=1 \$Right Clutter Box 13

414 0 102 -103 110 -111 213 -214 imp:n,p=1 \$Right Clutter Box 14

415 0 102 -103 110 -111 214 -215 imp:n,p=1 \$Right Clutter Box 15

416 0 102 -103 110 -111 215 -216 imp:n,p=1 \$Right Clutter Box 16

417 0 102 -103 110 -111 216 -217 imp:n,p=1 \$Right Clutter Box 17

418 0 102 -103 110 -111 217 -218 imp:n,p=1 \$Right Clutter Box 18

419 0 102 -103 110 -111 218 -219 imp:n,p=1 \$Right Clutter Box 19

420 0 102 -103 110 -111 219 -220 imp:n,p=1 \$Right Clutter Box 20

421 0 102 -103 110 -111 220 -221 imp:n,p=1 \$Right Clutter Box 21

422 0 102 -103 110 -111 221 -222 imp:n,p=1 \$Right Clutter Box 22

423 0 102 -103 110 -111 222 -223 imp:n,p=1 \$Right Clutter Box 23

424 4 -1.8500 102 -103 110 -111 223 -224 imp:n,p=1 \$Right Clutter Box 24

425 4 -1.8500 102 -103 110 -111 224 -225 imp:n,p=1 \$Right Clutter Box 25

426 4 -1.8500 102 -103 110 -111 225 -226 imp:n,p=1 \$Right Clutter Box 26

427 4 -1.8500 102 -103 110 -111 226 -227 imp:n,p=1 \$Right Clutter Box 27
 428 4 -1.8500 102 -103 110 -111 227 -228 imp:n,p=1 \$Right Clutter Box 28
 429 4 -1.8500 102 -103 110 -111 228 -229 imp:n,p=1 \$Right Clutter Box 29
 430 4 -1.8500 102 -103 110 -111 229 -230 imp:n,p=1 \$Right Clutter Box 30
 431 4 -1.8500 102 -103 110 -111 230 -231 imp:n,p=1 \$Right Clutter Box 31
 432 4 -1.8500 102 -103 110 -111 231 -232 imp:n,p=1 \$Right Clutter Box 32
 433 4 -1.8500 102 -103 110 -111 232 -233 imp:n,p=1 \$Right Clutter Box 33
 434 0 102 -103 110 -111 233 -234 imp:n,p=1 \$Right Clutter Box 34
 435 0 102 -103 110 -111 234 -235 imp:n,p=1 \$Right Clutter Box 35
 436 0 102 -103 110 -111 235 -236 imp:n,p=1 \$Right Clutter Box 36
 437 0 102 -103 110 -111 236 -237 imp:n,p=1 \$Right Clutter Box 37
 438 0 102 -103 110 -111 237 -238 imp:n,p=1 \$Right Clutter Box 38
 439 0 102 -103 110 -111 238 -239 imp:n,p=1 \$Right Clutter Box 39
 440 0 102 -103 110 -111 239 -240 imp:n,p=1 \$Right Clutter Box 40
 441 0 102 -103 110 -111 240 -241 imp:n,p=1 \$Right Clutter Box 41
 442 0 102 -103 110 -111 241 -242 imp:n,p=1 \$Right Clutter Box 42
 443 0 102 -103 110 -111 242 -243 imp:n,p=1 \$Right Clutter Box 43
 444 0 102 -103 110 -111 243 -244 imp:n,p=1 \$Right Clutter Box 44
 445 0 102 -103 110 -111 244 -245 imp:n,p=1 \$Right Clutter Box 45

c -----

201 0 101 -102 110 -111 200 -201 imp:n,p=1 \$Middle Clutter Box 1
 202 0 101 -102 110 -111 201 -202 imp:n,p=1 \$Middle Clutter Box 2
 203 0 101 -102 110 -111 202 -203 imp:n,p=1 \$Middle Clutter Box 3
 204 0 101 -102 110 -111 203 -204 imp:n,p=1 \$Middle Clutter Box 4
 205 0 101 -102 110 -111 204 -205 imp:n,p=1 \$Middle Clutter Box 5
 206 0 101 -102 110 -111 205 -206 imp:n,p=1 \$Middle Clutter Box 6
 207 0 101 -102 110 -111 206 -207 imp:n,p=1 \$Middle Clutter Box 7
 208 0 101 -102 110 -111 207 -208 imp:n,p=1 \$Middle Clutter Box 8
 209 0 101 -102 110 -111 208 -209 imp:n,p=1 \$Middle Clutter Box 9
 210 0 101 -102 110 -111 209 -210 imp:n,p=1 \$Middle Clutter Box 10
 211 0 101 -102 110 -111 210 -211 imp:n,p=1 \$Middle Clutter Box 11
 212 0 101 -102 110 -111 211 -212 imp:n,p=1 \$Middle Clutter Box 12
 213 0 101 -102 110 -111 212 -213 imp:n,p=1 \$Middle Clutter Box 13
 214 0 101 -102 110 -111 213 -214 imp:n,p=1 \$Middle Clutter Box 14
 215 0 101 -102 110 -111 214 -215 imp:n,p=1 \$Middle Clutter Box 15
 216 0 101 -102 110 -111 215 -216 imp:n,p=1 \$Middle Clutter Box 16
 217 0 101 -102 110 -111 216 -217 imp:n,p=1 \$Middle Clutter Box 17
 218 0 101 -102 110 -111 217 -218 imp:n,p=1 \$Middle Clutter Box 18
 219 0 101 -102 110 -111 218 -219 imp:n,p=1 \$Middle Clutter Box 19
 220 0 101 -102 110 -111 219 -220 imp:n,p=1 \$Middle Clutter Box 20
 221 0 101 -102 110 -111 220 -221 imp:n,p=1 \$Middle Clutter Box 21
 222 0 101 -102 110 -111 221 -222 imp:n,p=1 \$Middle Clutter Box 22
 223 0 101 -102 110 -111 222 -223 imp:n,p=1 \$Middle Clutter Box 23
 224 4 -1.8500 101 -102 110 -111 223 -224 imp:n,p=1 \$Middle Clutter Box 24
 225 4 -1.8500 101 -102 110 -111 224 -225 imp:n,p=1 \$Middle Clutter Box 25
 226 4 -1.8500 101 -102 110 -111 225 -226 imp:n,p=1 \$Middle Clutter Box 26

227 4 -1.8500 101 -102 110 -111 226 -227 imp:n,p=1 \$Middle Clutter Box 27
 228 4 -1.8500 101 -102 110 -111 227 -228 imp:n,p=1 \$Middle Clutter Box 28
 229 4 -1.8500 101 -102 110 -111 228 -229 imp:n,p=1 \$Middle Clutter Box 29
 230 4 -1.8500 101 -102 110 -111 229 -230 imp:n,p=1 \$Middle Clutter Box 30
 231 4 -1.8500 101 -102 110 -111 230 -231 imp:n,p=1 \$Middle Clutter Box 31
 232 4 -1.8500 101 -102 110 -111 231 -232 imp:n,p=1 \$Middle Clutter Box 32
 233 4 -1.8500 101 -102 110 -111 232 -233 imp:n,p=1 \$Middle Clutter Box 33
 234 0 101 -102 110 -111 233 -234 imp:n,p=1 \$Middle Clutter Box 34
 235 12 -1.8000 101 -102 110 -111 234 -235 imp:n,p=1 \$Sample Box 35
 236 12 -1.8000 101 -102 110 -111 235 -236 imp:n,p=1 \$Sample Box 36
 237 12 -1.8000 101 -102 110 -111 236 -237 imp:n,p=1 \$Sample Box 37
 238 12 -1.8000 101 -102 110 -111 237 -238 imp:n,p=1 \$Sample Box 38
 239 12 -1.8000 101 -102 110 -111 238 -239 imp:n,p=1 \$Sample Box 39
 240 12 -1.8000 101 -102 110 -111 239 -240 imp:n,p=1 \$Sample Box 40
 241 12 -1.8000 101 -102 110 -111 240 -241 imp:n,p=1 \$Sample Box 41
 242 12 -1.8000 101 -102 110 -111 241 -242 imp:n,p=1 \$Sample Box 42
 243 12 -1.8000 101 -102 110 -111 242 -243 imp:n,p=1 \$Sample Box 43
 244 12 -1.8000 101 -102 110 -111 243 -244 imp:n,p=1 \$Sample Box 44
 245 12 -1.8000 101 -102 110 -111 244 -245 imp:n,p=1 \$Sample Box 45

c -----

101 0 100 -101 110 -111 200 -201 imp:n,p=1 \$Left Clutter Box 1
 102 0 100 -101 110 -111 201 -202 imp:n,p=1 \$Left Clutter Box 2
 103 0 100 -101 110 -111 202 -203 imp:n,p=1 \$Left Clutter Box 3
 104 0 100 -101 110 -111 203 -204 imp:n,p=1 \$Left Clutter Box 4
 105 0 100 -101 110 -111 204 -205 imp:n,p=1 \$Left Clutter Box 5
 106 0 100 -101 110 -111 205 -206 imp:n,p=1 \$Left Clutter Box 6
 107 0 100 -101 110 -111 206 -207 imp:n,p=1 \$Left Clutter Box 7
 108 0 100 -101 110 -111 207 -208 imp:n,p=1 \$Left Clutter Box 8
 109 0 100 -101 110 -111 208 -209 imp:n,p=1 \$Left Clutter Box 9
 110 0 100 -101 110 -111 209 -210 imp:n,p=1 \$Left Clutter Box 10
 111 0 100 -101 110 -111 210 -211 imp:n,p=1 \$Left Clutter Box 11
 112 0 100 -101 110 -111 211 -212 imp:n,p=1 \$Left Clutter Box 12
 113 0 100 -101 110 -111 212 -213 imp:n,p=1 \$Left Clutter Box 13
 114 0 100 -101 110 -111 213 -214 imp:n,p=1 \$Left Clutter Box 14
 115 0 100 -101 110 -111 214 -215 imp:n,p=1 \$Left Clutter Box 15
 116 0 100 -101 110 -111 215 -216 imp:n,p=1 \$Left Clutter Box 16
 117 0 100 -101 110 -111 216 -217 imp:n,p=1 \$Left Clutter Box 17
 118 0 100 -101 110 -111 217 -218 imp:n,p=1 \$Left Clutter Box 18
 119 0 100 -101 110 -111 218 -219 imp:n,p=1 \$Left Clutter Box 19
 120 0 100 -101 110 -111 219 -220 imp:n,p=1 \$Left Clutter Box 20
 121 0 100 -101 110 -111 220 -221 imp:n,p=1 \$Left Clutter Box 21
 122 0 100 -101 110 -111 221 -222 imp:n,p=1 \$Left Clutter Box 22
 123 0 100 -101 110 -111 222 -223 imp:n,p=1 \$Left Clutter Box 23
 124 4 -1.8500 100 -101 110 -111 223 -224 imp:n,p=1 \$Left Clutter Box 24
 125 4 -1.8500 100 -101 110 -111 224 -225 imp:n,p=1 \$Left Clutter Box 25
 126 4 -1.8500 100 -101 110 -111 225 -226 imp:n,p=1 \$Left Clutter Box 26

```

127 4 -1.8500 100 -101 110 -111 226 -227 imp:n,p=1 $Left Clutter Box 27
128 4 -1.8500 100 -101 110 -111 227 -228 imp:n,p=1 $Left Clutter Box 28
129 4 -1.8500 100 -101 110 -111 228 -229 imp:n,p=1 $Left Clutter Box 29
130 4 -1.8500 100 -101 110 -111 229 -230 imp:n,p=1 $Left Clutter Box 30
131 4 -1.8500 100 -101 110 -111 230 -231 imp:n,p=1 $Left Clutter Box 31
132 4 -1.8500 100 -101 110 -111 231 -232 imp:n,p=1 $Left Clutter Box 32
133 4 -1.8500 100 -101 110 -111 232 -233 imp:n,p=1 $Left Clutter Box 33
134 0      100 -101 110 -111 233 -234 imp:n,p=1 $Left Clutter Box 34
135 0      100 -101 110 -111 234 -235 imp:n,p=1 $Left Clutter Box 35
136 0      100 -101 110 -111 235 -236 imp:n,p=1 $Left Clutter Box 36
137 0      100 -101 110 -111 236 -237 imp:n,p=1 $Left Clutter Box 37
138 0      100 -101 110 -111 237 -238 imp:n,p=1 $Left Clutter Box 38
139 0      100 -101 110 -111 238 -239 imp:n,p=1 $Left Clutter Box 39
140 0      100 -101 110 -111 239 -240 imp:n,p=1 $Left Clutter Box 40
141 0      100 -101 110 -111 240 -241 imp:n,p=1 $Left Clutter Box 41
142 0      100 -101 110 -111 241 -242 imp:n,p=1 $Left Clutter Box 42
143 0      100 -101 110 -111 242 -243 imp:n,p=1 $Left Clutter Box 43
144 0      100 -101 110 -111 243 -244 imp:n,p=1 $Left Clutter Box 44
145 0      100 -101 110 -111 244 -245 imp:n,p=1 $Left Clutter Box 45

```

C ***** BLOCK 2 -- SURFACES *****

```

20 RPP -50 50 -100 0 0 100 $aluminum box outer
21 RPP -50.2 50.2 -100.2 0.2 -0.2 100.2 $aluminum box inner
999 SO 500.0

```

c

c ===== surfaces for clutter boxes=====

c

c -----Planes parrallel to the beam-----

```

100 px -48 $left side of clutter
101 px -7.62 $left side of middle clutter/sample box
102 px 7.62 $right side of middle clutter/sample box
103 px 48 $right side of clutter
110 pz 40.0 $bottom plane
111 pz 60.0 $top plane

```

c

c ----- Planes perpendicular to the beam -----

c THE FIRST PLANE IS NEAREST TO THE SOURCE

c =====

```

200 py -98.0 $Plane 1
201 py -97.0 $Plane 2
202 py -96.0 $Plane 3
203 py -95.0 $Plane 4
204 py -94.0 $Plane 5
205 py -93.0 $Plane 6
206 py -92.0 $Plane 7
207 py -91.0 $Plane 8

```

208 py -90.0 \$Plane 9
209 py -89.0 \$Plane 10
210 py -88.0 \$Plane 11
211 py -87.0 \$Plane 12
212 py -86.0 \$Plane 13
213 py -85.0 \$Plane 14
214 py -84.0 \$Plane 15
215 py -83.0 \$Plane 16
216 py -82.0 \$Plane 17
217 py -81.0 \$Plane 18
218 py -80.0 \$Plane 19
219 py -79.0 \$Plane 20
220 py -78.0 \$Plane 21
221 py -77.0 \$Plane 22
222 py -76.0 \$Plane 23
223 py -75.0 \$Plane 24
224 py -74.0 \$Plane 25
225 py -73.0 \$Plane 26
226 py -72.0 \$Plane 27
227 py -71.0 \$Plane 28
228 py -70.0 \$Plane 29
229 py -69.0 \$Plane 30
230 py -68.0 \$Plane 31
231 py -67.0 \$Plane 32
232 py -66.0 \$Plane 33
233 py -65.0 \$Plane 34
234 py -64.0 \$Plane 35
235 py -63.0 \$Plane 36
236 py -62.0 \$Plane 37
237 py -61.0 \$Plane 38
238 py -60.0 \$Plane 39
239 py -59.0 \$Plane 40
240 py -58.0 \$Plane 41
241 py -57.0 \$Plane 42
242 py -56.0 \$Plane 43
243 py -55.0 \$Plane 44
244 py -54.0 \$Plane 45
245 py -53.0 \$Plane 46

C ***** BLOCK 3 -- COMMANDS *****

mode n p
PHYS:n 20.0 0.000000001 0 0
NPS 20000000
c
c ----- SOURCE: plane parallel cylindrical beam
SDEF POS= 0 -150 50

AXS= 0 1 0
 EXT= 0
 RAD= d1
 PAR= 1
 VEC= 0 1 0
 DIR= 1
 ERG= 14.1
 ARA= 182.4
 SI1 0 7.62
 SP1 -21 1
 c
 F15:n 100 -150 50 0 ND
 c
 c Note: ND implies do not include uncollided flux component
 c Energy Bins:
 E15 0.0000004 20
 c
 F25:n 200 -150 50 0 ND
 c
 c Note: ND implies do not include uncollided flux component
 c Energy Bins:
 E25 0.0000004 20
 c
 c
 F35:p 0 -150 85 0 ND
 c
 c Note: ND implies do not include uncollided flux component
 c Energy Bins:
 E35 0. 0.865 .869 .873 0.877 1.256
 1.260 1.264 1.268
 1.629 1.633 1.637 1.641
 2.217 2.221 2.225 2.229
 2.307 2.311 2.315 2.319
 3.372 3.376 3.380 3.384
 3.888 3.892 3.896 4.432 4.436
 4.440 4.444 4.908 4.912
 4.916 4.920 4.939 4.943
 4.947 4.951 5.099 5.103
 5.107 5.111 6.123 6.127
 6.131 6.135 6.439 6.443
 6.447 6.451 6.910 6.914
 6.918 6.922 7.009 7.113 7.117
 7.121 10.823 10.827 10.831 10.835
 c
 c
 c ----- MATERIALS:

```

c
c *****
c Aluminum density 2.70 g/cm^3
c *****
m3 13027.74c 1.00000
c -----
C RDX (C3H6N6O6) (WITH CHN0 STOICHIOMETRY)
C composition by weight
C density of 1.8 g/cm^3
C
C -----
m12
    1001.74c .142857
    6012.50c 0.28571
    7014.70c 0.28571
    8016.70c 0.28571
c -----
c Adobe Brick, rho = 1.8500
c
m4
    1001.74c -0.005962
    8016.66c -0.539829
    14000.60c -0.407098
    13027.70c -0.020181
    12000.50c -0.003876
    11023.70c -0.005034
    19000.50c -0.004160
    20000.50c -0.005830
    26000.50c -0.008030

```

Appendix C - Sample Compositions and Density

Table C.1 Inert Compositions (Williams III, 2006).

Material	Density	Element	ZAID	Atomic fraction (or mass fraction indicated by a - sign)
Air	0.00121	C	6012	0.000151
		N	7014	0.784437
		O	8016	0.21075
		Ar	18000	0.004671
Aluminum	2.7	Al	13027	1
Bricks	1.8	O	8016	0.663062
		Al	13027	0.003916
		Si	14000	0.32314
		Ca	20000	0.007272
		Fe	26000	0.00261
Concrete	2.35	H	1001	-0.0056
		O	8016	-0.4983
		Na	11023	-0.0171
		Mg	12000	-0.0024
		Al	13027	-0.0456
		Si	14000	-0.3158
		S	16032	-0.0012
		K	19000	-0.0192
		Ca	20000	-0.0826
		Fe	26000	-0.0122
Copper	8.92	Cu	29000	1
Cotton	1.55	H	1001	0.4762
		C	6000	0.2857
		O	8016	0.2381

Glass	2.4	O	8016	0.603858
		Na	11023	0.088145
		Si	14028	0.251791
		Ca	20000	0.056205
Limestone	2.35	C	6000	0.2
		O	8016	0.6
		Ca	20000	0.2
Nylon	1.14	H	1001	0.578932
		C	6012	0.315803
		N	7014	0.052632
		O	8016	0.052633
Propane	0.0019	H	1001	0.72726
		C	6012	0.27274
Steel	7.85	C	6012	-0.0015
		N	7014	-0.0025
		Si	14000	-0.0075
		Cr	24000	-0.16
		Mn	25055	-0.05
		Fe	26000	-0.7385
		Ni	28000	-0.04
Wood	0.75	H	1001	0.4762
		C	6012	0.2857
		O	8016	0.2381

Table C.2 Inert Compositions.

Adobe	1.85	H	1001	-0.006
Brick (Molnar, V. CEA-021227-A)		O	8016	-0.5398
		Na	11023	-0.005
		Mg	12000	-0.0039
		Al	13027	-0.0202
		Si	14000	-0.4071
		K	19000	-0.0042
		Ca	20000	-0.0058
		Fe	26000	-0.008

Clay (Likos, 2001) (Nelson, 2011) 50/50 Montmorillinite/ Halloysite	1.285	H	1001	-0.026
		O	8016	-0.5707
		Na	11023	-0.0098
		Mg	12000	-0.0104
Coal (Gloyn, 2003)	1.29	H	1001	-0.0636
		C	6012	-0.8159
		N	7014	-0.0146
		O	8016	-0.1059
Fruit & Vegetables (USDA)	1.081	H	1001	-0.6417
		C	6012	-0.0375
		O	8016	-0.3208
Gypsum Board (Park et al., 2009)	0.752	H	1001	-0.0234
		O	8016	-0.5576
		S	16000	-0.1862
		Ca	20000	-0.2328
Polyester (Chawla, 198)	1.4	H	1001	-0.042
		C	6012	-0.625
		O	8016	-0.333
Sand (Lo Presti et al., 1992)	1.391	O	8016	-0.5326
		Si	14000	-0.4674
Silk (Goodings & Turl, 1940)	1.16	H	1001	-0.07
		C	6012	-0.344
		N	7014	-0.166
		O	8016	-0.42
Slate (Nelson, 1906)	2.84	O	8016	-0.3424
		Na	11023	-0.0703
		Mg	12000	-0.0372
		Al	13027	-0.0825
		Si	14000	-0.0429
		K	19000	-0.1195
		Ca	20000	-0.0613
		Ti	22048	-0.0732
		Fe	26000	-0.1707
Tin	7.365	Sn	50000	-1

Table C.3 Explosive Compositions.

Material	Density	Element	ZAID	Atomic fraction (or mass fraction indicated by a - sign)
Cyclonite (RDX) $C_3H_6N_6O_6$ (Williams III, 2006)	1.8	H	1001	0.0272
		C	6012	0.1622
		N	7014	0.3784
		O	8016	0.4322
Urea nitrate (UNi) $CH_5N_3O_4$ (Woodfin, 2007) (Johll, 2009)	0.69	H	1001	0.0409
		C	6012	0.0976
		N	7014	0.3414
		O	8016	0.52

Appendix D - Sample Pearl Script and C++ Codes for MCNP5 Data Processing

Table D.1 Pearl Script for isolating neutron signatures.

```
#!/usr/bin/perl

open ($Neutron_Response, ">", "Neutron_Response.txt") or die "$!"; #opens the ouput file
named Neutron_Response.txt

@a;
@b;
@c;
$length;

@files = <*.o>; #stores the names of all .o files into an array named @files
foreach $filename (@files)
{
    open(INFILE, '<', $filename) || die("can't open inputfile: $!"); #opens each .o file for
reading
    # print $output "\n\nThe name of this file is: $filename\n" ;
    $i=0;
    while ($line = <INFILE>)
    {

        if($line =~ /^\\s*(\\d\\.\\d+E[+-]\\d+)\\s+(\\d\\.\\d+E[+-]\\d+)\\s(\\d\\.\\d+)/) #Finds the line of
#MCNP5 output for processing
        {

            $line =~ /^\\s*(\\d\\.\\d+E[+-]\\d+)\\s+(\\d\\.\\d+E[+-]\\d+)\\s(\\d\\.\\d+)/;
            @a[$i] = $1; #stores the left column
            @b[$i] = $2; #stores the middle column
            @c[$i] = $3; #stores the right column
            $i++;

        }

    }

    $length = $#a/2+1;
    for($i=0; $i<$length; $i++)
    {
        $az[$i]=$a[$i];
    }
}
```

```

    $bz[$i]=$b[$i];
    $cz[$i]=$c[$i];
}
for($i=$length; $i<=#a+1; $i++)
{
    $ax[$i-$length]=$a[$i];
    $bx[$i-$length]=$b[$i];
    $cx[$i-$length]=$c[$i];
}
print $Neutron_Response " $filename\n";
for($i=0; $i<=#a; $i++)
{
    if ($a[$i]==0.0000004){
        print $Neutron_Response "$a[$i] $b[$i] $c[$i]\n"
    }
    if ($a[$i]==20.0){
        print $Neutron_Response "$a[$i] $b[$i] $c[$i]\n"
    }
}
;

close INFILE;

    Neutron_Response
}

```


Table D.2 C++ code for extracting gamma-ray signatures.

```
#include <iostream>
#include <string>
#include <sstream>
#include <fstream>
#include <vector>
#include <cmath>

using namespace std;
//sets of signatures
struct Template {
    double column1, column2, column3;
};

//does not need to be a friend of template
istream& operator >> (istream& ins, Template& r) {
    ins >> r.column1 >> r.column2 >> r.column3;
    return ins;
}
int main(){

    ifstream input ("tin.txt");
    if ( !input ){

        cerr << "Cannot open file\n";
    }
    ofstream output1 ("Response.txt",ios::app);

    if (output1.is_open()){
        output1 << "tin" << endl;
        vector<Template> data;
        Template datum;
        //Test for end of file (eof)
        while ( input >> datum )
        {
            data.push_back (datum);
        }
        //This loop displays the data.

        double average;          //average of counts in the bins on either side of the desired energy bin.
        double net_peak;         //energy bin counts minus average of the bins on either side.
        double three_sigma_check; //variable used to determine if an energy bin is a 'peak'.
```

```

double peak;          //variable assigned to a bin that is investigated to determine if it is a
                      //'peak'.
double sigma;        //relative standard error determined by MCNP.

for ( double i=0; i < data.size(); ++i)
{
  if (data[i].column1==2.31500E+00){
    average = (data[i-1].column2 + data[i+1].column2)/2;
    peak = data[i].column2;
    sigma = data[i].column3;
    three_sigma_check = average + 3 * sigma * peak;
    net_peak = peak - average;

    if (peak > three_sigma_check){
      net_peak = net_peak;
    }
    else {
      net_peak = 0;
    }
    output1 << net_peak << endl;
    if (net_peak > 0){
      sigma = sqrt((((data[i].column2*data[i].column3)*(data[i].column2*data[i].column3))+
                    0.25*((data[i-1].column2*data[i-1].column3)*(data[i-1].column2*
                    data[i-1].column3))+0.25*((data[i+1].column2*data[i+1].column3)*
                    (data[i+1].column2*data[i+1].column3))));
    }
    else{
      sigma =0;
    }
    output1 << sigma << endl;
  }

  if (data[i].column1==2.22500E+00){
    average = (data[i-1].column2 + data[i+1].column2)/2;
    peak = data[i].column2;
    sigma = data[i].column3;
    three_sigma_check = average + 3 * sigma * peak;
    net_peak = peak - average;

    if (peak > three_sigma_check){
      net_peak = net_peak;
    }
    else {
      net_peak = 0;
    }
    output1 << net_peak << endl;
  }
}

```

```

if (net_peak > 0){
sigma = sqrt((((data[i].column2*data[i].column3)*(data[i].column2*data[i].column3))+
0.25*((data[i-1].column2*data[i-1].column3)*(data[i-1].column2*
data[i-1].column3))+0.25*((data[i+1].column2*data[i+1].column3)*
(data[i+1].column2*data[i+1].column3))));
}
else{
sigma =0;
}
output1 << sigma << endl;
}

```

```

if (data[i].column1==3.38000E+00){
average = (data[i-1].column2 + data[i+1].column2)/2;
peak = data[i].column2;
sigma = data[i].column3;
three_sigma_check = average + 3 * sigma * peak;
net_peak = peak - average;

```

```

if (peak > three_sigma_check){
net_peak = net_peak;
}
else {
net_peak = 0;
}
output1 << net_peak << endl;
if (net_peak > 0){
sigma = sqrt((((data[i].column2*data[i].column3)*(data[i].column2*data[i].column3))+
0.25*((data[i-1].column2*data[i-1].column3)*(data[i-1].column2*
data[i-1].column3))+0.25*((data[i+1].column2*data[i+1].column3)*
(data[i+1].column2*data[i+1].column3))));
}
else{
sigma =0;
}
output1 << sigma << endl;
}

```

```

if (data[i].column1==4.44000E+00){
average = (data[i-1].column2 + data[i+1].column2)/2;
peak = data[i].column2;
sigma = data[i].column3;
three_sigma_check = average + 3 * sigma * peak;
net_peak = peak - average;

```

```

if (peak > three_sigma_check){

```

```

net_peak = net_peak;
}
else {
net_peak = 0;
}
output1 << net_peak << endl;
if (net_peak > 0){
sigma = sqrt((((data[i].column2*data[i].column3)*(data[i].column2*data[i].column3))+
0.25*((data[i-1].column2*data[i-1].column3)*(data[i-1].column2*
data[i-1].column3))+0.25*((data[i+1].column2*data[i+1].column3)*
(data[i+1].column2*data[i+1].column3))));
}
else{
sigma =0;
}
output1 << sigma << endl;
}

```

```

if (data[i].column1==4.91600E+00){
average = (data[i-1].column2 + data[i+1].column2)/2;
peak = data[i].column2;
sigma = data[i].column3;
three_sigma_check = average + 3 * sigma * peak;
net_peak = peak - average;

```

```

if (peak > three_sigma_check){
net_peak = net_peak;
}
else {
net_peak = 0;
}
output1 << net_peak << endl;
if (net_peak > 0){
sigma = sqrt((((data[i].column2*data[i].column3)*(data[i].column2*data[i].column3))+
0.25*((data[i-1].column2*data[i-1].column3)*(data[i-1].column2*
data[i-1].column3))+0.25*((data[i+1].column2*data[i+1].column3)*
(data[i+1].column2*data[i+1].column3))));
}
else{
sigma =0;
}
output1 << sigma << endl;
}

```

```

if (data[i].column1==5.10700E+00){
average = (data[i-1].column2 + data[i+1].column2)/2;

```

```

peak = data[i].column2;
sigma = data[i].column3;
three_sigma_check = average + 3 * sigma * peak;
net_peak = peak - average;

    if (peak > three_sigma_check){
        net_peak = net_peak;
    }
    else {
        net_peak = 0;
    }
    output1 << net_peak << endl;
    if (net_peak > 0){
        sigma = sqrt((((data[i].column2*data[i].column3)*(data[i].column2*data[i].column3))+
            0.25*((data[i-1].column2*data[i-1].column3)*(data[i-1].column2*
            data[i-1].column3))+0.25*((data[i+1].column2*data[i+1].column3)*
            (data[i+1].column2*data[i+1].column3))));
    }
    else{
        sigma =0;
    }
    output1 << sigma << endl;
}

if (data[i].column1==6.13100E+00){
average = (data[i-1].column2 + data[i+1].column2)/2;
peak = data[i].column2;
sigma = data[i].column3;
three_sigma_check = average + 3 * sigma * peak;
net_peak = peak - average;

    if (peak > three_sigma_check){
        net_peak = net_peak;
    }
    else {
        net_peak = 0;
    }
    output1 << net_peak << endl;
    if (net_peak > 0){
        sigma = sqrt((((data[i].column2*data[i].column3)*(data[i].column2*data[i].column3))+
            0.25*((data[i-1].column2*data[i-1].column3)*(data[i-1].column2*
            data[i-1].column3))+0.25*((data[i+1].column2*data[i+1].column3)*
            (data[i+1].column2*data[i+1].column3))));
    }
    else{
        sigma =0;
    }

```

```

    }
    output1 << sigma << endl;
}

if (data[i].column1==6.44700E+00){
average = (data[i-1].column2 + data[i+1].column2)/2;
peak = data[i].column2;
sigma = data[i].column3;
three_sigma_check = average + 3 * sigma * peak;
net_peak = peak - average;

    if (peak > three_sigma_check){
net_peak = net_peak;
    }
    else {
net_peak = 0;
    }
    output1 << net_peak << endl;
    if (net_peak > 0){
sigma = sqrt((((data[i].column2*data[i].column3)*(data[i].column2*data[i].column3))+
0.25*((data[i-1].column2*data[i-1].column3)*(data[i-1].column2*
data[i-1].column3))+0.25*((data[i+1].column2*data[i+1].column3)*
(data[i+1].column2*data[i+1].column3)));
    }
    else{
sigma =0;
    }
    output1 << sigma << endl;
}

if (data[i].column1==6.91800E+00){
average = (data[i-1].column2 + data[i+1].column2)/2;
peak = data[i].column2;
sigma = data[i].column3;
three_sigma_check = average + 3 * sigma * peak;
net_peak = peak - average;

    if (peak > three_sigma_check){
net_peak = net_peak;
    }
    else {
net_peak = 0;
    }
    output1 << net_peak << endl;
    if (net_peak > 0){
sigma = sqrt((((data[i].column2*data[i].column3)*(data[i].column2*data[i].column3))+

```

```

        0.25*((data[i-1].column2*data[i-1].column3)*(data[i-1].column2*
        data[i-1].column3))+0.25*((data[i+1].column2*data[i+1].column3)*
        (data[i+1].column2*data[i+1].column3));
    }
    else{
        sigma =0;
    }
    output1 << sigma << endl;
}

}
output1 << endl;

output1.close();
}

else cout << "Unable to open file";
return 0;
}

```

Appendix E - Sample MATLAB (2010a) codes for calculating Figures-of-Merit.

Table E.1 Code calling “Response” script to retrieve signatures for templates and responses of targets.

```

%Code for determining the FOM for Samples Vs. Templates
%Program is configured for beta=1 and alpha=1/N (uniform weight factors)
%Author: CPT Heider, Samuel 04MAR12
%Revised: 17MAR12
%-----
%Initializes values to be used in calculating FOM for each
T=80;           %T=number of templates
S=21;           %S=number of samples
G=9;            %G=number of gamma signatures
N=2;            %N=number of neutron signatures
G_N=G+N;        %G-N=sum of gamma and neutron signatures
FOM_gamma=zeros(G,1); %Figure of Merit from gammas array
FOM_neutron=zeros(N,1); %Figure of Merit from neutrons array
FOM=zeros(T,S); %Total Figure of Merit array
Sigma_FOM=zeros(T,S); %Error in the Figure of Merit array
Norm=zeros(G_N,1); %Norm=vetor of normalization vlaues for
                    %each template
Norm_z=0;        %Norm_z=variable used to hold value of
                    %sum(Norm)
Norm_zeta=zeros(T,S); %Norm_zeta=array of normalized FOM values
alpha=1/G_N;     %Alpha value for uniform weight factors
beta=1;          %Beta value
k=1;
l=1;
Response         %Calls “Response” script

```


**Table E.2 “Response” script, places signatures inside response vectors and calls
“Template” script.**

```

while k<=S
  if k<=1
    Response_gamma=adobeg;      %Gamma sample signature vector
    Response_neutron=adobe1;    %Neutron sample signature vector
    Template                    %Uses 'Template' script
    k=k+1;
  end
  if k>=2 && k<3
    Response_gamma=airg;        %Gamma sample signature vector
    Response_neutron=air1;      %Neutron sample signature vector
    Template                    %Uses 'Template' script
  end
  .
  .
  .
  if k>=21 && k<22
    Response_gamma=woodoakg;    %Gamma sample signature vector
    Response_neutron=woodoak1;  %Neutron sample signature vector
    Template                    %Uses 'Template' script
  end

  k=k+1;
end

```

Table E.3 “Template” script, places signatures inside template vectors and calls “FOM_Calc” script.

```

while l<=T
  if l<=1
    Template_gamma=N000C50H50hdg; %Gamma template signature vector

    Template_neutron=N000C50H50hd; %Neutron template signature vector

    FOM_Calc %"FOM_Calc" Script file to calculate FOM

    %Puts calculated zeta values in FOM Matrix
    FOM(l,k)=sum(FOM_gamma)+sum(FOM_neutron);

    Sigma_FOM(l,k)=2*(sqrt(alpha*FOM(l,k))); %Puts error in zeta into Sigma_FOM matrix

    Norm_zeta(l,k)=100*FOM(l,k)/(sum(Norm)); %Normalized FOM

    Norm_sigma(l,k)=100*Sigma_FOM(l,k)/(Norm_z); %Normalized error
  end
  .
  .
  .
  if l>=80 && l<81
    Template_gamma=N0030C0H70vldgU; %Gamma template signature vector

    Template_neutron=N0030C0H70vldU; %Neutron template signature vector

    FOM_Calc %"FOM_Calc" Script file to calculate FOM

    %Puts calculated zeta values in FOM Matrix
    FOM(l,k)=sum(FOM_gamma)+sum(FOM_neutron);

    Sigma_FOM(l,k)=2*(sqrt(alpha*FOM(l,k))); %Puts error in zeta into Sigma_FOM matrix

    Norm_zeta(l,k)=100*FOM(l,k)/(sum(Norm)); %Normalized FOM

    Norm_sigma(l,k)=100*Sigma_FOM(l,k)/(Norm_z); %Normalized error
  end

  l=l+1;
end
l=1;

```

Table E.4 “FOM_Calc” script, calculates FOM and normalization factor

```
i=1;j=1;
while i<=23
  if i<=17
    if Response_gamma(i+1,1)<=0 && Template_gamma(i+1,1)<=0
      FOM_gamma(j)=0;
    else
      FOM_gamma(j)=alpha*(beta*Response_gamma(i,1)-
Template_gamma(i,1))^2/(beta^2*Response_gamma(i+1,1)^2+Template_gamma(i+1,1)^2);
    end

    if Template_gamma(i,1)<=0 || Template_gamma(i+1,1)<=0
      Norm(j)=0;
    else
      Norm(j)=alpha*Template_gamma(i,1)^2/Template_gamma(i+1,1)^2;
    end
  end

  if i>17 && i<=21
    if Response_neutron(i-17,1)<=0 && Template_neutron(i-17,1)<=0
      FOM_neutron(j-9)=0;
    else
      FOM_neutron(j-9)=alpha*(beta*Response_neutron(i-18,1)-Template_neutron(i-
18,1))^2/(beta^2*Response_neutron(i-17,1)^2+Template_neutron(i-17,1)^2);

    end

    if Template_neutron(i-18,1)<=0 || Template_neutron(i-17,1)<=0
      Norm(j)=0;
    else
      Norm(j)=alpha*Template_neutron(i-18,1)^2/Template_neutron(i-17,1)^2;
    end

  end
  j=j+1;
  i=i+2;

end
Norm_z=sum(Norm);
```

Appendix F - Lowest Figures-of-Merit for RDX, UNi, and inert samples versus all templates.

Clutter/Sample	ζ_ℓ	$\pm\sigma(\zeta_\ell)$
Adobe/RDX	2.4080	0.0128
Air/RDX	0.2118	0.0036
Bricks/RDX	2.0787	0.0119
Clay/RDX	3.8880	0.0156
Coal/RDX	1.9142	0.0113
Concrete/RDX	1.7713	0.0111
Copper/RDX	8.7227	0.0170
Cotton/RDX	3.9496	0.0160
Fruit/RDX	0.9979	0.0089
Glass/RDX	2.5814	0.0132
Gypsum/RDX	1.6510	0.0114
Limestone/RDX	0.7369	0.0058
Nylon/RDX	2.2934	0.0132
Polyester/RDX	3.1304	0.0146
Propane/RDX	0.2122	0.0036
Sand/RDX	2.8063	0.0133
Silk/RDX	2.5657	0.0132
Slate/RDX	1.5944	0.0105
Steel/RDX	6.0619	0.0142
Tin/RDX	6.8798	0.0151
Wood/RDX	2.1119	0.0120

Clutter/Sample	ζ_ℓ	$\pm\sigma(\zeta_\ell)$
Adobe/UNi	6.1140	0.0203
Air/UNi	1.0406	0.0117
Bricks/UNi	6.2493	0.0117
Clay/UNi	5.0489	0.0220
Coal/UNi	1.9395	0.0114
Concrete/UNi	2.1009	0.0129
Copper/UNi	8.6382	0.0170
Cotton/UNi	3.7716	0.0156
Fruit/UNi	1.7303	0.0131
Glass/UNi	5.7851	0.0198
Gypsum/UNi	3.7568	0.0199
Limestone/UNi	0.8009	0.0074
Nylon/UNi	2.1941	0.0138
Polyester/UNi	2.7965	0.0138
Propane/UNi	1.0884	0.0120
Sand/UNi	3.9812	0.0195
Silk/UNi	3.2220	0.0174
Slate/UNi	1.9696	0.0125
Steel/UNi	6.1358	0.0143
Tin/UNi	7.1576	0.0154
Wood/UNi	3.7194	0.0187

Clutter/Sample	ζ_ℓ	$\pm\sigma(\zeta_\ell)$
Adobe/Inert	7.3040	0.0222
Air/Inert	80.9972	0.0921
Bricks/Inert	7.8681	0.0249
Clay/Inert	10.0060	0.0260
Coal/Inert	5.6373	0.0195
Concrete/Inert	3.3602	0.0163
Copper/Inert	10.5538	0.0187
Cotton/Inert	2.4273	0.0125
Fruit/Inert	9.8975	0.0314
Glass/Inert	6.7111	0.0213
Gypsum/Inert	8.1638	0.0297
Limestone/Inert	1.9068	0.0114
Nylon/Inert	5.1086	0.0197
Polyester/Inert	5.9022	0.0170
Propane/Inert	80.3154	0.0918
Sand/Inert	9.5333	0.0274
Silk/Inert	2.6971	0.0136
Slate/Inert	4.6184	0.0193
Steel/Inert	7.1532	0.0154
Tin/Inert	8.8412	0.0172
Wood/Inert	4.9532	0.0216

Appendix G - Lowest Figures-of-Merit using density filter.

Density Group-1			Density Group-2		
Clutter/Sample	ζ_ℓ	$\pm\sigma(\zeta_\ell)$	Clutter/Sample	ζ_ℓ	$\pm\sigma(\zeta_\ell)$
Air/UNi	1.0406	0.0117	Adobe/Uni	6.1140	0.0203
Air/RDX	0.2118	0.0036	Adobe/RDX	2.4080	0.0128
Air/Inert	80.9972	0.0921	Adobe/Inert	7.3040	0.0222
Clay/UNi	5.0489	0.0220	Bricks/Uni	6.2493	0.0246
Coal/UNi	2.1363	0.0140	Bricks/RDX	2.0787	0.0119
Fruit/UNi	1.7303	0.0131	Bricks/Inert	7.8681	0.0249
Gypsum/UNi	3.7568	0.0199	Clay/RDX	3.8880	0.0156
Gypsum/Inert	8.1638	0.0297	Clay/Inert	10.0060	0.0260
Nylon/UNi	2.1941	0.0138	Coal/RDX	1.9142	0.0113
Propane/UNi	1.0884	0.0120	Coal/Inert	5.6373	0.0195
Propane/RDX	0.2122	0.0036	Concrete/Uni	2.1009	0.0129
Propane/Inert	80.3154	0.0918	Cotton/Uni	3.7716	0.0156
Silk/UNi	3.2220	0.0174	Cotton/RDX	3.9496	0.0160
Wood/UNi	3.7194	0.0187	Cotton/Inert	2.4273	0.0125
Wood/Inert	4.9532	0.0216	Fruit/RDX	0.9979	0.0089
			Fruit/Inert	9.8975	0.0314
			Glass/Uni	5.7851	0.0198
			Gypsum/RDX	1.6510	0.0114
			Limestone/Uni	0.8009	0.0074
			Nylon/RDX	2.2934	0.0132
			Nylon/Inert	5.1086	0.0197
			Polyester/Uni	2.7965	0.0138
			Polyester/RDX	3.1304	0.0146
			Polyester/Inert	5.9022	0.0170
			Sand/Uni	3.9812	0.0195
			Sand/RDX	2.8063	0.0133
			Sand/Inert	9.5333	0.0274
			Silk/RDX	2.5657	0.0132
			Silk/Inert	2.6971	0.0136
			Slate/Uni	1.9696	0.0125
			Wood/RDX	2.1119	0.0120

Density Group-3

Clutter/Sample	ζ_ℓ	$\pm\sigma(\zeta_\ell)$
Concrete/RDX	1.7713	0.0111
Concrete/Inert	3.3602	0.0163
Limestone/RDX	2.5814	0.0132
Limestone/Inert	6.7111	0.0213
Glass/RDX	0.7369	0.0058
Glass/Inert	1.9068	0.0114
Slate/RDX	1.5944	0.0105
Slate/Inert	4.6184	0.0193

Density Group-4 & Group-5

Clutter/Sample	ζ_ℓ	$\pm\sigma(\zeta_\ell)$
Tin/UNi	7.1576	0.0154
Copper/UNi	8.6382	0.0170
Copper/RDX	8.7227	0.0170
Copper/Inert	10.5538	0.0187
Steel/UNi	6.1358	0.0143
Steel/RDX	6.0619	0.0142
Steel/Inert	7.1532	0.0154
Tin/RDX	6.8798	0.0151
Tin/Inert	8.8412	0.0172

Appendix H - Lowest Figures-of-Merit using neutron signatures and density filter.

Density Group-1			Density Group-2		
Clutter/Sample	ζ_ℓ	$\pm\sigma(\zeta_\ell)$	Clutter/Sample	ζ_ℓ	$\pm\sigma(\zeta_\ell)$
Air/RDX	0.0100	0.0010	Limestone/UNi	0.0050	0.0007
Propane/RDX	0.0103	0.0010	Slate/UNi	0.0092	0.0010
Silk/UNi	0.0380	0.0027	Clay/Inert	0.0110	0.0013
Fruit//Uni	0.0970	0.0047	Clay/RDX	0.0134	0.0014
Gypsum/Inert	0.1604	0.0056	Polyester/Inert	0.0155	0.0017
Nylon//Uni	0.2053	0.0060	Glass/UNi	0.0156	0.0012
Clay//Uni	0.2638	0.0061	Adobe/UNi	0.0197	0.0014
Air//Uni	0.3004	0.0098	Sand/Uni	0.0260	0.0019
Propane/UNi	0.3155	0.0101	Concrete/UNi	0.0375	0.0019
Wood/Uni	0.5798	0.0091	Sand/Inert	0.0401	0.0024
Woodoak/Inert	0.5813	0.0091	Bricks/UNi	0.0404	0.0020
Gypsum/Uni	0.6647	0.0114	Bricks/RDX	0.0406	0.0020
Coal//Uni	0.8140	0.0124	Fruit/RDX	0.0421	0.0030
Propane/Inert	74.0004	0.1032	Sand/RDX	0.0428	0.0021
Air/Inert	74.5940	0.1036	Adobe/Inert	0.0435	0.0021
			Gypsum/RDX	0.0528	0.0028
			Silk/Inert	0.0584	0.0033
			Adobe/RDX	0.0599	0.0024
			Polyester/RDX	0.1217	0.0047
			Bricks/Inert	0.1592	0.0040
			Fruit/Inert	0.1858	0.0065
			Polyester/UNi	0.2209	0.0054
			Silk/RDX	0.2284	0.0065
			Coal/Inert	0.2532	0.0058
			Nylon/RDX	0.2585	0.0070
			Coal/RDX	0.3204	0.0076
			Nylon/Inert	0.3458	0.0081
			Woodoak/RDX	0.4375	0.0091
			Cotton/UNi	0.4810	0.0080
			Cotton/RDX	0.5804	0.0088
			Cotton/Inert	0.7084	0.0097

Density Group-3

Clutter/Sample	ζ_ℓ	$\pm\sigma(\zeta_\ell)$
Concrete/RDX	0.0035	0.0006
Glass/RDX	0.0049	0.0007
Limestone/RDX	0.0319	0.0018
Slate/RDX	0.0415	0.0020
Glass/Inert	0.1126	0.0034
Slate/Inert	0.1571	0.0032
Concrete/Inert	0.1684	0.0041
Limestone/Inert	0.2226	0.0047

Density Group-4 & 5

Clutter/Sample	ζ_ℓ	$\pm\sigma(\zeta_\ell)$
Tin/UNi	0.3326	0.0035
Steel/UNi	0.0481	0.0013
Steel/RDX	0.1800	0.0025
Steel/Inert	0.6288	0.0048
Tin/RDX	0.8062	0.0054
Tin/Inert	1.4511	0.0072
Copper/UNi	1.8618	0.0082
Copper/RDX	2.2958	0.0091
Copper/Inert	3.3025	0.0109

**Appendix I - Lowest Figures-of-Merit using gamma-ray signatures
and density filter.**

Density Group-1			Density Group-2		
Clutter/Sample	ζ_ℓ	$\pm\sigma(\zeta_\ell)$	Clutter/Sample	ζ_ℓ	$\pm\sigma(\zeta_\ell)$
Air/UNi	0.4788	0.0141	Limestone/UNi	0.9617	0.0142
Propane/UNi	0.5027	0.0144	Fruit/RDX	1.5433	0.0139
Air/RDX	0.5490	0.0096	Gypsum/RDX	1.5933	0.0164
Propane/RDX	0.5534	0.0097	Coal/RDX	1.6306	0.0144
Gypsum/UNi	2.8299	0.0315	Nylon/RDX	2.4694	0.0177
Fruit/UNi	2.9972	0.0230	Silk/Inert	3.0659	0.0201
Coal/UNi	3.4082	0.0248	Woodoak/RDX	3.5343	0.0215
Nylon/UNi	4.0642	0.0261	Silk/RDX	3.5381	0.0216
Woodoak/UNi	5.3895	0.0318	Sand/RDX	3.8631	0.0266
Silk/UNi	6.4073	0.0347	Polyester/RDX	3.8881	0.0226
Woodoak/Inert	8.6298	0.0402	Cotton/Inert	4.0414	0.0234
Clay/Urea Nitrate	13.4083	0.0622	Polyester/UNi	4.4829	0.0243
Gypsum/Inert	19.8781	0.0927	Clay/RDX	4.5004	0.0287
Propane/Inert	96.0094	0.2036	Bricks/RDX	4.7147	0.0314
Air/Inert	97.9901	0.1995	Cotton/RDX	5.1931	0.0256
			Cotton/UNi	6.0011	0.0285
			Adobe/RDX	6.3240	0.0363
			Nylon/Inert	6.4903	0.0287
			Concrete/UNi	7.0968	0.0515
			Slate/UNi	7.4362	0.0527
			Coal/Inert	8.7873	0.0335
			Sand/UNi	9.3434	0.0462
			Polyester/Inert	10.8018	0.0329
			Bricks/UNi	12.2106	0.0521
			Adobe/UNi	13.0611	0.0522
			Glass/UNi	15.1728	0.0581
			Fruit/Inert	15.2405	0.0316
			Sand/Inert	18.8638	0.0648
			Clay/Inert	19.5457	0.0639
			Bricks/Inert	19.9873	0.0667
			Adobe/Inert	20.6238	0.0656

Density Group-3

Clutter/Sample	ζ_l	$\pm\sigma(\zeta_l)$
Glass/Inert	0.1575	0.0048
Glass/RDX	0.5253	0.0092
Slate/Inert	2.0191	0.0248
Concrete/Inert	2.2058	0.0260
Concrete/RDX	3.9268	0.0300
Slate/RDX	5.1477	0.0343
Limestone/RDX	7.4496	0.0330
Limestone/Inert	16.3698	0.0490

Density Group-4 & 5

Clutter/Sample	ζ_l	$\pm\sigma(\zeta_l)$
Tin/UNi	91.0308	0.1520
Steel/RDX	78.6175	0.1868
Steel/UNi	81.2290	0.1899
Tin/RDX	81.7996	0.1906
Steel/Inert	87.6330	0.1972
Copper/RDX	88.0004	0.1976
Copper/UNi	92.2280	0.2023
Copper/Inert	100.0000	0.2107
Tin/Inert	100.0000	0.2107